DEVELOPMENT OF WAFER-LEVEL VACUUM PACKAGING FOR MEMS DEVICES WITH TRANSIENT LIQUID PHASE (TLP) BONDING: A COMBINATORIAL APPROACH

A THESIS SUBMITTED TO
THE GRADUATE SCHOOL OF NATURAL AND APPLIED SCIENCES
OF
MIDDLE EAST TECHNICAL UNIVERSITY

BY

ÖZGÜN YURDAKUL

IN PARTIAL FULFILLMENT OF THE REQUIREMENTS
FOR
THE DEGREE OF MASTER OF SCIENCE
IN
METALLURGICAL AND MATERIALS ENGINEERING

JANUARY 2023

Approval of the thesis:

DEVELOPMENT OF WAFER-LEVEL VACUUM PACKAGING FOR MEMS DEVICES WITH TRANSIENT LIQUID PHASE (TLP) BONDING: A COMBINATORIAL APPROACH

submitted by **ÖZGÜN YURDAKUL** in partial fulfillment of the requirements for the degree of **Master of Science** in **Metallurgical and Materials Engineering, Middle East Technical University** by,

Prof. Dr. Halil Kalıpçılar
Dean, Graduate School of **Natural and Applied Sciences** ________________

Prof. Dr. Ali Kalkanlı
Head of the Department, **Metallurgical and Materials Eng.** ________________

Prof. Dr. Yunus Eren Kalay
Supervisor, **Metallurgical and Materials Eng., METU** ________________

Examining Committee Members:

Prof. Dr. Cemil Hakan Gür
Metallurgical and Materials Eng., METU ________________

Prof. Dr. Yunus Eren Kalay
Metallurgical and Materials Eng., METU ________________

Prof. Dr. Tayfun Akın
Electrical-Electronics Eng., METU ________________

Assist. Prof. Dr. Eda Aydoğan
Metallurgical and Materials Eng., METU ________________

Prof. Dr. Yüksel Ergün
Physics., ESTU ________________

Date: 25.01.2023

I hereby declare that all information in this document has been obtained and presented in accordance with academic rules and ethical conduct. I also declare that, as required by these rules and conduct, I have fully cited and referenced all material and results that are not original to this work.

Name Last name : Özgün Yurdakul

Signature :

ABSTRACT

DEVELOPMENT OF WAFER-LEVEL VACUUM PACKAGING FOR MEMS DEVICES WITH TRANSIENT LIQUID PHASE (TLP) BONDING: A COMBINATORIAL APPROACH

Yurdakul, Özgün
Master of Science, Metallurgical and Materials Engineering
Supervisor: Prof. Dr. Yunus Eren Kalay

January 2023, 138 pages

Electronic systems may be sealed by slicing the wafer into individual circuits and then packaging them or by packaging an integrated circuit while still part of the wafer. The latter enables the packaging of all detectors on complementary metal oxide semiconductors (CMOS) simultaneously, considerably decreasing manufacturing costs and increasing efficiency. Regarding a suitable packaging process for microbolometers, the most crucial parameter appears to be the compatibility of the packaging procedure with the detectors and the CMOS-based chips. Besides, as the MEMS's complexity and durability increase, more robust packaging is needed to achieve better packaging.

For this purpose, in this study, a combinatorial approach that obtains multiple compositions for bonding purposes in a single deposition run was studied to investigate the best composition-property relation for MEMS packaging using binary Gold-Indium (Au-In) material system and Transient Liquid Phase (TLP) bonding method. In addition, a Gold – Indium – Tin (Au-In-Sn) ternary material system that

has not been studied before in the literature for Wafer Level Packaging (WLP) has been studied to enhance the properties of the MEMS package.

As a result of studies in this thesis, various compositions for the Au-In binary system were achieved with a combinatorial approach. According to comparing the results of characterization stages, the most efficient composition value was found for packaging MEMS devices with the Au-In TLP bonding method. Concerning that, almost %40 of the AuIn – $AuIn_2$ intermetallic region has been investigated with only 3 In deposition run with a combinatorial approach. Furthermore, with single In deposition run via combinatorial deposition, up to 8% wt In composition range has been obtained. After combinatorial optimizations, 22 MPa average shear strength was achieved with 46.0 wt% In composition. Therefore, this thesis has studied optimizing the composition/property relationship with the combinatorial approach.

Furthermore, after optimization of the composition of the In in Au-In binary system, WLP was done with a cap cavity to observe of hermetic properties of the structure. 8 µm cap deflection depth has been achieved with 24 µm membrane thickness, providing 0.2 mbar pressure inside the package without any gas penetration. Moreover, with an optimized composition value, 28 MPa package strength was observed in that sample.

Although Au-In-Sn ternary bonding system seems to be one of the candidate materials systems for WLP packaging of MEMS since TLP bonding conditions have been obtained according to Differential Scanning Calorimetry results, higher than 49 MPa shear strength was achieved and high bond integrity has been acquired concerning Scanning Acoustic Microscope inspection, this system requires re-evaluation for use as a result of the low yield of successfully packaged chips after bonding experiments.

Keywords: Wafer-Level Packaging, Combinatorial Approach, Au-In Alloy, Transient Liquid Phase Bonding, MEMS Packaging

ÖZ

MEMS AYGITLARININ GEÇİCİ SIVI FAZ BAĞLAMA YÖNTEMİ İLE DİSK SEVİYESİNDE VAKUM PAKETLENMESİNİN KOMBİNATORYAL YAKLAŞIM İLE GELİŞTİRİLMESİ

Yurdakul, Özgün
Yüksek Lisans, Metalurji ve Malzeme Mühendisliği
Tez Yöneticisi: Prof. Dr. Yunus Eren Kalay

Ocak 2023, 138 sayfa

Elektronik sistemler, plakaların ayrı devreler için dilimlenip ardından paketlenmesiyle veya entegre bir devre hala plakanın üzerindeyken paketlenmesiyle beraber birleştirilebilir. İkinci birleştirme yöntemi, bütün dedektörlerin tamamlayıcı metal oksit yarı iletkenler (CMOS) üzerinde eş zamanlı olarak paketlenebilmesini sağlar, bu da üretim maliyetini önemli ölçüde azaltır ve verimliliği arttırır. Mikrobolometreler için uygun bir paketleme sürecine karar vermek açısından en önemli parametre, paketleme işleminin dedektörlere ve CMOS tabanlı çiplere uyumluluğu olarak görünmektedir. Ayrıca, MEMS'in karmaşıklığı ve gerekli dayanıklığı arttıkça, daha iyi paketleme elde etmek için daha güçlü paketleme gerekmektedir.

Bu amaçla, bu çalışmada, ikili Altın – İndiyum (Au-In) malzeme sistemi ve Geçici Sıvı Faz (TLP) bağlama yöntemi kullanılarak, MEMS paketleme için en iyi kompozisyon-özellik ilişkisinin araştırılması amacıyla tek bir kaplama işleminde bağlama işlemi için birden fazla kompozisyon elde edilebilmesini sağlayan kombinatoryal yaklaşım çalışılmıştır. Ayrıca, Disk Seviyesi Paketleme (WLP) için daha önce literatürde çalışılmamış olan Altın – İndiyum – Kalay (Au-In-Sn) üçlü malzeme sistemi MEMS paketinin özelliklerini geliştirme amacıyla çalışılmıştır.

Bu tez kapsamında yapılan çalışmalar sonucunda, kombinatoryal yaklaşım ile Au-In ikili sistemi için çeşitli kompozisyonlar elde edilmiştir. Karakterizasyon aşamalarının sonuçları karşılaştırılarak, Au-In TLP bağlama yöntemi ile MEMS cihazlarının paketlenmesi için en verimli kompozisyon değeri bulunmuştur. Buna bağlı olarak AuIn-$AuIn_2$ intermetalik bölgesinin yaklaşık %40'lık bir kısmı kombinatoryal yaklaşım sayesinde yalnızca 3 In kaplamasıyla incelenmiştir. Ayrıca kombinatoryal yaklaşımla gerçekleştirilen tekli In kaplaması ile ağırlık olarak %8'e varan In kompozisyon aralığı elde edilmiştir. Kombinatoryal optimizasyonlar sonucunda ağırlıkça %46.0 In kompozisyonuyla beraber 22 MPa kesme dayancı elde edilmiştir. Bu sayede, bu tez kapsamında kompozisyon/özellik ilişkisinin kombinatoryal yaklaşım ile optimizasyonu çalışılmıştır.

Ayrıca Au-In ikili sistemi için kompozisyon optimizasyonu yapıldıktan sonra, hermetik özellikleri gözlemleyebilmek için kapak boşluğu oluşturulan örnekler ile pul seviyesi paketleme gerçekleştirilmiştir. Sonuç olarak 8 μm kapak bükülme derinliğine 24 μm membran kalınlığı ile ulaşılmıştır bu da paket içerisinde herhangi bir gaz girişi olmadan 0.2 mbar basınç elde edildiğini göstermektedir. Ayrıca, optimize edilmiş kompozisyon değeri ile bu örnekte 28 MPa paket mukavemeti gözlemlenmiştir.

Au-In-Sn üçlü bağlama sistemi, Diferansiyel Taramalı Kalorimetre sonuçlarına göre TLP bağlanma şartlarına uygunluk, 49 MPa kesme dayanımından daha fazla kayma mukavemeti ve Taramalı Akustik Mikroskop ile inceleme sonuçlarına göre yüksek bağ bütünlüğü gibi uygun sonuçlar verdiğinden MEMS cihazlarının WLP paketlemesi için aday malzeme sistemlerinden biri gibi görünse de, bağlama deneylerinden sonra elde edilen paketlenen ürünlerin düşük verimi sonucunda bu sistemin kullanımı için yeniden değerlendirme yapılması gerekmektedir.

Anahtar Kelimeler: Disk Seviyesi Paketleme, Kombinatoryal Yaklaşım, Au-In Alaşımı, Geçici Sıvı Faz İle Bağlama, MEMS Paketleme

To the Future

ACKNOWLEDGMENTS

First, I would like the thank to my supervisor Prof. Dr. Yunus Eren Kalay for all guidance and supports during my graduate studies. He has always been a supportive and encouraging supervisor since I started my master's degree with him.

I would also like to thank to Ali Can Atik for helps about COMSOL Multiphysics Simulation Software and other fabrication and characterization methods, Sedat Mert for helping me DRIE process and many characterization steps during my experimental procedures, Oytun Demirörs for helping me on sputter metallization processes, Taylan Töral for many contributions with his knowledge and helping on my experimental procedures, my colleague Gürel Dimez for helping during packaging processes and Adem Saraç for giving me guidance on lithography steps.

I am also thankful to my workmates Gülşah Demirhan, Mert Uslu, Esin Gül and Evren Erdil for their helps with grateful contributions on experimental and characterization stages. I am also thankful to all members of the METU MEMS Research Center for their valuable friendship and nice environment.

I would like to express my gratefulness to my laboratory mates Can Okuyucu and Doğuhan Sarıtürk for their advice at my graduate works.

I am also thankful to clean room support team of METU MEMS Research Center for all their helps which includes, Levent Abat, Ali Aytekin, Macit Araz, Fatih Aykut Bakırcı and Yusuf Murat.

I am also grateful to my parents who raised me and brought me to this day with their endless love and support. I would like to thank my sister Özge, with whom I have always had a good friendship, as well as her sisterhood.

I would also like to thank my cousins Ozan Yurdakul and my colleague Kıvanç Yurdakul, who helped me with their advice and information about my academic and business life. I would also like to thank my friends for their help and friendship.

TABLE OF CONTENTS

ABSTRACT v

ÖZ vii

ACKNOWLEDGMENTS x

TABLE OF CONTENTS xi

LIST OF TABLES xiv

LIST OF FIGURES xvi

1 INTRODUCTION 1

1.1 Overview of Micro-Electro-Mechanical Systems (MEMS) 1

1.2 MEMS Packaging Systems and Requirements 3

1.2.1 Die Level Packaging 8

1.2.2 Wafer Level Packaging (WLP) and Methods 9

1.3 Combinatorial Deposition Method 20

1.4 Ternary Material System Approach 21

1.5 Objective and Outline of Thesis 22

2 LITERATURE REVIEW 25

2.1 Au-In TLP Bonding 25

2.2 Au-Sn Eutectic Bonding and Combination with TLP 32

2.3 Ternary WLP Approaches 36

2.4 Combinatorial Deposition 39

3 EXPERIMENTAL PROCEDURE 43

3.1 Overview 43

3.2 Fabrication Steps 43

3.2.1 Dehydration of Wafers 44
3.2.2 Photoresist (PR) Spinning 45
3.2.3 UV Exposure 46
3.2.4 Photoresist (PR) Development 47
3.2.5 Thin Film Metal Deposition 49
3.2.6 Lift-Off 51
3.2.7 Cap Cavity Opening 53
3.2.8 Bond Alignment 56
3.2.9 Wafer Bonding 57
3.2.10 Dicing 61
3.3 Characterization 62
3.3.1 Scanning Acoustic Microscopy (SAM) 64
3.3.2 Scanning Electron Microscopy (SEM) and Energy Dispersive Spectroscopy (EDS) 65
3.3.3 Differential Scanning Calorimetry (DSC) 67
3.3.4 Die Level Shear Test 68
3.3.5 Cap Deflection Test 68
3.3.6 He Leak Test 71
4 RESULTS & DISCUSSION 73
4.1 WLP Trials with Combinatorial Au-In Material System 74
4.1.1 Combinatorial Au-In Sample 1 74
4.1.2 Combinatorial Au-In Sample 2 and Combinatorial Au-In Sample 3 81
4.1.3 Combinatorial Au-In Sample 4 and Combinatorial Au-In Sample 5 90
4.1.4 Comparison of Combinatorial Au-In Samples 101

4.1.5 Au-In WLP Sample with Cap Cavity 103
4.2 WLP Trials with Au-In-Sn Ternary System 113
4.2.1 Au-In-Sn Sample 7 118
4.2.2 Au-In-Sn Sample 8 122
4.2.3 Au-In-Sn Sample 9 125
5 CONCLUSION AND FUTURE RECOMMENDATIONS 129
REFERENCES 132

LIST OF TABLES

TABLES

Table 1.1 Required Pressure Values for Working of some MEMS Devices [7] 4

Table 1.2 Examples of Eutectic Metal Combinations with Eutectic Temperature Values [32] 16

Table 1.3 Candidate Metal Stacks for TLP Bonding with Bonding Process Parameters and Remelting Temperature Values [33] 19

Table 3.1 He Leakage Test Rejection Limits Concerning MIL-STD 883 [12] 72

Table 4.1 Indium Thickness Values and Statistical Data for Combinatorial Au-In Sample 1 76

Table 4.2 Indium Composition Values and Statistical Data for Combinatorial Au-In Sample 1 76

Table 4.3 Shear Strength Values of Combinatorial AuIn Sample 1 81

Table 4.4 Indium Thickness Values and Statistical Data for Combinatorial Au-In Sample 2 83

Table 4.5 Indium Composition Values and Statistical Data for Combinatorial Au-In Sample 2 84

Table 4.6 Indium Thickness Values and Statistical Data for Combinatorial Au-In Sample 3 84

Table 4.7 Indium Composition Values and Statistical Data for Combinatorial Au-In Sample 3 85

Table 4.8 Shear Strength Values of Combinatorial AuIn Sample 2 90

Table 4.9 Indium Thickness Values and Statistical Data for Combinatorial Au-In Sample 4 92

Table 4.10 Indium Composition Values and Statistical Data for Combinatorial Au-In Sample 4 92

Table 4.11 Indium Thickness Values and Statistical Data for Combinatorial Au-In Sample 5 93

Table 4.12 Indium Composition Values and Statistical Data for Combinatorial Au-In Sample 5 93
Table 4.13 Shear Strength Values of Combinatorial AuIn Sample 4 100
Table 4.14 Shear Strength Values of Combinatorial AuIn Sample 5 100
Table 4.15 Properties of Combinatorial AuIn Samples 102
Table 4.16 Indium Thickness Values and Statistical Data for Cavity AuIn Sample 6.. 105
Table 4.17 Indium Composition Values and Statistical Data for Cavity Au-In Sample 6.. 105
Table 4.18 Shear Strength Values of Cavity AuIn Sample 6 with Statistical Data 108
Table 4.19 Shear Strength Values of Au-In-Sn Sample 7 with Statistical Data .. 121
Table 4.20 Shear Strength Values of Au-In-Sn Sample 8 with Statistical Data .. 124
Table 4.21 Shear Strength Values of Au-In-Sn Sample 9 with Statistical Data .. 127

LIST OF FIGURES

FIGURES

Figure 1.1 Global Market Size of MEMS Technology from 2017 to 2023 Forecast [3] 2
Figure 1.2 Schematic Representation of Microbolometer Structure [8]. 4
Figure 1.3 Heat Transfer Mechanisms of Microbolometer Systems [9] 5
Figure 1.4 Microbolometer Efficiency with respect to Pressure Value Inside the Package [9] 6
Figure 1.5 Schematic Representation of Die Level Packaging [17] 9
Figure 1.6 Schematic Representation of Wafer Level Packaging (WLP) [17] 10
Figure 1.7 Schematic Representation of Anodic Bonding with Scanning Electron Microscope (SEM) Image [20] 11
Figure 1.8 Schematic Representation of Glass Frit Bonding with Phase Changes and SEM Images [27] 13
Figure 1.9 Estimation of Hermetic Properties of Different Material Types with respect to Time as a function of Thickness [29] 14
Figure 1.10 Schematic Representation of Eutectic Phase Diagram 15
Figure 1.11 Schematic Representation of TLP Bonding with Stages [34] 17
Figure 1.12 Phase Diagram of Au-In System to Demonstrate TLP Bonding with Stages [35] 18
Figure 1.13 Example of Combinatorial Deposition Method [39] 20
Figure 1.14 Combinatorial Deposition Method with Varied Composition Across Substrate [40] 21
Figure 2.1 Gold-Indium (Au-In) Phase Diagram [35] 26
Figure 2.2 Schematic Representation of Au-In TLP Bonding with Stages of Bonding and In Distribution [43] 27
Figure 2.3 a) Schematic Representation of WLP Bonding Procedure with Au-In System Before Bonding, and b) Scanning Electron Microscope (SEM) Image of Cross Section of Bonding System After Bonding [44] 28

Figure 2.4 a) Temperature and Chamber Pressure Values that Applied during Bonding Operation, and b) Pressure Values Inside the Package after Bonding with respect to Time [44] 29
Figure 2.5 Schematic Representation of 3D Integrated Microelectronic System which joined with Au-In Binary System [45] 30
Figure 2.6 a) Shear Strength Change with respect to Bonding Time and Bonding Pressure and b) Shear Strength Change with respect to Bonding Time and Annealing Temperature [45] 31
Figure 2.7 Electrical Resistance Change of Au-In Bonding System with respect to Change in the Annealing Time at 120 °C Annealing Temperature [45] 31
Figure 2.8 Gold-Tin (Au-Sn) Phase Diagram [35] 33
Figure 2.9 Schematical representation of MEMS Device Design with Design of Bonding Material Stack with Thicknesses [47] 34
Figure 2.10 SEM Image of the Cross-Section of Bonding Area with EDS Analysis [47] 35
Figure 2.11 a), b) Schematic Representation of Bonded Structure with Cu-In-Sn System with Cross-Sectional View, c) and d) Fracture Surface after Mechanical Test on Bonded Sample [41] 37
Figure 2.12 a), b), and c) Selected Bonded Area for EDS Analysis with Different Magnifications with Elemental Distribution [41] 38
Figure 2.13 a) Combinatorial Deposition Method with in-situ Co-Sputtering Method, b) Distribution of the Samples at Holder for Combinatorial Deposition, and c) Composition Values of the Samples after Combinatorial Deposition (shown with blue dots) [50] 40
Figure 2.14 Schematic Representation of Combinatorial Deposition with Single Target and Substrate [51] 41
Figure 2.15 a) Schematic Illustration of Combinatorial Deposition with Thermal Evaporation System (left) and b) Obtained Phases concerning Elemental Composition and X-Ray Diffraction (XRD) Analysis (right) [52] 42

Figure 2.16 Schematic Representation of Combinatorial Deposition of Al and Fe Elements with Thermal Evaporation Technique and b) Compositional Gradient on Substrate after Combinatorial Deposition [53]..42
Figure 3.1 Fabrication Steps of Substrate and Cap Wafers for WLP.....................44
Figure 3.2 Imperial IV Furnace 45
Figure 3.3 a) SUSS MicroTec Spinner System (left) and b) Torrey Pines Hot Plate (right)..46
Figure 3.4 EVG 6200 Contact Aligner System 47
Figure 3.5 Development Procedure 48
Figure 3.6 a) Varian 3119 Thermal Evaporator System, b) BESTEC Sputtering System, c) AJA Sputtering System, and d) Nanovak NVTH 500 Thermal Evaporator System...50
Figure 3.7 Holder Types of In Thermal Evaporator for 4" Wafer In Deposition...51
Figure 3.8 a) Nanovak NVTH 500 In Thermal Evaporator Inside the Chamber and b) Magnified View of Wafer Holder 51
Figure 3.9 Schematic Representation of Process Steps for Patterning Metal Structure with Lift-off 52
Figure 3.10 a) Ultrasonic Cleaner for Lift-Off Process and b) Avenger Ultra-Pure 8 SRD System...53
Figure 3.11 STS Pegasus DRIE System..54
Figure 3.12 a) Branson O_2 Plasma Cleaner and b) Wet Bench of PR Strip Process 55
Figure 3.13 Schematic Illustration of Cap Cavity Opening Process 56
Figure 3.14 EVG 520 IS Wafer Bonder System 57
Figure 3.15 Recipe CombAuIn 1 Temperature and Pressure vs. Time Diagram...59
Figure 3.16 Recipe AuInSn 1 Temperature and Pressure vs. Time Diagram 60
Figure 3.17 Recipe AuInSn 2 Temperature and Pressure vs. Time Diagram 61
Figure 3.18 DAD 3350 Dicing System 62
Figure 3.19 Veeco DEKTAK 8 Surface Profiler...63

Figure 3.20 a) PVA TepLA 301 HD SAM System, b and c) Positions of the Transducer and WLP Sample during SAM Analysis, and d) SAM Software Interface with Peak Positions and SAM Image 65
Figure 3.21 Hitachi Regulus 8230 SEM System 66
Figure 3.22 Perkin Elmer Diamond DSC System... 67
Figure 3.23 a) Dage 4000 Bond Tester System, b) Cross View of Shear Tool with Packaged Die During Die Level Shear Test, and c) Optic Microscope Image of Shear Tool and Sample 68
Figure 3.24 Schematic Illustration of Cap Deflection Process 69
Figure 3.25 Package Vacuum Level Equation... 69
Figure 3.26 a) Maximum Deflection vs. Membrane Thickness from 20 µm to 200 µm for 10 mbar Package Pressure, b) Deflection Distribution vs. Length along Max. Deflection Cross Section for 25 µm Membrane Thickness, c) Max. Deflection vs. Pressure Inside the Package for 25 µm Membrane Thickness and d) Schematization of Deflection along Maximum Deflection Cross Sectional Region for 25 µm Membrane Thickness. 70
Figure 3.27 a) Pressure Vessel for He Bombardment and b) He Leak Detector ... 71
Figure 4.1 Schematic Representation of Regions of 4” Wafer 73
Figure 4.2 Representation of the Nomenclature of dies for 4” Wafer System 74
Figure 4.3 a) Schematized Illustration of Obtained Thickness Values Inside the In Chamber and b) Cross Sectional View of Deposited Thicknesses of Bonding Material System with Seed Layer 75
Figure 4.4 Combinatorial AuIn Sample 1 - d 10.9 a) Cross Sectional SEM Image with Package Parts, b) Cross-Sectional View of Bond Area, c) EDS Elemental Analysis and d) Elemental Distribution across Bond Area.................................... 78
Figure 4.5 a) SAM Image of Combinatorial AuIn Sample 1 with Different Die Types and b) Optic Image of Combinatorial AuIn Sample 1 in Wafer just after SAM Analysis 79
Figure 4.6 Optic Microscope Images of Combinatorial AuIn Sample 1 after WLP 79

Figure 4.7 a) Photo of Combinatorial AuIn Sample 1 after Dicing and b) Dicing Yield Analysis of Combinatorial AuIn Sample 1 with Schematic Illustration 80
Figure 4.8 Schematic Representation of In Deposition Stage with Thickness Values 82
Figure 4.9 SAM Image of Combinatorial AuIn Sample 2 86
Figure 4.10 SAM Image of Combinatorial AuIn Sample 3 86
Figure 4.11 Optic Image of Combinatorial AuIn Sample 3 after Dicing Process .. 88
Figure 4.12 Combinatorial AuIn Sample 2 - d 10.9 a) Cross Sectional SEM Image with Package Parts, b) Cross-Sectional View of Bond Area, c) EDS Elemental Analysis and d) Elemental Distribution across Bond Area 88
Figure 4.13 a) Photo of Combinatorial AuIn Sample 2 after Dicing and b) Dicing Yield Analysis of Combinatorial AuIn Sample 2 with Schematic Illustration 89
Figure 4.14 a) Schematized Illustration of Obtained Thickness Values Inside the In Chamber and b) Cross Sectional View of Deposited Thicknesses of Bonding Material System with Seed Layer 91
Figure 4.15 a) SAM Image of Combinatorial AuIn Sample 4 with Different Die Types and b) Optic Image of Combinatorial AuIn Sample 4 after WLP and SAM Analysis 95
Figure 4.16 SAM Image of Combinatorial AuIn Sample 5 95
Figure 4.17 Optic Microscope Image of Squeezed-Out Region of Combinatorial AuIn Sample 4 between d 11.15 and d 12.15 96
Figure 4.18 Combinatorial AuIn Sample 4 - d 10.9 a) Cross Sectional SEM Image with Package Parts, b) Cross-Sectional View of Bond Area, c) EDS Elemental Analysis and d) Elemental Distribution across Bond Area 97
Figure 4.19 Combinatorial AuIn Sample 5 - d 10.9 a) Cross Sectional SEM Image with Package Parts, b) Cross-Sectional View of Bond Area, c) EDS Elemental Analysis and d) Elemental Distribution across Bond Area 98
Figure 4.20 a) Photo of Combinatorial AuIn Sample 4 after Dicing and b) Dicing Yield Analysis of Combinatorial AuIn Sample 4 with Schematic Illustration 99

Figure 4.21 Optic Image of Combinatorial AuIn Sample 5 after Dicing Process (In this Figure, missing dies were taken for Shear Test) 99
Figure 4.22 Position of All Combinatorial Samples in Au-In Phase Diagram and In Compositions Examined with Combinatorial Approach 102
Figure 4.23 Schematized Illustration of Obtained Thickness Values Inside the In Chamber and b) Cross Sectional View of Deposited Thicknesses of Bonding Material System with Seed Layer 104
Figure 4.24 SAM Image of Cavity AuIn Sample 6 with Different Die Types 106
Figure 4.25 Image of Cavity AuIn Sample 6 After Dicing Process 107
Figure 4.26 a) Cap Cavity Depth Measurement Result with Optic Surface Profiler for Cavity AuIn Sample 6 and b) Iso-sectional View of the Cap Cavity Depth with Optic Surface Profiler 108
Figure 4.27 Cavity AuIn Sample 6 a) Cross Sectional SEM Image with Package Parts, b) Bond Region and Squeeze-out Parts of the Packaged System, c) Cross-Sectional View of Bond Area, d) EDS Elemental Analysis and e) Elemental Distribution across Bond Area 109
Figure 4.28 Photos of the Dies after DRIE Process with Cap Cavity Formation and Ruptured Si Part of the Die 111
Figure 4.29 a) Iso-sectional View from COMSOL Multiphysics Software, b) Magnified View of the Cavity Deflection Area of the Image of COMSOL Multiphysics Simulation Image c) 2D Depth Image of Cap Deflection with Optic Surface Profiler, d) Iso-sectional Representation of Cap Cavity with Optic Surface Profiler and e) 3 Different Cap Cavity Depth Measurements with Optic Surface Profiler 112
Figure 4.30 Schematic Representation of Bonding System for WLP with Au-In-Sn Ternary System with Definition of the Layers 114
Figure 4.31 DSC Result of Au-In-Sn Ternary System 115
Figure 4.32 a) Isothermal Ternary Phase Diagram of Au-In-Sn Material System at 300 °C and b) Isothermal Ternary Phase Diagram of Au-In-Sn Material System at 350 °C 116

Figure 4.33 Sample that Annealed at 350 °C – 1 hour – Vacuum Atmosphere a) SEM Image with Secondary Electron Detector, b) SEM Image with High Angle Back Scattered Electron Detector c) Point and Map EDS Analyzes with Compositions and d) Elemental Distribution 117
Figure 4.34 Sample that Annealed at 350 °C – 5 hours – N_2 Atmosphere a) SEM Image with Secondary Electron Detector, b) SEM Image with High Angle Back Scattered Electron Detector c) Point and Map EDS Analyzes with Compositions and d) Elemental Distribution 117
Figure 4.35 SAM Image of Au-In-Sn Sample 7 119
Figure 4.36 Au-In-Sn Sample 7 – Location 1 a) Cross Sectional SEM Image, b) Map EDS Analysis with Elemental Compositions and c) Elemental Distributions 120
Figure 4.37 Au-In-Sn Sample 7 – Location 2 a) Cross Sectional SEM Image, b) Map EDS Analysis with Elemental Compositions and c) Elemental Distributions 120
Figure 4.38 SAM Image of Au-In-Sn Sample 8 123
Figure 4.39 Photo of Au-In-Sn Sample 8 After Dicing Process 124
Figure 4.40 a) SAM Image of Au-In-Sn Sample 9 and b) Photo of Au-In-Sn Sample 9 after SAM Inspection 125
Figure 4.41 Photo of Sample Au-In-Sn Sample 9 After Dicing 126

CHAPTER 1

INTRODUCTION

1.1 Overview of Micro-Electro-Mechanical Systems (MEMS)

Micro-Electro-Mechanical Systems (MEMS) can be defined as the integration of mechanical systems with electrical components in microscales to perceive the outside effects such as radiation, pressure, and thermal effects and give desired reactions. MEMS sense the external effects through the physical counteraction of the materials in these devices, such as temporary dimensional changes with contraction, expansion, or displacement of some parts. These changes convert to changes in MEMS devices' electrical properties, such as resistance or current. Changes in electrical properties can be read by Read-Out-Integrated-Circuit (ROIC), which can be built onto substrate semiconductor structures such as Complementary Metal Oxide Semiconductor (CMOS) systems and n or p-type doped silicon semiconductors [1].

MEMS devices are produced with microfabrication techniques such as photolithography, thin film deposition techniques such as Chemical Vapor Deposition (CVD) or Physical Vapor Deposition (PVD), and dry or wet etching; therefore, these devices have microscaled feature sizes. Since most of these microfabrication techniques require high purity to eliminate any contamination which causes unacceptable operating conditions for these devices, a clean room with a specific classification is needed to manufacture. Therefore, MEMS devices are highly technological and susceptible to outside effects, providing highly developed research areas and broad multidisciplinary working areas [2]. For instance, the global market size for MEMS technology with the 2023 forecast and 2017 values was given in Figure 1.1 [3].

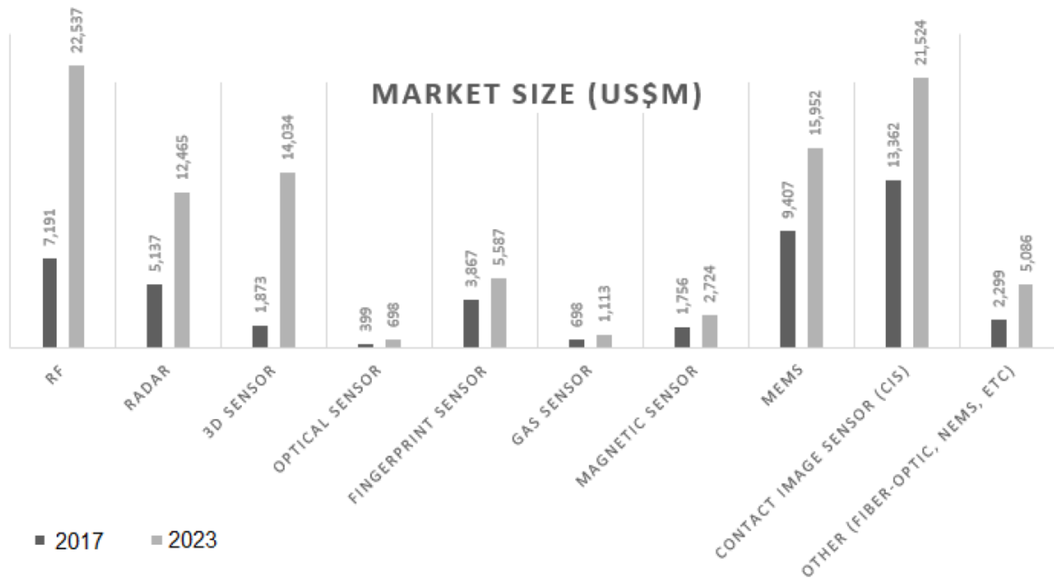

Figure 1.1 Global Market Size of MEMS Technology from 2017 to 2023 Forecast [3]

Accelerometers and gyroscopes are the most common examples of MEMS devices used in industry and commercially. For example, the most common usage area of MEMS is airbag systems of automobiles, and accelerometers are used in them. Besides the automobile industry, MEMS is also used in defense, medicine, and chemical industries. Furthermore, Radio Frequency (RF) MEMS, BioMEMS, pressure or vacuum sensors, and infrared imaging systems such as photon detectors and microbolometers are other types of MEMS or MEMS-based structures [4].

The packaging process of the MEMS devices requires the highest cost concerning other fabrication processes of MEMS [5]. In addition, packaging presents some of the most significant challenges in MEMS production since the package must sustain the atmospheric conditions it was manufactured in (such as vacuum or depressurized inert gas), keep its robust structure for the stability of the entire device, have hermeticity with high bond integrity and significant thermal resistance. Furthermore, used packaging materials must be compatible with other parts of the MEMS devices. Concerning these, some crucial parameters must be taken into account for the packaging system, such as the selection of proper metal candidates, combinability of selected metals for obtaining robust, hermetic, and thermal resistance, deposition

techniques of these metals, and diffusion phenomenon of these metals between them [6].

Furthermore, as the complexity of the MEMS devices is increasing concerning developed fabrication technologies and increased demands for properties of MEMS devices, the required conditions for packaging MEMS are getting more compelling. For providing all these conditions with sustaining compatibility of the package with MEMS devices, new material systems or production methods should be considered to enhance these properties. For this purpose, in this study, a combinatorial metal deposition approach was tried to optimize the composition amount for the candidate metal system, which is Gold-Indium (Au-In) Transient Liquid Phase (TLP) system for this study. Furthermore, to enhance the properties of the packaging of MEMS, a novel Gold-Indium-Tin (Au-In-Sn) ternary metallic system was studied with the addition of In to the eutectic Au-Sn system, which provides the combination of TLP and eutectic bonding techniques for Wafer Level Packaging (WLP) of MEMS devices.

1.2 MEMS Packaging Systems and Requirements

After the production of MEMS devices, packaging may be obligatory for some of these devices. Moreover, since packaging these devices requires extra process steps just after the fabrication of devices, compatibility of packaging steps to the main MEMS device is one of the most crucial parameters. This compatibility may be changed concerning MEMS device type and required conditions because packaging processes were planned concerning these requirements.

First, the vacuum inside the packaged MEMS is one of the essential required parameters for some MEMS devices to work properly. While the working conditions of some devices can be optimized with an inert or controlled gas atmosphere, for some systems, a certain vacuum level has to be reached with proper encapsulation. Required vacuum or pressure of required gas inside the package change concerning

the working mechanism or principle of the manufactured MEMS device. Table 1.1 shows the needed pressure values for some MEMS devices [7].

Table 1.1 Required Pressure Values for Working of some MEMS Devices [7]

Sensor	Working Pressure
Accelerometer	300-700 mbar
Resonator	10^{-1}-10^{-4} mbar
Gyroscope	10^{-1}-10^{-4} mbar
RF switch	10^{-1}-10^{-4} mbar
Microbolometers	$<10^{-4}$ mbar

As seen from Table 1.1, required pressure values vary with the device type. Regarding other MEMS devices, the microbolometers' working pressure, which was studied in this thesis to encapsulate, has relatively lower values.

Microbolometer system is the one type of infrared imaging sensor in the subgroup of uncooled infrared detectors. A schematic representation of the microbolometer structure is shown in Figure 1.2 [8].

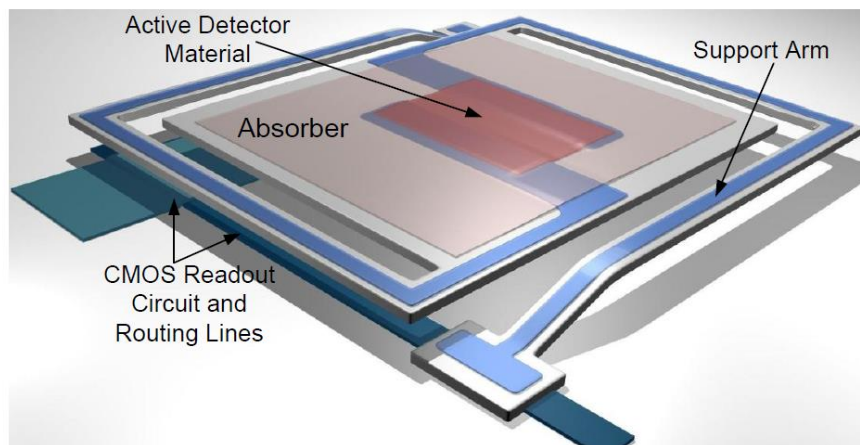

Figure 1.2 Schematic Representation of Microbolometer Structure [8].

In microbolometers, when Infrared Radiation (IR) comes from the outside environment, this IR is absorbed by the absorber of the microbolometer. This causes heating of the active detector material and, with respect to that, resistivity changes. This resistivity change due to temperature change is read by a CMOS-based ROIC system. Therefore, besides the importance of some parameters like low coefficient of thermal resistivity (TCR) value for active material, low thermal conductance but high electrical conductivity of support arms, and high vacuum level inside the package for preventing any heat flow with convection is another critical parameter [8]. Since microbolometers have suspended structures, as shown in Figure 1.2, thermal isolation caused by any conduction between the active part and CMOS can be satisfied in these ways. Nevertheless, any possible heat transfer via convection is directly related to the number of gas molecules inside the package, which is associated with the quality of the package system. Furthermore, heat transfer from the device to any gas trapped inside the package can also affect the proper working of the microbolometer. Possible heat transfer mechanisms of microbolometers are schematized in Figure 1.3 [9].

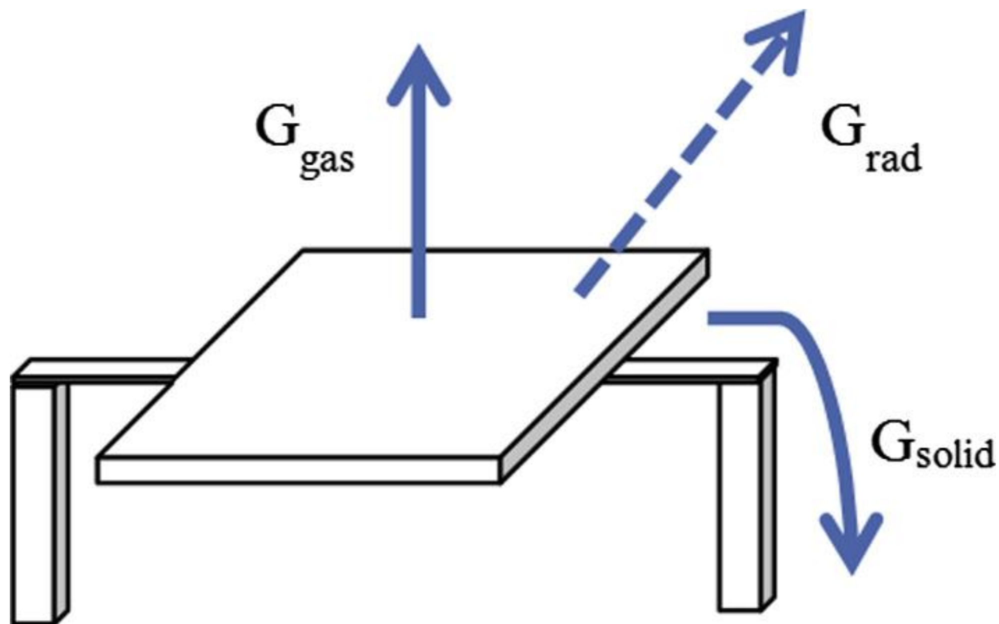

Figure 1.3 Heat Transfer Mechanisms of Microbolometer Systems [9]

With simulations, testing the singular microbolometer or directly observing the Infrared Focal Plane Array (IRFPA) system, which is sequentially placed in many individual microbolometer pixel systems, the pressure effect on sensor output efficiency can be measured just as shown in Figure 1.4 [9].

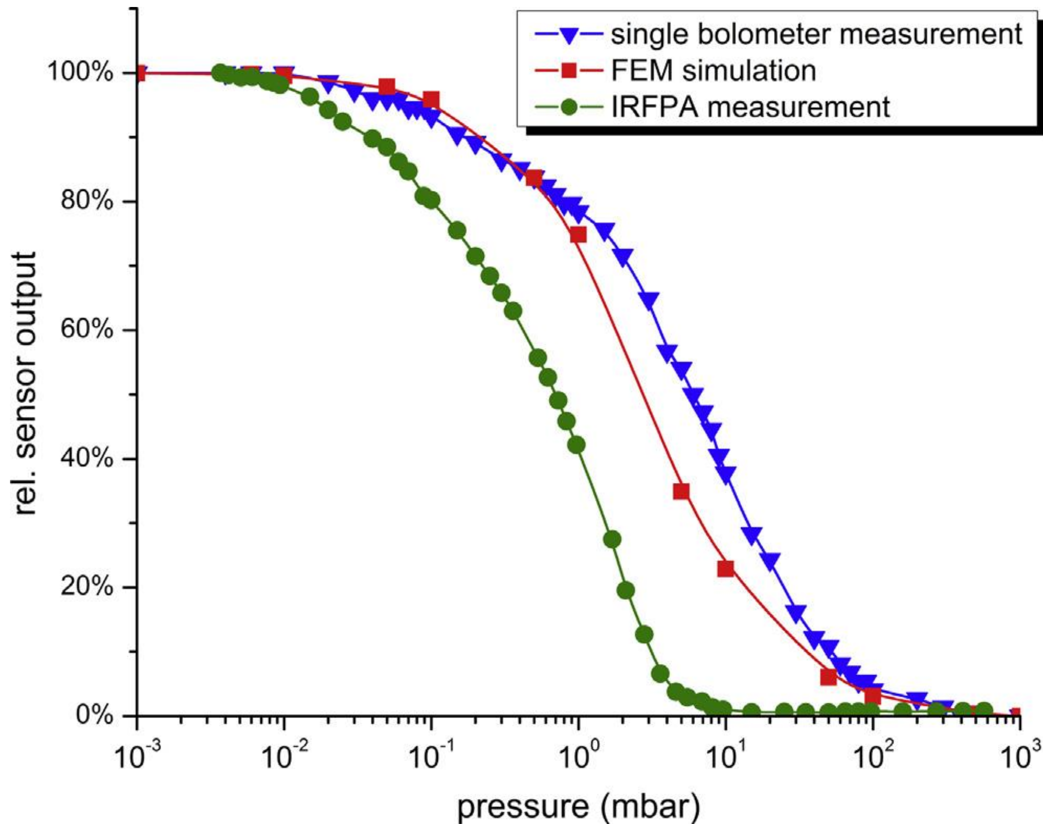

Figure 1.4 Microbolometer Efficiency with respect to Pressure Value Inside the Package [9]

As seen from Figure 1.4, the vacuum environment inside the package of the microbolometer system is critical for the yield of the device since the pressure amount inside the package effect some parameters like Noise Equivalent Temperature Difference (NETD) and Thermal Conductance values that directly image quality of these detectors [10], [11]. For that reason, for the efficient working condition of microbolometers, the pressure inside the package must be below at least 10 mTorr.

Therefore, hermeticity, the quantitative calculable value of permeability of the package system against gas or liquid penetration, is an essential parameter for this device system. Thus, the candidate material system for WLP should have a voidless structure to eliminate penetration of any liquid or gas flow inside and outside the package. This situation can be measured with some characterization techniques like the He Leak Test, which is standardized with Military Standards concerning package volume, or Cap Deflection Test [12], [13], [14].

Another vital criterion is obtaining the stage of this pressure level during the fabrication of microbolometers. For this purpose, before the cap and substrate wafer was encapsulated, getter material, a gas absorber, inside the package to provide the required vacuum level was deposited. Since Titanium (Ti) is one of the most used getter materials, the getter activation temperature of Ti should be considered as a temperature resistance level of the candidate packaging material system. Since Ti getter activation is applied around 400 °C and about 15 minutes which is lower than the CMOS maximum temperature allowance, which is 450 °C, package material must be withstood against 400 °C for the Ti case [15]. If any liquefication, extra void formation, or dimensional change exists during the thermal treatment stage of getter activation at the package system, hermeticity, bond integrity, or robustness will be lost for the device system, which can cause failure to work. The getter activation temperature can vary with respect to the selected material type as the getter. In general, reactive metals that gas absorbing efficiency high materials are selected as getters generally like Ti, Zr, or V [16]. Lower getter activation temperature values can be obtained with respect to that; however, in any case, the getter should satisfy the required vacuum level for the encapsulated system.

Mechanical integrity is another required parameter for packaged MEMS devices. This parameter is standardized under the military microelectronics standard MIL-STD 883. Due to that standardization, MEMS packages should stand at least 6 MPa shear stress [12]. After the dicing operation of the WLP system, the shear strength value of each die can be measured quantitatively with the die-level shear test characterization technique.

To conclude, the requirements of the package system of the MEMS devices, hermeticity, standing against a certain degree of temperature, and passing the limit of the specific shear strength value are essential parameters that provide proper working conditions for specific MEMS devices. Two main approaches are applied to encapsulating MEMS devices to obtain these parameters: die-level packaging and wafer-level packaging (WLP) methods.

1.2.1 Die Level Packaging

Die (also known as device or chip) level packaging is one of the methods for encapsulating MEMS devices. Before the packaging procedure, the device wafer is diced; therefore, identical devices are obtained at the chip level. Later, to eliminate the excessive polymer structure placed on the MEMS device as a sacrificial layer or protective layer against dicing, die-level devices are placed on a chip placer which can be required to set the system to a Printed Circuit Board (PCB). Afterward, both diced chip level device and the pre-prepared metal or ceramic package are aligned and encapsulated in a vacuum environment. Lastly, the entire system has placed the PCB. A schematic representation of die-level packaging is shown in Figure 1.5 [17].

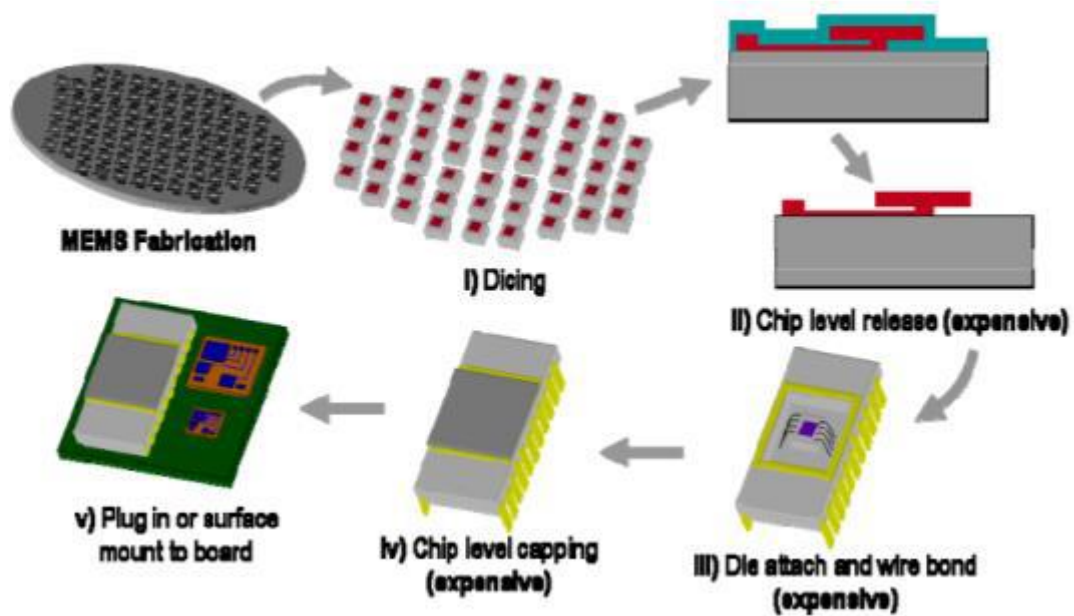

Figure 1.5 Schematic Representation of Die Level Packaging [17]

As seen in Figure 1.5, each die-level device has to be processed individually for packaging operation inherently. Since the packaging operation is done for each die separately, it can vary in obtaining identical properties for each die, and this may cause a negative effect on total yield. Moreover, this situation causes high time and labor energy consumption. Therefore, die-level packaging has become a relatively expensive procedure for MEMS encapsulation operation. Since the packaging cost of MEMS devices is around 70% of the total manufacturing cost, expense during this type of packaging has a considerable effect [5].

1.2.2 Wafer Level Packaging (WLP) and Methods

Wafer Level Packaging (WLP) is another packaging method that provides encapsulation before the dicing operation of the device wafer. Except for the thin film deposition bonding technique, which is a method that includes encapsulation with thin film layers onto the device at the wafer level, other WLP techniques provide encapsulation with the usage of a cap wafer. After the production and release stages of the device are completed at the wafer level, the cap wafer, which has the

same dimension as the device wafer, is bonded with each other. Therefore, all devices are encapsulated at the same time. Since the dicing process is applied after the bonding operation of wafers, diced devices can be directly ready to be placed on the PCB. A schematic representation of the WLP procedure is shown in Figure 1.6 [17].

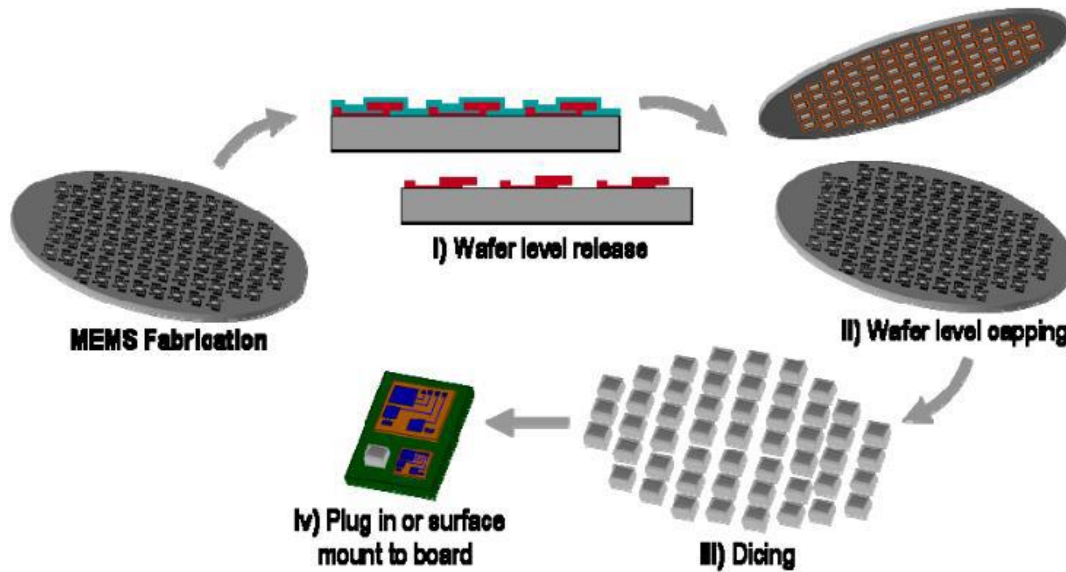

Figure 1.6 Schematic Representation of Wafer Level Packaging (WLP) [17]

Since packaging is done before the dicing operation with this method, the package can protect the device against any harmful effect of the dicing operation, such as mechanical vibration or shock effect. These can be beneficial for obtaining the final product efficiently. Furthermore, as all processes are done at the wafer level instead of the individual approach, just like at the die-level case, the equivalency of each device is increased, which can provide an increased yield of the final product. Moreover, since there is no requirement for individual packaging operation for each die, this situation offers less time consumption and labor work, satisfying a significant decrease in the cost. Several WLP methods exist in that the literature and package material type, required cap wafer type, or applied process parameters can vary with respect to the selected method.

1.2.2.1 Anodic Bonding

Anodic bonding (also called assisted bonding or electrostatic sealing) is one of the packaging methods that does not require any bonding material. However, some requirements exist in this method, such as only a pyrex glass wafer that contains Na inside can be bonded with Si wafers. During the appliance of voltage and temperature, diffusion of these Na atoms happens inside the glass wafer; oxygen atoms bond with the Si wafer and create a SiO_2 layer, which provides strong bonding. For instance, hermetic wafer-level vacuum packaged MEMS resonant-based temperature sensors were obtained with anodic bonding method at METU-MEMS Research Center [18]. However, since no usage of the intermediate bonding layer, surface roughness tolerance is very low (nanometer scale) [19]. A schematic representation of the anodic bonding process is shown in Figure 1.7 [20].

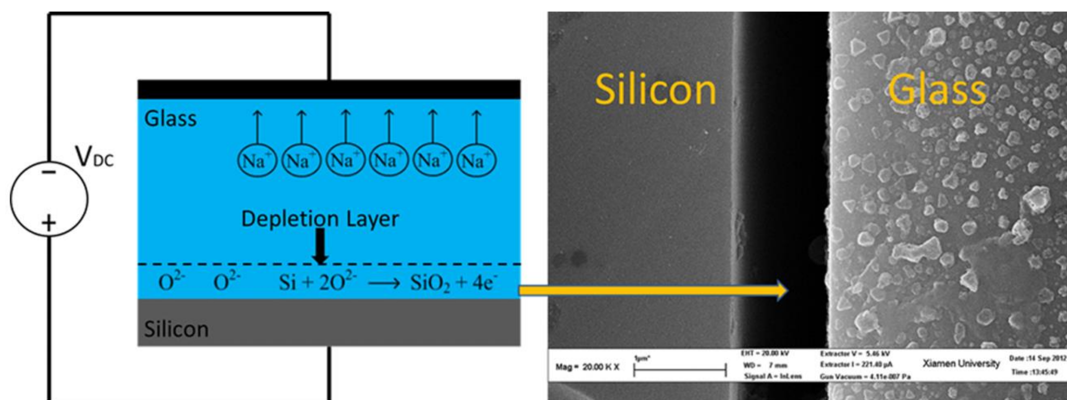

Figure 1.7 Schematic Representation of Anodic Bonding with Scanning Electron Microscope (SEM) Image [20]

1.2.2.2 Fusion Bonding

Fusion bonding is another direct bonding method that means an intermediate bonding layer is not required, just like anodic bonding; however, fusion bonding has more variety on wafer type than anodic bonding's requirement to pyrex glass. The bonding mechanism is similar to anodic bonding in the chemical kind of view.

Before bonding, the wafers' surfaces must be activated to obtain a hermetic and robust bond. High temperatures might be required in conventional fusion bonding, like approximately 1000 °C for Silicon (Si) – Si wafer bonding [21]. Process temperature for this bonding type can be decreased with surface preparation methods with wet or dry activation processes [22]. For instance, around 300 °C, two wafers with Si_3N_4 passivation layers on their surface were bonded with that method [23]. Nevertheless, for hermetic bonding with this method, the surface of the bonding area of wafer couples must be extremely smooth so that roughness tolerance must be below 2-3 nanometer (nm) level for successful bonding [24].

1.2.2.3 Thermocompression Bonding

In the thermocompression bonding method, the bonded wafer stack has the same intermediate bonding metal type. Furthermore, this bonding method does not require liquidation of that bonding metal, which means bonding occurs at a solid state in this bonding type. Thus, temperature generally preferred around 400 °C and pressure with respect to selected temperature are two main parameters for this method. Generally, compatible metals for MEMS devices like Au, Al, or Cu are preferred for this method as the bonding material. Since no liquid formation exists in this method, high surface smoothness is required in thermocompression bonding to obtain a hermetic structure [25].

1.2.2.4 Glass Frit Bonding

In glass frit bonding, pre-prepared paste that contains low melting point glass is used as the bonding material. With the help of temperature and pressure, this paste can provide strong and hermetic bonding for WLP. During the bonding procedure, the paste becomes softened; hence this bonding material can tolerate surface roughness during the bonding operation. After bonding, the softened paste becomes glass-like due to cooling; thus, the rigid structure is obtained after WLP. The screen printing

method spreads this paste across the patterned wafer. A temperature of around 400-450 °C is required to soften the paste. For instance, with optimized bonding parameters for the selected glass-frit paste, a shear strength of up to 45 MPa has been achieved for the package at METU-MEMS Research Center [26]. Still, since lead (Pb) is generally used to decrease paste softening temperature and Pb count is a hazardous metal type for the environment since it is toxic, this type of glass frit can be problematic for applications. Furthermore, even though most of the glass frit paste is nonconductive, with the addition of silver particles into glass frit, acquiring conductive glass frit material could be possible, which can be beneficial for vertical feedthroughs for some MEMS device type package [27] - [28]. The process cycle with bonding conditions of glass frit is shown in Figure 1.8.

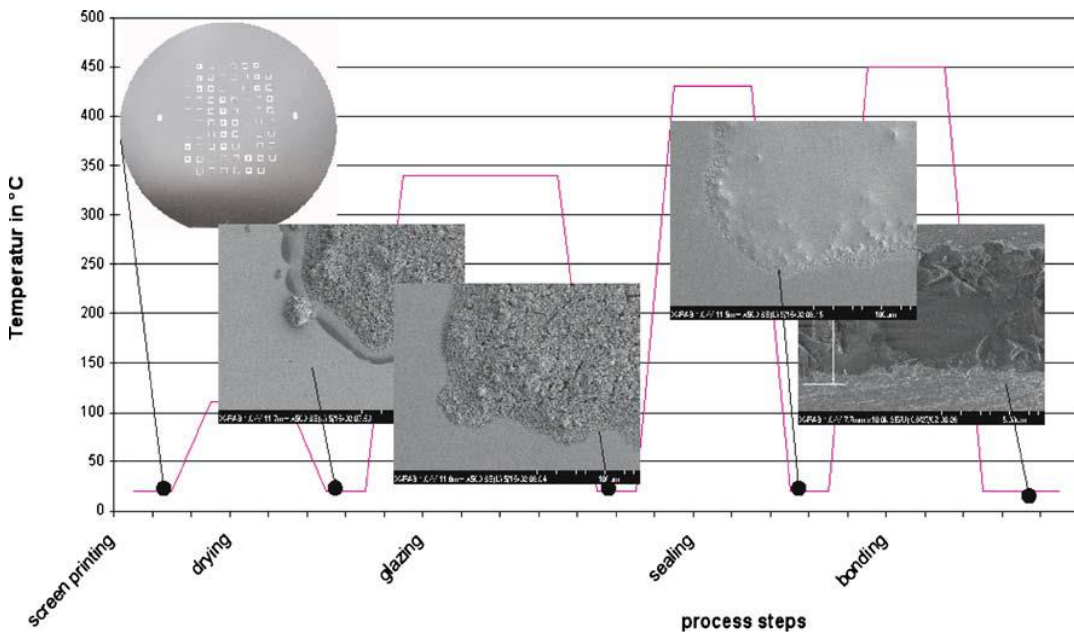

Figure 1.8 Schematic Representation of Glass Frit Bonding with Phase Changes and SEM Images [27]

1.2.2.5 Eutectic and Transient Liquid Phase (TLP) Bonding

Both eutectic and Transient Liquid Phase (TLP) (also known as Solid Liquid Interdiffusion (SLID) Bonding) combination of the metal stack or alloy type of intermediate bond material is used to obtain WLP. Since liquid formation exists in

both systems during bonding, high surface topology tolerance is achieved along the bond area. Furthermore, with respect to the wide variety for selecting a candidate metal stack for this type of bonding, high bonding temperature variance can be achieved in both methods. Moreover, metal systems generally have better hermeticity properties concerning other material types, which is beneficial to protect the package's vacuum or inert gas state environment. The estimated hermeticity properties of materials with respect to time as a function of thickness are shown in Figure 1.9 [29]. Due to all of the advantages of these methods, the Eutectic and TLP bonding methods are the most commonly used methods for WLP.

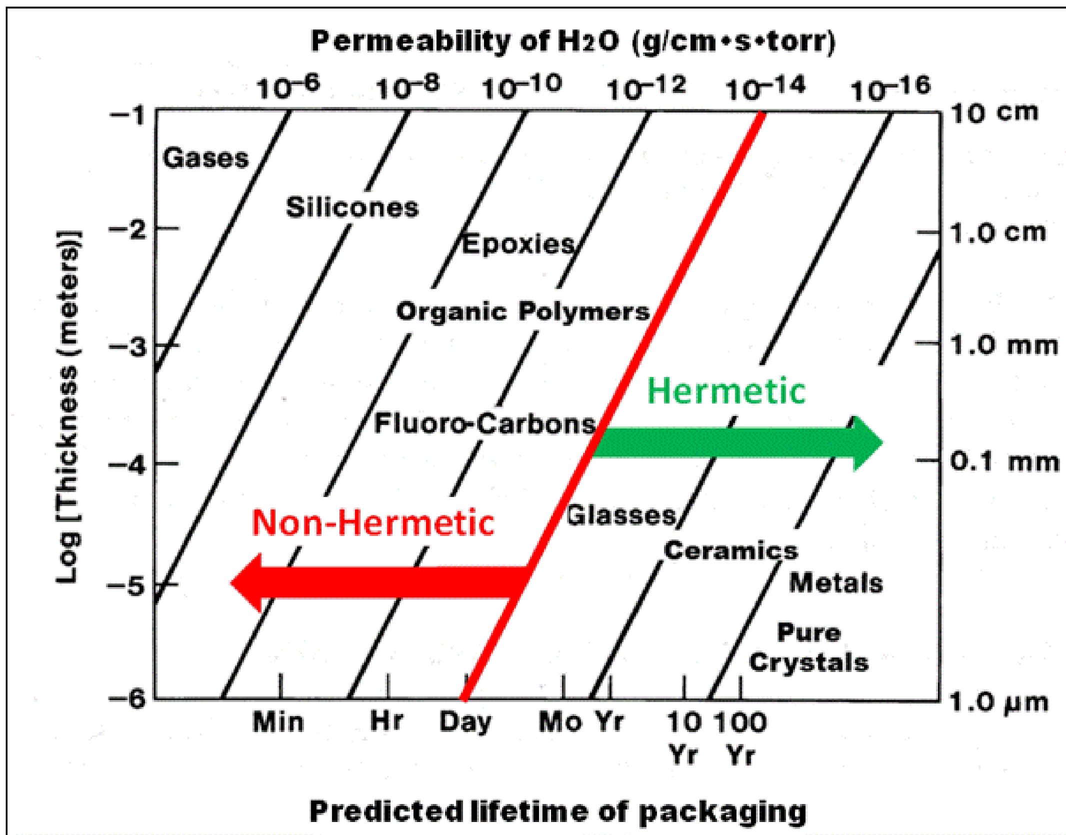

Figure 1.9 Estimation of Hermetic Properties of Different Material Types with respect to Time as a function of Thickness [29]

In the eutectic bonding method, candidate metal materials are deposited in specific thickness values to reach eutectic composition, which is the exact composition for the formation of only pure liquid phase above the eutectic temperature constant

temperature between liquefaction and solidification of the two-phase stack. In this bonding technique, metal candidates can be deposited to the bonding area layer by layer or as a eutectic alloy mixture with exact eutectic composition. In the layer-by-layer case, as temperature increases during the process, solid-state diffusion between candidate metals is occurred to reach eutectic temperature. After the eutectic temperature, liquid formation with respect to time provides a liquid phase with exact eutectic composition [30]. In the eutectic mixture case, which can be pre-prepared before the deposition process with an arc melting-like technique, a direct liquid phase can be obtained upon passing the eutectic temperature [31]. In both cases, liquid formation exists at eutectic composition, and after cooling, a solid, complete eutectic structure is obtained, which provides sealing. A representative phase diagram for eutectic bonding is shown in Figure 1.10.

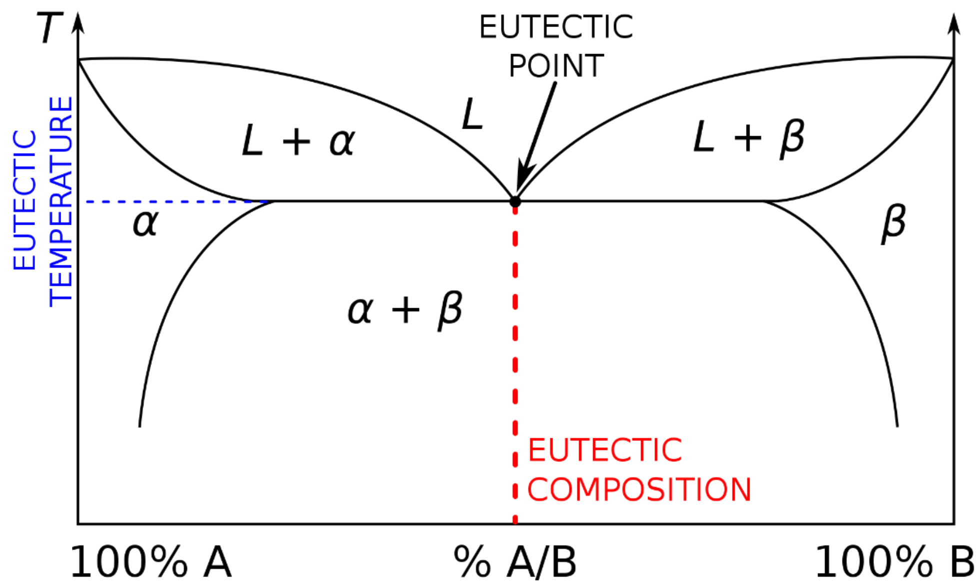

Figure 1.10 Schematic Representation of Eutectic Phase Diagram

There are several candidate binary eutectic cases that exist in literature. There is also possible that the usage of the ternary mixture to obtain eutectic bonding. With respect to the selected metal type, eutectic temperature varies. Since the maximum temperature durability of the eutectic bonding system is eutectic temperature because liquefication is started at that temperature even after bonding, the selected eutectic

stack should withstand the getter activation process, which requires a specific temperature with respect to the getter type. For instance, since Ti getter activation needs 400 °C, the eutectic stack must stand against that temperature during the process. Some metal combinations for eutectic bonding used in literature and industry are generally shown in Table 1.2 [32].

Table 1.2 Examples of Eutectic Metal Combinations with Eutectic Temperature Values [32]

Material System	Eutectic Temperature (°C)
Au – Sn	280
Au – Si	380
Au – Ge	380
Al – Ge	420

As shown in Table 1.2, Aluminium – Germanium (Al-Ge) stacks bonding temperature can provide requirements for both durabilities against Ti getter activation and harmlessness against CMOS stability. Additionally, since the Al-Ge stack can provide adhesion without any additional adhesion layer, that offers no necessity for an extra adhesion layer deposition step on the CMOS wafer. Therefore, bonding metal deposition only cap wafer is enough to complete WLP at the Al-Ge system [31].

Transient Liquid Phase Bonding (TLP), also known as Solid Liquid Interdiffusion Bonding (SLID), is based on two types of bonding material. While one stack has a high melting point, the other is metal with a low melting point with respect to the other. During the deposition procedure, a metal with a low melting point is placed just at the center of the bonding area, which means the upmost part of the cap or substrate wafer to complete the bonding operation. For this bonding system, two wafers can be coated symmetric or asymmetric with candidate metals; nevertheless, the amount of composition shall be satisfied concerning pre-settled thickness values. Instead of eutectic bonding that requires a specific composition of candidate metals,

in TLP, a varied composition range can be used because the formation of the Intermetallic Phase (IMC) or alloy plays quite a role in successful bonding. In TLP bonding, metal with a low melting point liquefies during heating. As this situation increases the diffusion phenomenon between candidate metals and provides sticking of metals in each other, the formation of alloy or IMCs between the candidate interface starts. When the consumption of the low melting metal is completed, the entire bonding area is transformed into a new formatted phase, which means complete alloy or IMC formation is obtained [33]. A schematic representation of TLP bonding with stages is shown in Figure 1.11 [34].

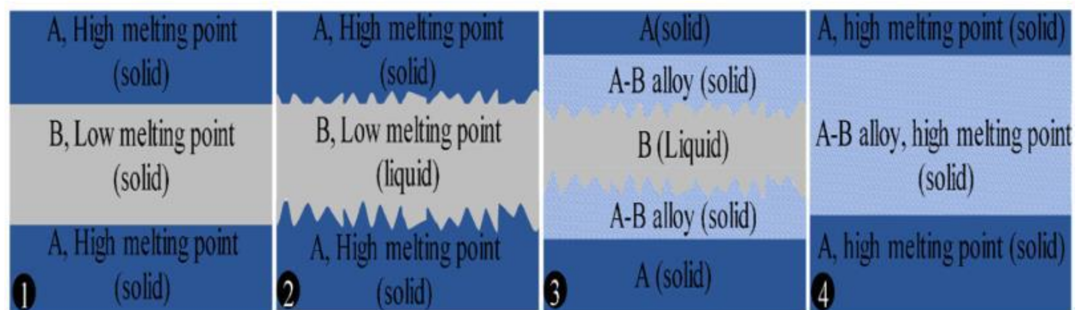

Figure 1.11 Schematic Representation of TLP Bonding with Stages [34]

Furthermore, to demonstrate the TLP mechanism on phase diagram, the phase diagram of the Au-In system which generally used for that purpose is shown in Figure 1.12 with respect to TLP stages which is shown in Figure 1.11 [35].

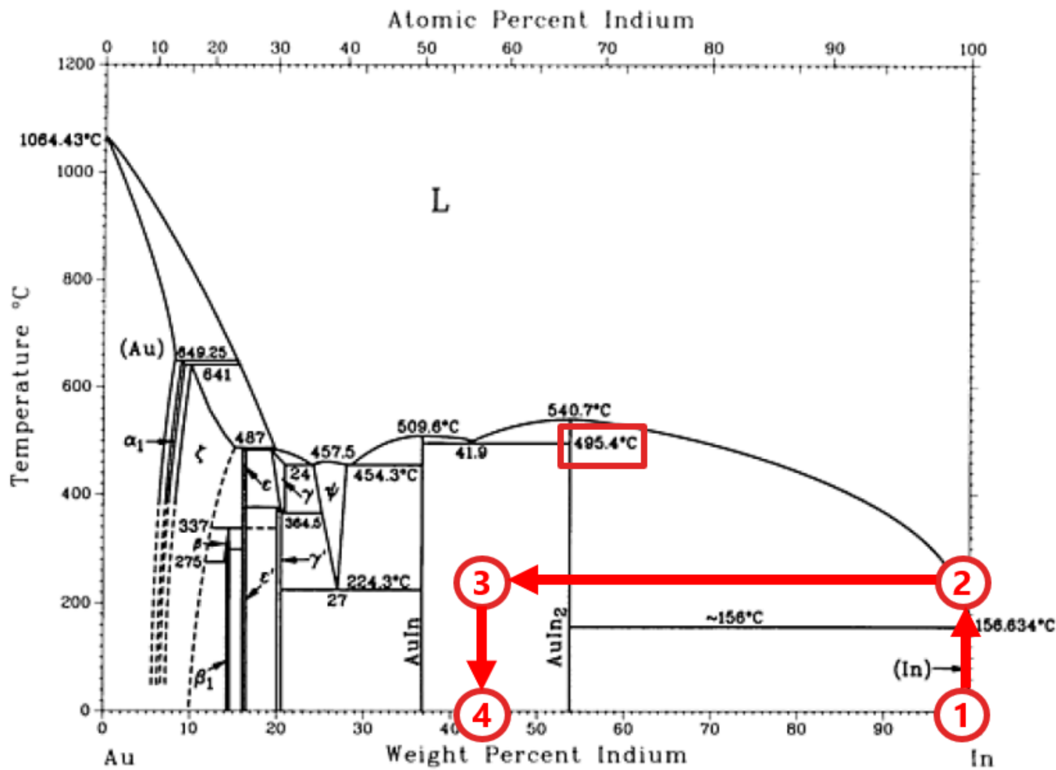

Figure 1.12 Phase Diagram of Au-In System to Demonstrate TLP Bonding with Stages [35]

As seen from Figures 1.11 and 1.12, new generated phase from candidate TLP materials has a higher melting point with respect to interbonding metal with a low melting point. That means with a low bonding temperature of just enough to pass the melting point of the low melting point candidate, a high-standing new bonded structure can be generated, which stands up to the melting point of the generated new phase. For example, for the Au-In system shown in Figure 1.12, exceeding the melting temperature of In is sufficient to initiate the TLP bonding process. During the process, Au and In start to diffuse between each other, and with respect to that, AuIn and $AuIn_2$ phases are started to formatted. When the TLP process is completed, since consumption of Au and In is completed to form new IMCs, AuIn, and $AuIn_2$, the new system can stand temperature up to 495 °C approximately. Just like Au-In binary metal stack, other metal candidates can be used for the TLP process. With respect to that, some materials system that can be used for TLP bonding is shown in Table 1.3 [33].

Table 1.3 Candidate Metal Stacks for TLP Bonding with Bonding Process Parameters and Remelting Temperature Values [33]

Material System	Process Time and Temp.	Re-melt Temp.
Copper-Indium	4 min at 180 °C	> 307 °C
Copper-Tin	4 min at 280 °C	> 415 °C
Silver-Tin	60 min at 250 °C	> 600 °C
Silver-Indium	120 min at 175 °C	> 880 °C
Gold-Tin	15 min at 260 °C	> 278 °C
Gold-Indium	0.5 min at 200 °C	> 495 °C
Nickel-Tin	6 min at 300 °C	> 400 °C

As seen from Table 1.3, Indium (In) and Tin (Sn) are the most commonly used metal candidates for low melting temperature because of their low melting temperature value and high diffusive property. In every material stack, while low bonding temperatures were used, new generated phase with TLP can stand higher temperatures with respect to bonding temperature.

While the most significant advantage of the TLP bonding method is obtaining high re-melting properties with a relatively low-temperature bonding process, some possible drawbacks exist in that system. First, since two different metal types are used in that method, different diffusion rates exist in the system, which means an increment in the probability of the formation of Kirkendall Voids during the process that may cause a decrease in hermeticity and bond integrity for packaging [36]. Secondly, since most IMCs have inherently brittle properties, this can cause breakage during dicing operation [37]. Third, the number of possible IMCs can play a critical role in package properties. For instance, even though the Au-In system has a noncomplex phase diagram, the ratio between AuIn and $AuIn_2$ has a critical role.

1.3 Combinatorial Deposition Method

Since package and bonding quality are directly related to the composition ratio of metal systems used for bonding, this parameter must be optimized for enhanced properties. For this purpose, different compositions are investigated by trying many experiments that cause lots of time, material, and energy consumption. With the combinatorial deposition method, which provides a continuous compositional gradient along the substrate, the effect of different compositions on packaging and bonding can be investigated with fewer experiments. Even combinatorial composition variety can be obtained for discrete substrates, and compositional gradient along the same sample can also be achieved with a single deposition [38]. Schematic representation of the combinatorial deposition approach is shown in Figure 1.13 and Figure 1.14 to visualize this event [39], [40].

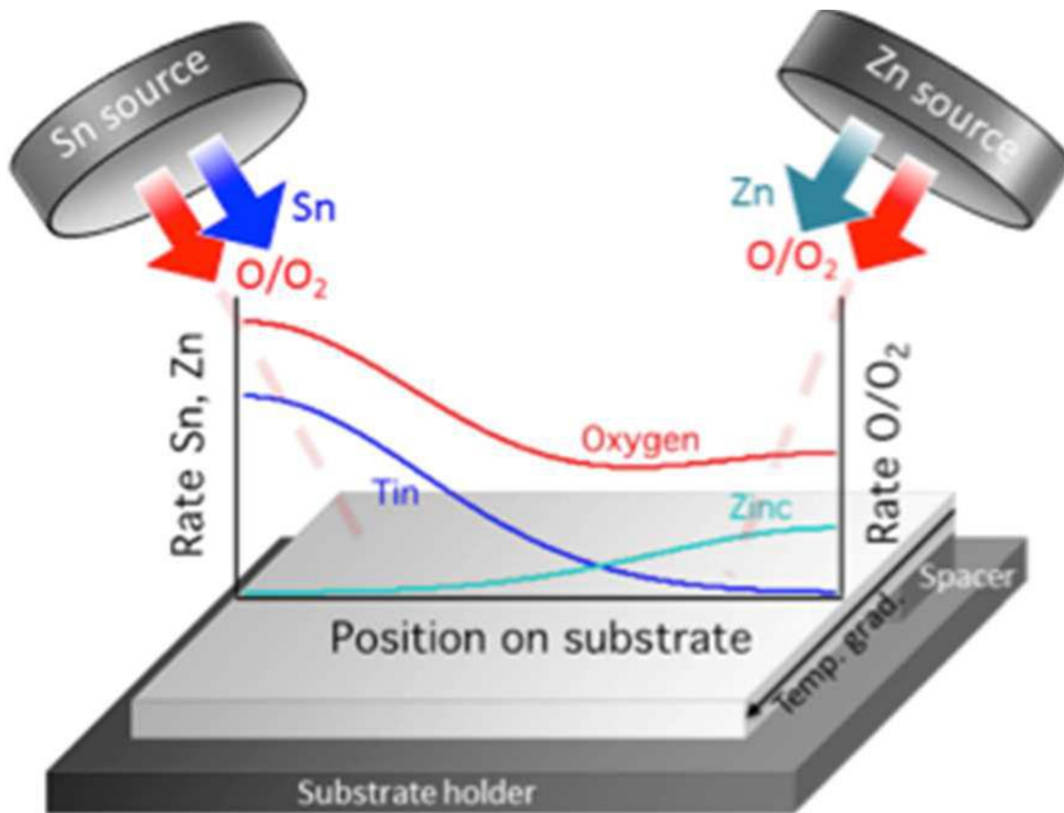

Figure 1.13 Example of Combinatorial Deposition Method [39]

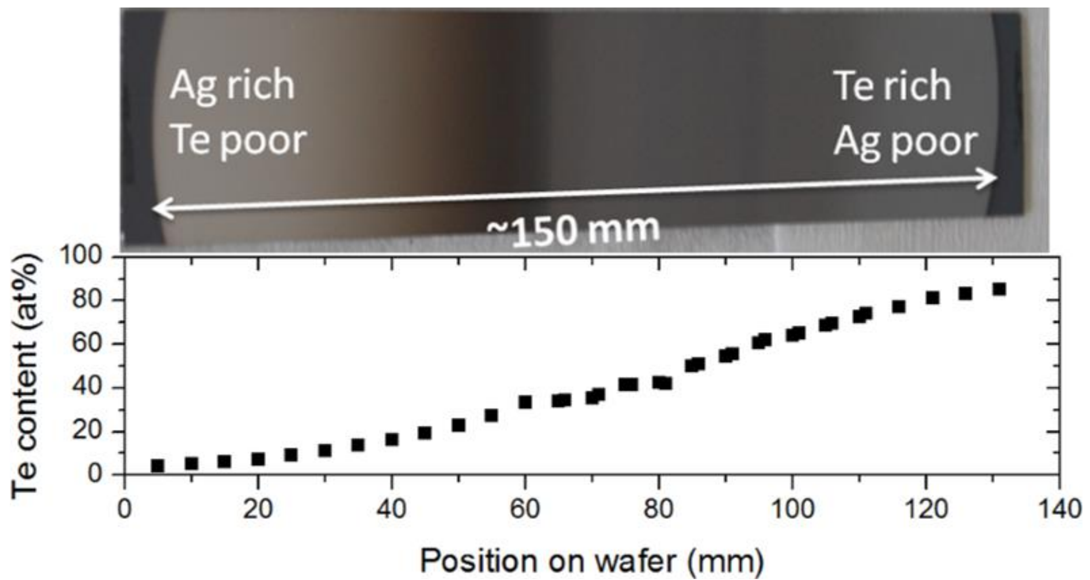

Figure 1.14 Combinatorial Deposition Method with Varied Composition Across Substrate [40]

As seen in Figure 1.13 and Figure 1.14, a composition gradient can be achieved along the entire substrate. This can provide different mechanical, chemical, or optical properties at various locations on a single substrate. Thus, with characterization and testing procedures, the composition that gives the best property for the selected application can be detected thanks to that method.

1.4 Ternary Material System Approach

In eutectic and TLP bonding approaches, binary metal systems that include two different metal types are generally used, as shown in Tables 1.2 and 1.3. Ternary systems have three different material system different with respect to each other. With ternary system usage, from bonding process parameters to obtained properties from the package can be varied. This situation requires new metallurgical approaches since ternary systems are more complicated concerning binary systems. Nevertheless, the aim of adding the additional metal candidate to the selected binary system is to improve the package quality, such as obtaining a more robust structure, higher temperature resistance, or decreasing bonding temperature and time, which is

beneficial for manufacturing. Furthermore, with that approach, TLP and eutectic bonding methods can be combined to improve properties. For instance, with Copper-Tin-Indium (Cu-Sn-In) ternary system, the WLP process was done successfully, and 30 MPa mechanical strength was obtained at 150 °C, which is a relatively low bonding temperature [41].

1.5 Objective and Outline of Thesis

In this thesis, the main aim is to improve the properties of the WLP system, which are obtaining robustness of the package and providing hermeticity level according to military standards, which is MIL-STD 883, and to optimize servicing temperature that shall provide standing against Ti getter activation temperature which is 400 °C while not passing bonding temperature that can be harmful to CMOS structure. For this purpose, to obtain the best composition ratio for superior properties of the packaging system, the combinatorial approach investigated the on Au-In system with varying thicknesses with one or two trials instead of the requirement of many trials. Furthermore, besides the Au-In system, Au-In-Sn ternary system that was not researched before in the literature for WLP was investigated to obtain a more robust, rigid, and hermetic structure with improving properties of the WLP system. With that ternary system, the main aim is combining the eutectic Au-Sn system with TLP candidate In material to enhance the properties of the packaging system with a combination of eutectic and TLP bonding techniques. Since this ternary system and combinatorial method did not research before, the obtained results can contribute to the literature for that purpose. The main advantage of the combinatorial approach is that it can also contribute to the optimization of the best composition ratio for metal candidates that can be a new material stack for WLP besides the Au-In structure.

According to the objective of this thesis, the organizational scheme of this work is given below as listed.

In Chapter 1, with a brief explanation of the terminology of the significant terms, general knowledge of packaging of the MEMS systems is tried to be explained.

In Chapter 2, previous studies in the literature and the METU MEMS Research Center, the facility used for this thesis, were reviewed to design the experimental pathway for this thesis.

In Chapter 3, all experimental procedures, from fabrication to characterization, were described in detail.

In Chapter 4, obtained results for combinatorial Au-In trials and new Au-In-Sn ternary systems were discussed in detail.

In Chapter 5, all studies in this thesis were concluded. Moreover, future recommendations were suggested about these topics in this work.

CHAPTER 2

LITERATURE REVIEW

2.1 Au-In TLP Bonding

Attributed to its robust mechanical and hermetic properties, Gold – Indium (Au-In) is one of the most common binary TLP material systems used for WLP. First, this system provides a low bonding temperature with a high re-melting point in a short time with respect to other systems shown in Table 1.3, which gives possible candidate material systems. Second, a low-temperature requirement in this system during bonding can satisfy avoiding the formation of residual stress during bonding, which can be beneficial for package durability against any mechanical effect [42]. The phase diagram of the Au-In system is shown in Figure 2.1 [35].

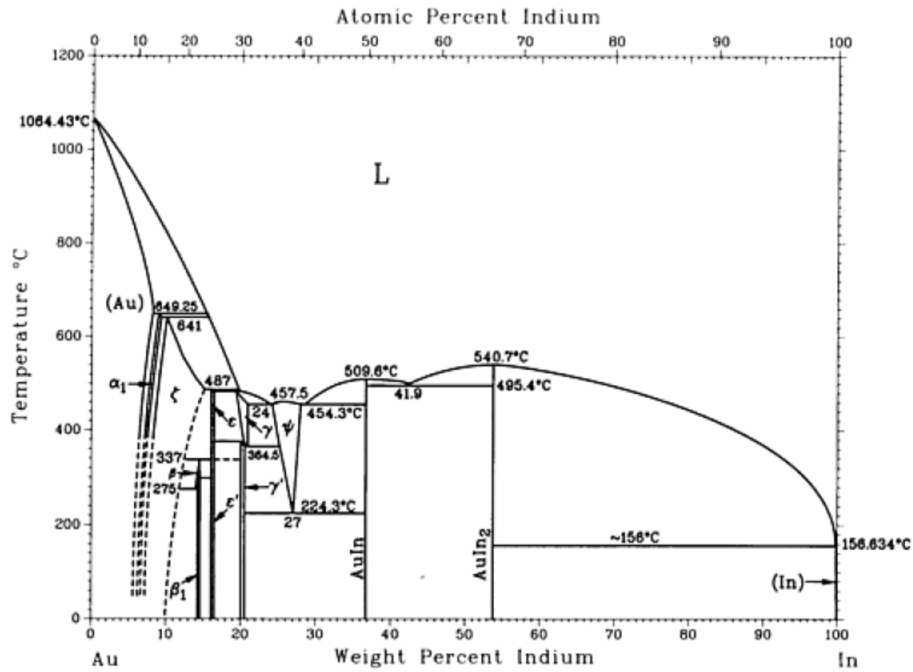

Figure 2.1 Gold-Indium (Au-In) Phase Diagram [35]

With respect to the selection of Indium and Gold content on the TLP system, the main aim is obtaining a homogeneous solid structure across the bonding area at the end of the bonding procedure with superior properties. According to that, reaction stages at this TLP system with change of In distribution are shown in Figure 2.2 schematically [43].

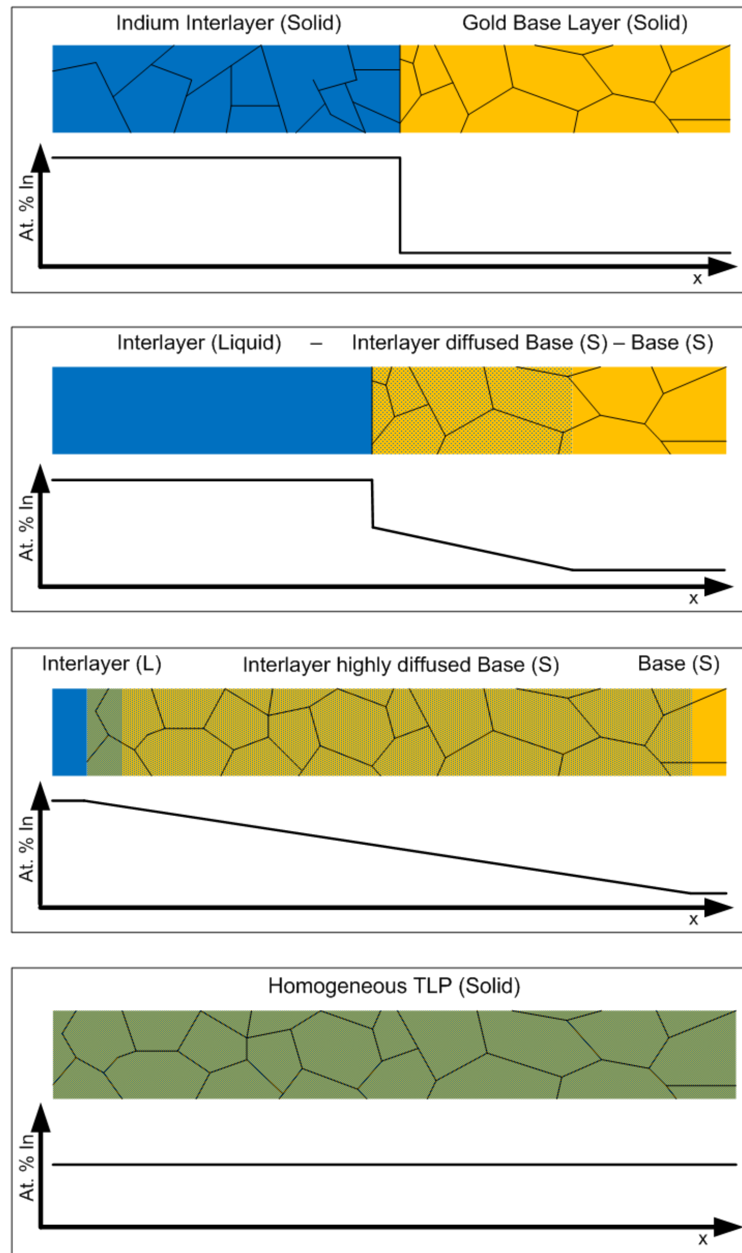

Figure 2.2 Schematic Representation of Au-In TLP Bonding with Stages of Bonding and In Distribution [43]

The bonding process can be applied with desired pressure, temperature, and time parameters based on the selected thickness for Au and In. Moreover, the deposition of these metals can be symmetric or asymmetric to cap and device (or substrate) wafers based on the selected design. Nevertheless, in both cases, this TLP system requires a seed layer that includes an adhesion and diffusion barrier layer to enhance

the sticking of the bonding system to the wafers and prevent diffusion between the wafer and bonding system, respectively. This system shows an example of a WLP system based on Au-In TLP bonding schematically with Scanning Electronic Microscope analysis in Figure 2.3 [44].

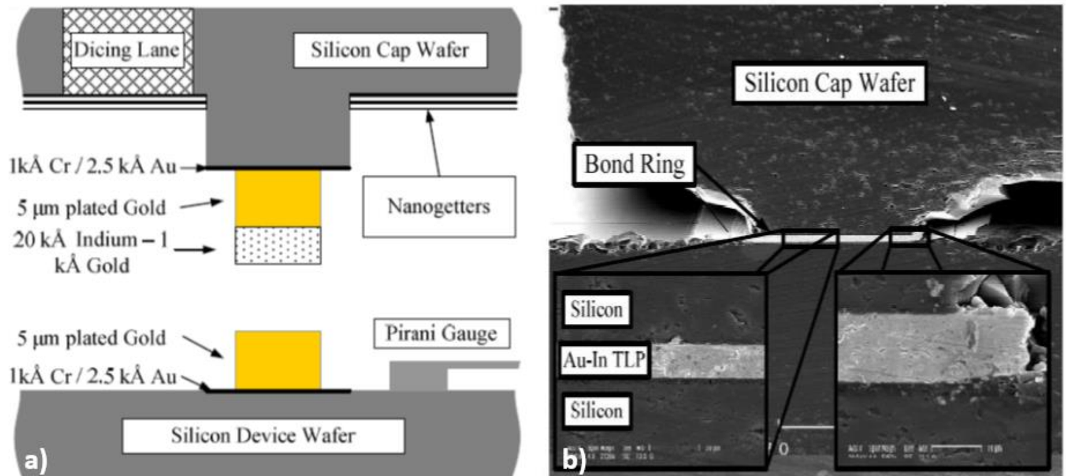

Figure 2.3 a) Schematic Representation of WLP Bonding Procedure with Au-In System Before Bonding, and b) Scanning Electron Microscope (SEM) Image of Cross Section of Bonding System After Bonding [44]

Figure 2.3a shows the asymmetric deposition of Au and In with different thicknesses at the bond ring area in this work. Furthermore, getter placement was done in this system with proper dicing lane design to obtain chip operation after the dicing operation. In Figure 2.3b, the observed SEM image shows that bond integrity was satisfied with this system properly because no void formation was observed. Process parameters and pressure values after the bonding operation for this WLP operation are shown in Figure 2.4 [44].

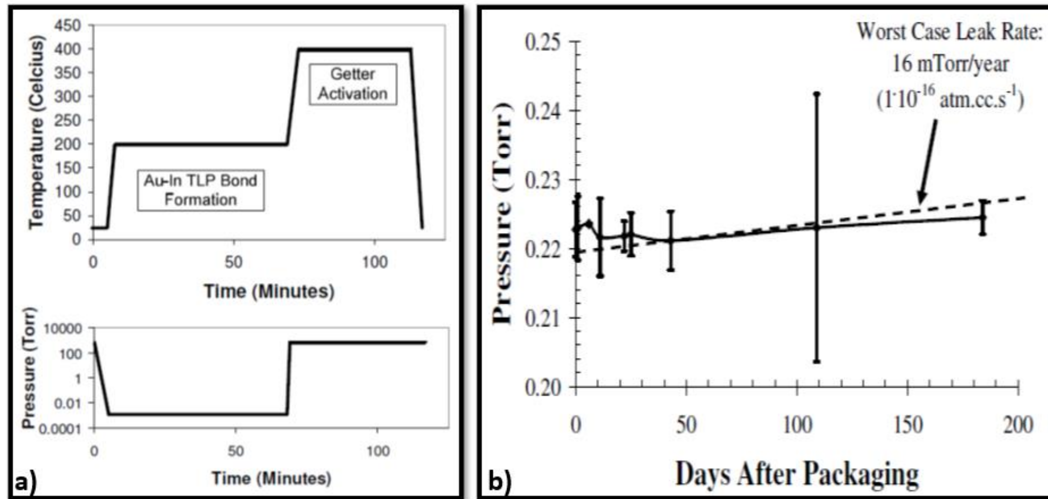

Figure 2.4 a) Temperature and Chamber Pressure Values that Applied during Bonding Operation, and b) Pressure Values Inside the Package after Bonding with respect to Time [44]

As seen in Figure 2.4a and with respect to this article, the bonding operation was completed at 200 °C with 3000 N force at approximately 0.01 Torr chamber pressure for 1 hour. After the bonding operation, for getter activation, the temperature was raised to 400 °C at atmosphere-level chamber pressure for around 40 minutes. As shown in Figure 2.4b, the package leak rate was found as 1.10-16 atm.cc.s^{-1} for 0.15 μL package volume, which is highly sufficient to provide hermeticity for this package.

Furthermore, besides using the Au-In binary system for WLP, this material system can be used as a solder system to obtain joints for other MEMS-based or related systems. For instance, since the Au-In system has a low temperature for bonding operation, avoiding degradation during bonding for many MEMS-based systems can be obtained. Moreover, since this material system provides good conductivity, low resistance values can be achieved, which is advantageous for vertical feedthrough for microelectronics. According to these, this material system can be used for 3D integration, providing multifunctionality for microelectronic products. Schematic representation for the joint solder system based on Au-In binary stack of 3D integration is shown in Figure 2.5 [45].

Figure 2.5 is a diagram with no detected image: a 3rd chip, a 2nd chip and a 1st chip stacked on each other.

Figure 2.5 Schematic Representation of 3D Integrated Microelectronic System which joined with Au-In Binary System [45]

As seen in Figure 2.5, instead of the bond ring system used for WLP, Au-In binary TLP bonding is obtained with the formation of a bump form of In. Therefore, besides the hermeticity property of the selected material system, other parameters such as robustness, thermal durability, and conductivity play a significant role in the same TLP bonding procedures applied. Based on these requirements, different bonding pressures and annealing temperatures that a heat treatment after bonding to aim enhancing properties were tried to investigate the changes in shear strength and electrical properties. The experimental results are shown in Figure 2.6 and Figure 2.7 [45].

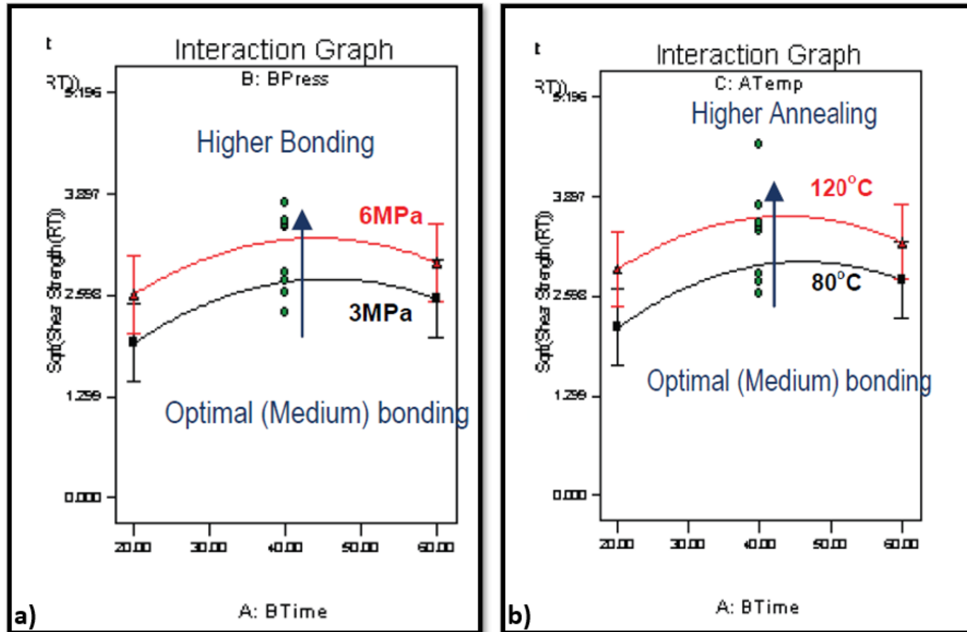

Figure 2.6 a) Shear Strength Change with respect to Bonding Time and Bonding Pressure and b) Shear Strength Change with respect to Bonding Time and Annealing Temperature [45]

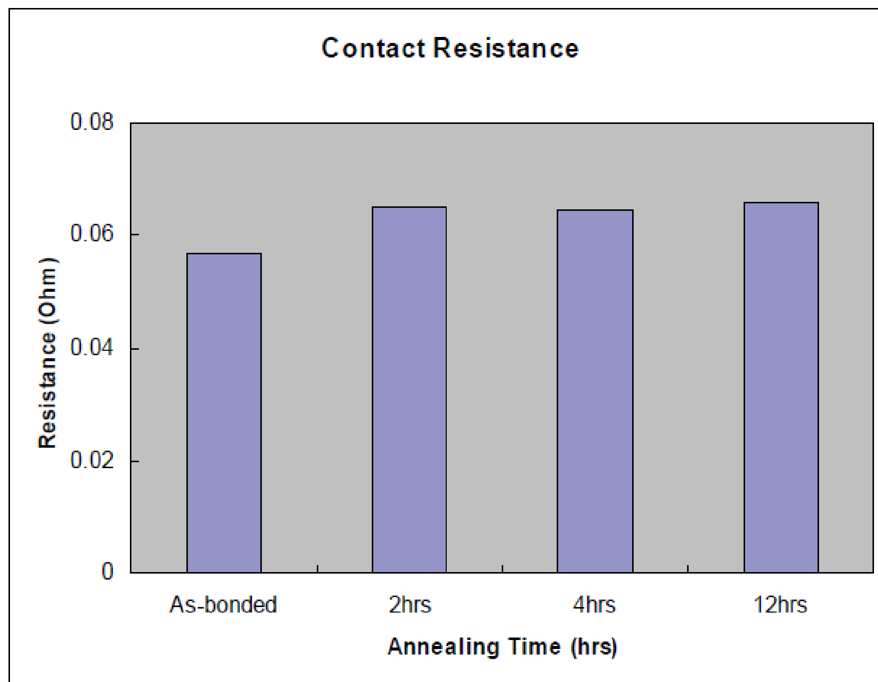

Figure 2.7 Electrical Resistance Change of Au-In Bonding System with respect to Change in the Annealing Time at 120 °C Annealing Temperature [45]

As seen from Figure 2.6 and Figure 2.7, changing process parameters for Au-In binary stack can achieve optimized bonding properties or package with respect to aimed design for the selected system. With respect to these approaches, utilization for bonding parameters of the Au-In system was tried in this thesis with the addition of a combinatorial deposition approach detailed in Chapter 2.3. Furthermore, with respect to literature and previous studies held on METU MEMS Research Center, used Au and In thicknesses are relatively high due to the used thickness values in this thesis. Therefore, decreasing Au and In thickness, values are another aim in this thesis because decreasing thickness can be advantageous in several ways, just like reducing material usage, time during coating, and energy usage at the packaging.

2.2 Au-Sn Eutectic Bonding and Combination with TLP

Gold – Tin (Au-Sn) is one of the most used binary material stacks for eutectic bonding. Even the Au-Sn system is widely used in flip-chip bonding for optoelectronic packaging or microwave due to superior properties like good wettability, adequately low melting point, good yield strength, and corrosion resistance since it has no required flux usage. Besides these advantages, this system is a good candidate for WLP [46]. The phase diagram of the Au-Sn system is shown in Figure 2.8 [35].

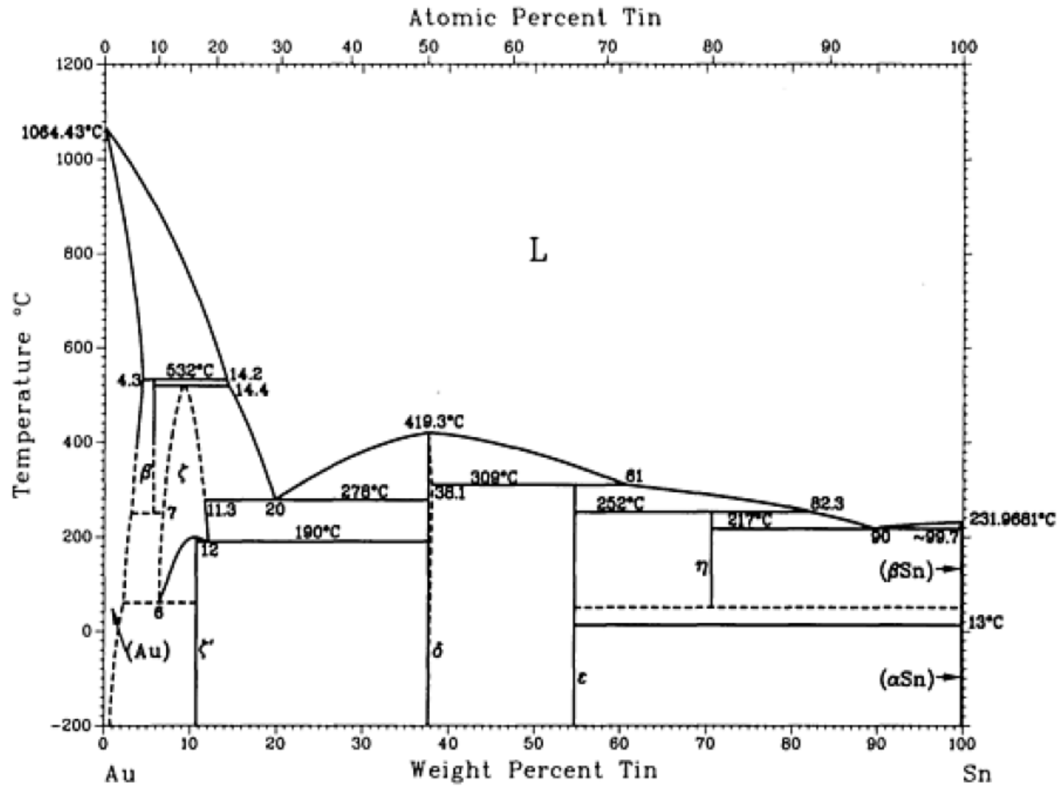

Figure 2.8 Gold-Tin (Au-Sn) Phase Diagram [35]

Figure 2.8 shows two eutectic points exist, while one has 90 wt % Sn, and the other has 20 wt % Sn. Since the binary Au-Sn stack that has 20 wt % Sn is a more reliable system, it is generally used as a candidate bonding material system for the eutectic bonding of WLP. For instance, with a study held at METU MEMS Research Center, a package that can provide robustness, hermeticity, and temperature resistance was obtained with Au-Sn eutectic bonding. A schematic representation of the box and Au-Sn material stack design is shown in Figure 2.9 [47].

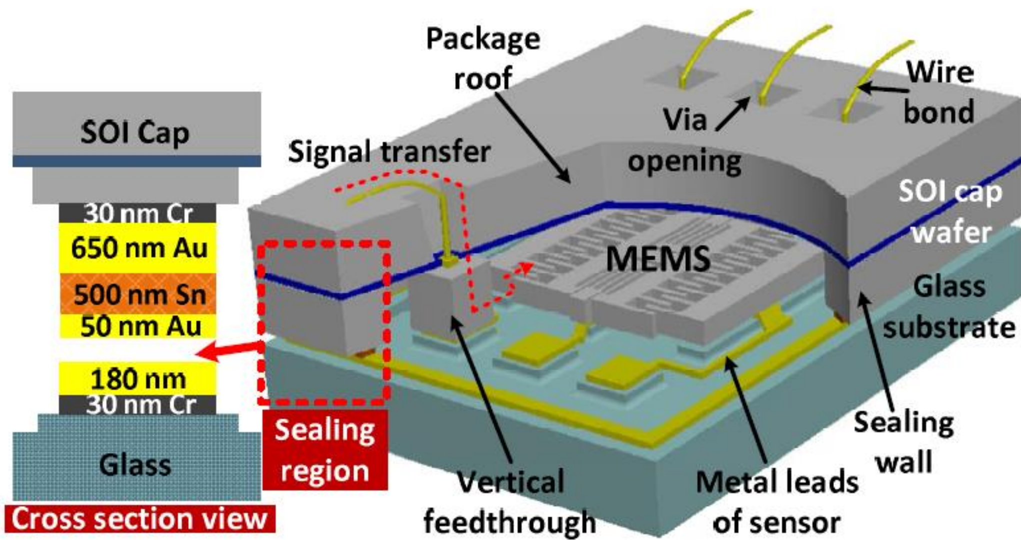

Figure 2.9 Schematical representation of MEMS Device Design with Design of Bonding Material Stack with Thicknesses [47]

As seen in Figure 2.9, asymmetric deposition of candidate Au-Sn materials was applied to bonding area. Nevertheless, the thickness ratio between Au and Sn was selected to reach the eutectic composition of this binary material system. During bonding, 300 °C temperature was applied with 2 MPa bonding pressure. SEM image and elemental analysis concerning EDS analysis of the bonding region are shown in Figure 2.10 [47].

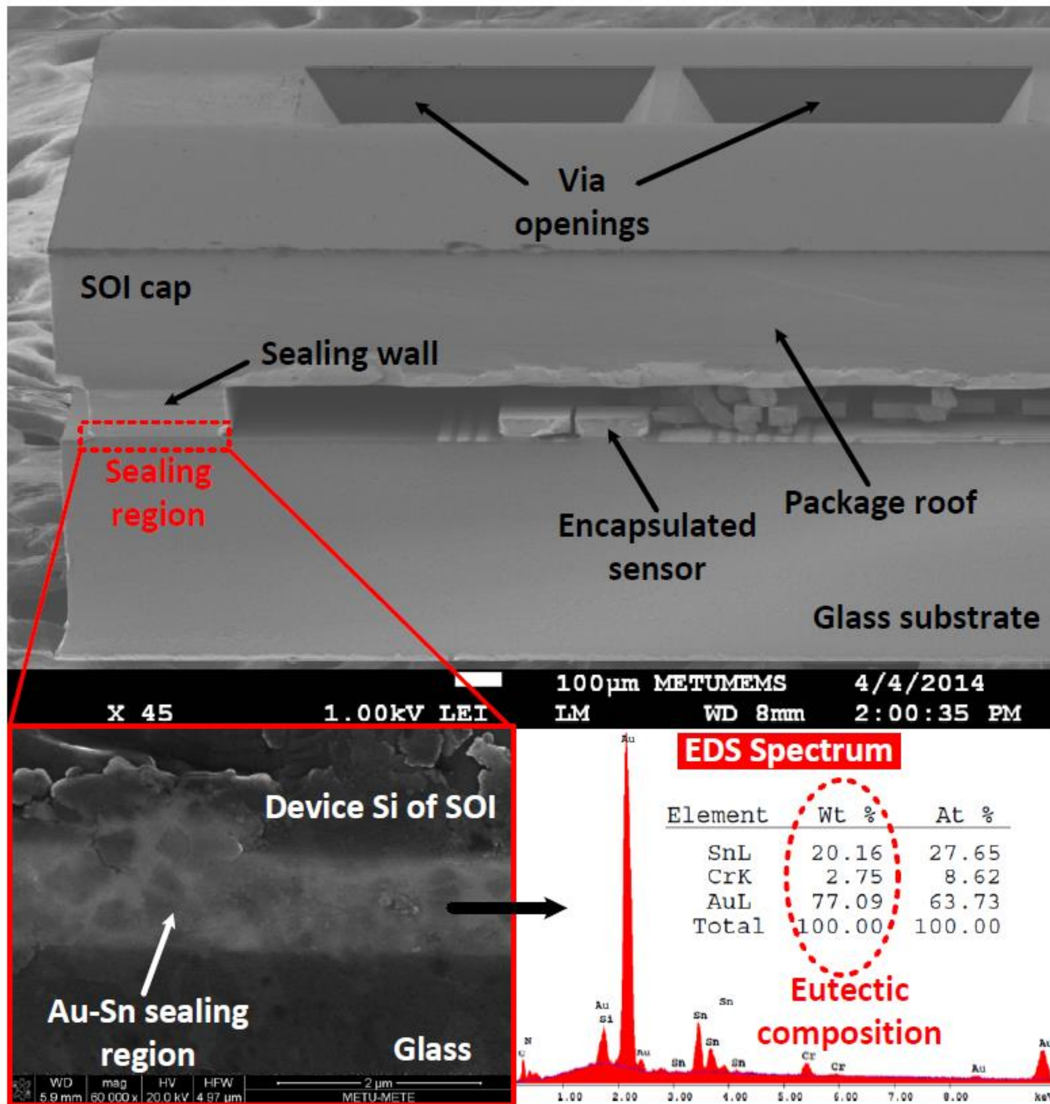

Figure 2.10 SEM Image of the Cross-Section of Bonding Area with EDS Analysis [47]

As seen from Figure 2.10, concerning EDS analysis, the eutectic composition is obtained with used Au and Sn thicknesses. Furthermore, after the shear test, the shear strength of the packaged devices is measured to be above 20 MPa, which means robust bonding is obtained with that candidate system.

One of the main ideas of this thesis is combining the superiorities of the eutectic Au-Sn bonding system with the advantages of Indium (In), which has been used for TLP bonding because of many beneficial properties to enhance WLP properties with

easing bonding parameters. For this purpose, the new Au-In-Sn ternary system, which does not exist in the literature, was tried for WLP to design candidate metal thicknesses and bonding process parameters.

2.3 Ternary WLP Approaches

In WLP, binary material systems are generally used as bonding material at eutectic and TLP bonding systems due to their general simplicity and controllability for bonding operation. However, as the MEMS's complexity and durability increase, more robust packaging is needed to achieve better packaging. For this purpose, ternary systems that include three different material types may overcome this situation. Ternary systems have more complicated phase formations and kinetics during the formation of IMCs due to binary systems that can cause more complex structure and bonding phenomena during packaging. Nevertheless, a more robust, rigid bonded structure can be achieved for WLP with ternary systems with other beneficial features such as decreasing bonding temperature or increased bond integrity.

For example, in the study of Vuorinen et al., that tried bonding with bumps instead of a bond ring system, decreased bonding temperature and time usage with more stabilized liquid formation and existence during bonding is achieved with Copper-Tin-Indium (Cu-Sn-In) ternary system with respect to Cu-Sn or Cu-In binary systems. A decrement in the bonding temperature is achieved with the help of the Sn-In binary system that has a lower melting point than Sn or In. This situation can also provide lower residual stress after bonding, improving bond reliability [48]. Furthermore, according to the study of Golim et al., faster Cu diffusion into the liquid Sn-In binary system is observed compared to pure Sn, which provides fastened bonding process. Schematic representation of bonded structure and situation of the bonding system after the mechanical test is shown in Figure 2.11 [41].

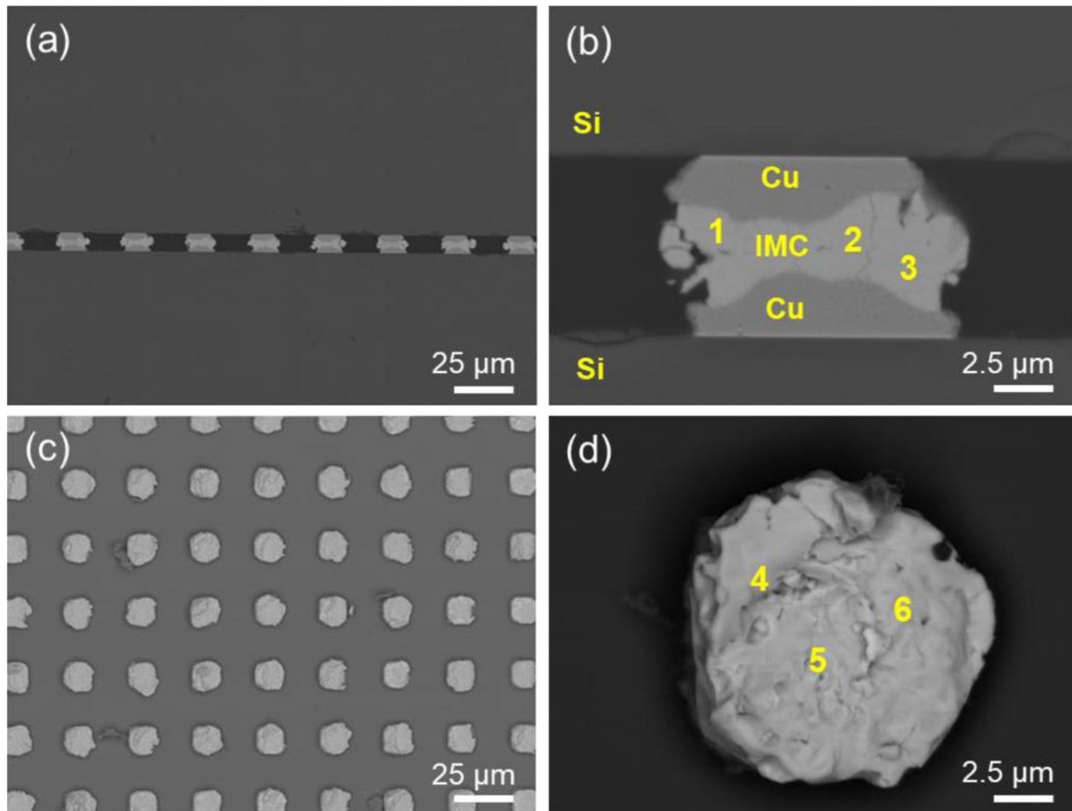

Figure 2.11 a), b) Schematic Representation of Bonded Structure with Cu-In-Sn System with Cross-Sectional View, c) and d) Fracture Surface after Mechanical Test on Bonded Sample [41]

According to this study, a total 252 mm^2 bonding area which includes bumps, was bonded with 7500 Newton force at 150 °C for 1 hour under a vacuum environment. In-Sn stack used in this study consist of Sn48-In52 composition, which indicates that the eutectic composition of this binary stack is met with pure Cu in that system during the bonding operation.

Furthermore, EDS analysis was done after bonding to observe each element's elemental distribution and atomic percent in the formatted IMCs at the bonding system. According to the EDS analyses, 55.5 at. % Cu, 29.1 at. % Sn and 15.4 at. % In were observed in the bonding area that closely indicates commonly known Cu_6Sn_5 IMCs composition value; however, in this system, In substitution with Sn in some amount was observed. That means instead of Cu_6Sn_5 IMC, $Cu_6(Sn, In)_5$, like IMCs,

are formed at the bonding area. The selected location for EDS analysis and elemental distributions in this work is shown in Figure 2.12 [41].

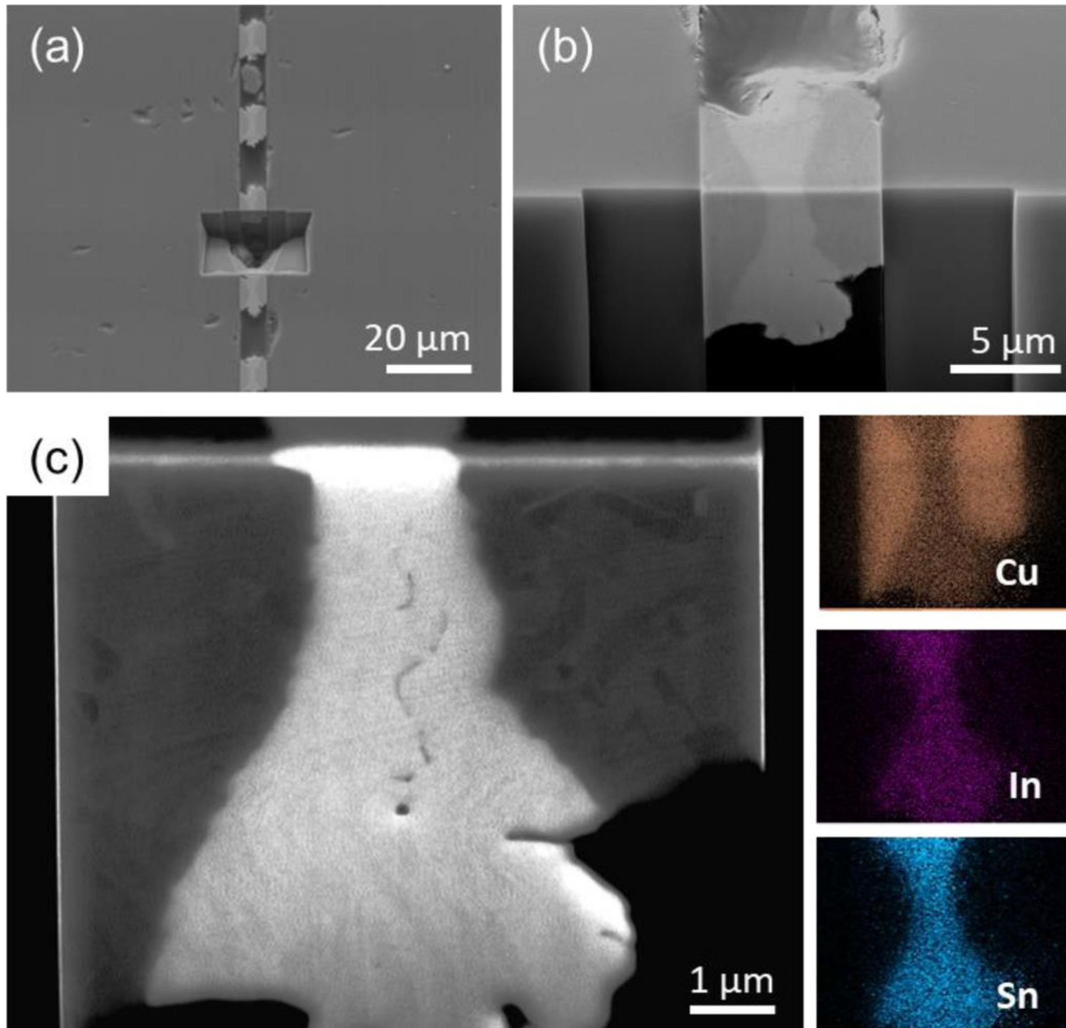

Figure 2.12 a), b), and c) Selected Bonded Area for EDS Analysis with Different Magnifications with Elemental Distribution [41]

After the mechanical chip level pull test, 32.7 MPa tensile strength was observed in this bonding system which is a relatively high value for provide requirements. With respect to all consequences of that work, the Cu-In-Sn system can be an alternative material system for WLP.

In the literature, trials of a ternary material system for WLP do not exist generally. Only a few articles about the Cu-In-Sn system for that purpose. In this thesis, instead

of Cu main metal, Au-In-Sn new ternary material system was tried for WLP that does not exist in the literature.

2.4 Combinatorial Deposition

One of the most critical parameters for WLP application is the candidate bonding materials' thickness since thickness directly affects the bonding's composition and properties. To optimize thickness value, distinct compositions must be tried that enhance properties. Nonetheless, multiple samples must be prepared for this purpose, which causes high energy, time, and material consumption [49]. Furthermore, this situation also causes the requirement for high effort since lots of process steps are required to produce WLP wafers. To decrease these requirements, a combinatorial deposition method that provides a compositional gradient along the sample was applied in this thesis with a known Au-In system. A combinatorial deposition is tried and used for many material areas to investigate composition-property relationships, such as optical or electrical properties. However, this approach has never been tested on WLP in the literature. Besides reducing the testing requirement, the widely known advantage of this method, this process approach can also enable more efficient and rapid optimization of the composition for new material systems that can be tested for WLP.

The main aim of the combinatorial deposition approach is obtaining compositional gradients along single or multiple samples with single deposition. This can be obtained with several techniques like co-coating, masking certain regions of sample or samples during coating with selected time intervals, setting holder geometry of sample or samples, and non-rotating samples or samples during coating that can generate non-uniform coating for thickness.

For instance, according to Pişkin et al., 21 discs were arranged in triangular form with triangularly placed three different sputter targets. A wide compositional range has been obtained discretely with the in-situ co-sputtering operation. In the results of

this experiment, instead of several run operations of the deposition, 21 compositionally different samples were achieved that can provide a large compositional database to investigate the effect of composition on a selected topic. With respect to that data, based on the resistivity values of the samples, an optimized design for hydrogen separation with Silver (Ag), Titanium (Ti), and Palladium (Pd) targets was obtained. Schematical representations of combinatorial deposition operation and obtained compositional distribution are shown in Figure 2.13 [50].

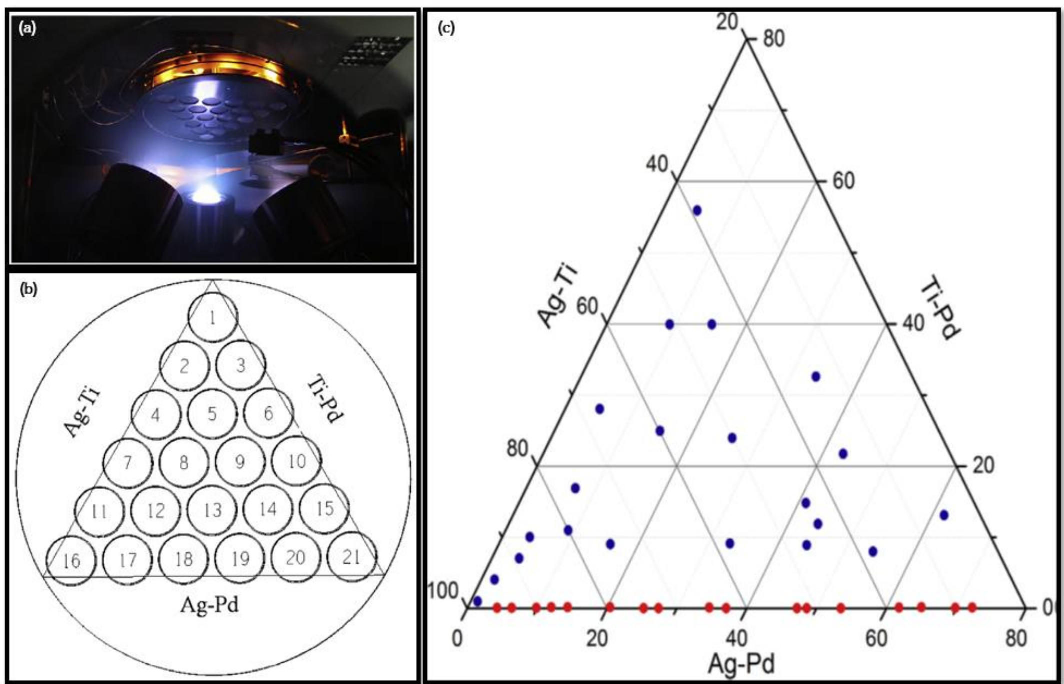

Figure 2.13 a) Combinatorial Deposition Method with in-situ Co-Sputtering Method, b) Distribution of the Samples at Holder for Combinatorial Deposition, and c) Composition Values of the Samples after Combinatorial Deposition (shown with blue dots) [50]

Another approach for combinatorial material deposition is using the distance and angle of the target with respect to the substrate during coating. According to the work of Siol et al., the In_2S_3 target was placed left side of the substrate at a certain angle and distance. Regarding that, while the close part of the substrate to the target is coated thicker, the distant part of the substrate has a thinner thickness concerning

another part of the substrate. Schematic representation of this study's combinatorial deposition and resulting structure are shown in Figure 2.14 [51].

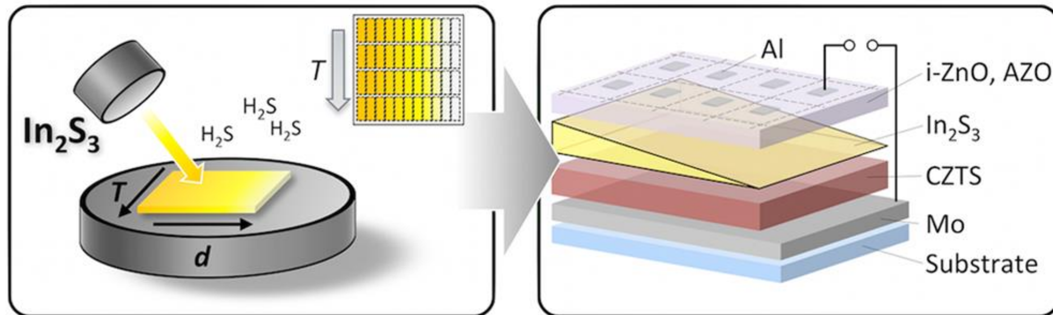

Figure 2.14 Schematic Representation of Combinatorial Deposition with Single Target and Substrate [51]

According to this work and with respect to Figure 2.14, from 75 nm to 25 nm, thickness variance along the width is obtained in this work. Based on that, electrical and photovoltaic properties of different thicknesses can be investigated.

Furthermore, the combinatorial deposition method can also be applied with a thermal evaporation system besides sputter deposition. In literature, composition gradient is achieved with two-boat systems generally. Different material types are used in each boat individually to create a compositional gradient along the sample in this method. Using the distance difference between the boat and sample, the compositional gradient is achieved with respect to the varied coated amount of candidate material. Schematic representations of some examples with compositional distributions are shown in Figure 2.15 and Figure 2.16 [52], [53].

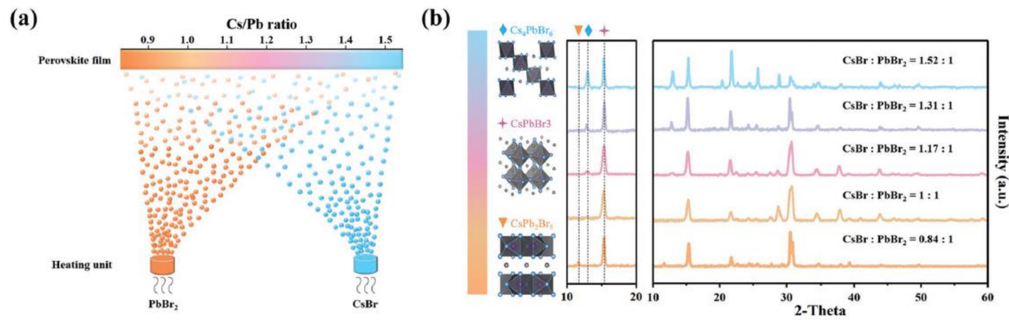

Figure 2.15 a) Schematic Illustration of Combinatorial Deposition with Thermal Evaporation System (left) and b) Obtained Phases concerning Elemental Composition and X-Ray Diffraction (XRD) Analysis (right) [52]

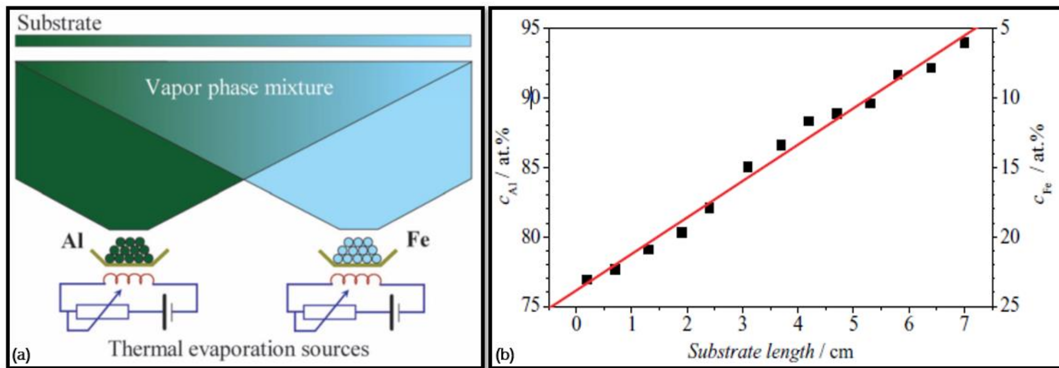

Figure 2.16 Schematic Representation of Combinatorial Deposition of Al and Fe Elements with Thermal Evaporation Technique and b) Compositional Gradient on Substrate after Combinatorial Deposition [53]

As seen from both Figure 2.15 and Figure 2.16, the compositional gradient can be achieved along the sample surface with thermal evaporation using a combinatorial deposition system. Based on the distance parameter between the certain substrate surface area and target position, the amount of coated element is varied, and regarding this phenomenon, gradual compositional variance can be achieved.

In this thesis, the combinatorial deposition method is tried with thermal evaporation coating technique for the Au-In system. While Au was uniformly deposited along all samples, to vary the thickness of the In, only one boat was used, and no rotation was applied during coating to keep constant the distance between specific locations of the wafer that was designed for packaging and In boat target. The designed system for this purpose was explained more detail in Chapter 3.

CHAPTER 3

EXPERIMENTAL PROCEDURE

3.1 Overview

In this thesis, Wafer Level Packaging (WLP) was tried using the combinatorial deposition method and the ternary metal system as bond material. As for material design, Gold – Indium (Au-In) binary metal system was selected as the bonding material system for combinatorial deposition studies since it is a well-known material stack for TLP bonding and suitable to manipulate In thickness with respect to the combinatorial approach, while Au thickness was kept constant along all area of wafers. For the ternary system, Gold – Indium – Tin (Au-In-Sn) ternary system was selected as a candidate bonding metal since this system can provide a combination of eutectic and TLP bonding with a combination of Au-Sn eutectic stack with one of the most used In TLP material. Bonding procedures were held on with 4” wafers. While silicon (Si) wafer was used as substrate wafer, glass wafers were used as cap wafer. Fabrication steps and characterization methods were explained in detail in this chapter.

3.2 Fabrication Steps

Schematic illustrations of fabrication steps for substrate and cap wafers were shown in Figure 3.1 in an ordered way.

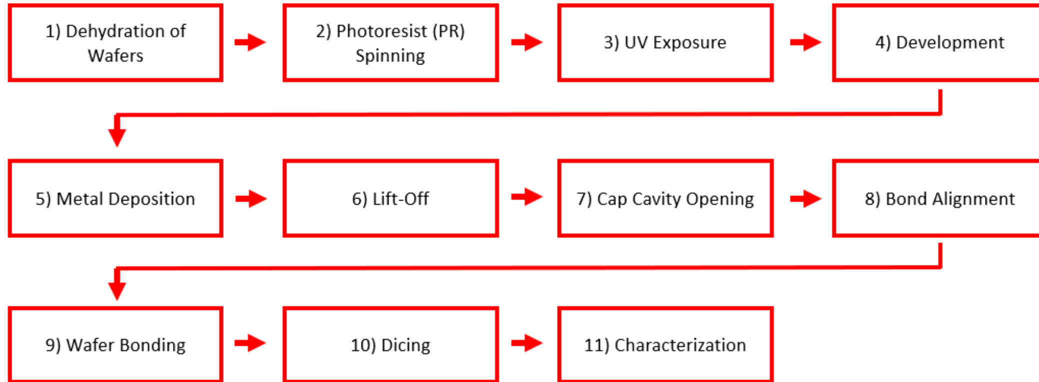

Figure 3.1 Fabrication Steps of Substrate and Cap Wafers for WLP

Some of the process steps have yet to be applied for some samples because the new process and material approaches were tried in this work to investigate the behavior and effect of these new approaches on WLP. After the WLP was completed, the characterization steps were started for the packaged samples. The fabrication process steps were explained in a detailed manner in this chapter.

3.2.1 Dehydration of Wafers

Before beginning the lithography steps, which include photoresist (PR) spinning, UV exposure, and development procedures, the wafers must be subjected to a dehydration step to remove moisture from the surface. For this purpose, wafers are placed in a furnace at 110 °C for 10 minutes. After the dehydration step was completed, for cooling, wafers were placed outside the oven for 5 minutes. A photo of the used furnace that is Imperial IV for the dehydration step is shown in Figure 3.2.

Figure 3.2 Imperial IV Furnace

3.2.2 Photoresist (PR) Spinning

Photoresist (PR) coating along all wafer surfaces is obligatory to embed the designed pattern in the wafer. For this purpose, the wafer is placed in the spinner system that provides uniform PR thickness along the surface of wafers with the help of the centrifugal force of the spinning phenomenon for consistent PR spread. Before PR addition, to prepare the wafer's surface and provide better sticking of the PR to the wafer surface, hexamethyldisilane (HMDS) coating is applied with the same method. After that process, PR coating is used with the spinning method. Later, a soft baking process, a heat treatment to become PR more solid for the following processes, is applied at a specific temperature and time. In this thesis, SUSS MicroTec Spinner was used for PR deposition. Furthermore, positive PR types were used for wafers because the photolithography mask for WLP was designed with respect to that. While SPR 220-7 PR was used for silicon substrate wafers, SPR 220-3 PR was used for cap glass wafers. PR types were selected with respect to designed metal thicknesses deposited onto the surface of the wafer. Each PR and HMDS were spun

at 3000 rpm for 30 seconds. For soft baking of SPR 220-3 PR, 115 °C temperature was applied for 90 seconds with a Torrey Pines hot plate system, while the same temperature was applied for 120 seconds for soft baking of SPR 220-7 PR. The spinner system and hot plate for soft bake process are shown in Figure 3.3.

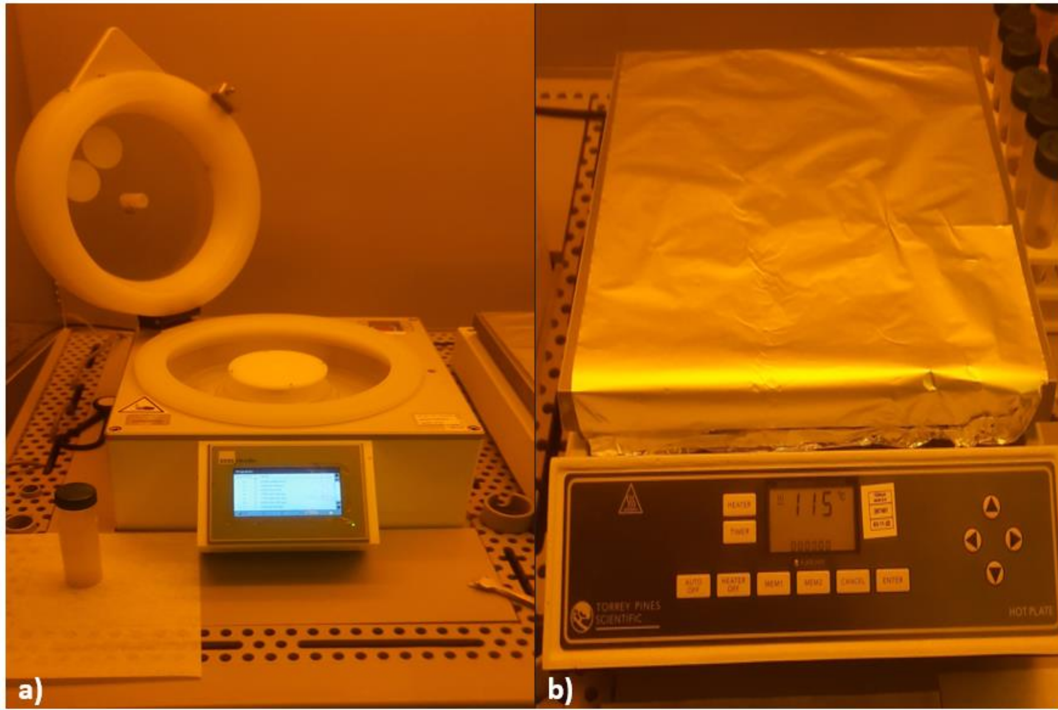

Figure 3.3 a) SUSS MicroTec Spinner System (left) and b) Torrey Pines Hot Plate (right)

3.2.3 UV Exposure

After PR coating onto the wafer was completed, UV exposure must be applied to pattern the designed structure onto the wafer. Since the positive PR type is used in this study and PR is a photosensitive material, the areas exposed to UV are degraded. With the help of a pre-designed photolithography mask that provides UV light to the designed area, while desired parts of the PR are exposed to UV light, other PR parts remain on the wafer surface since these parts do not expose by light. The patterned structure can be obtained on the wafer surface with this phenomenon. In this thesis, two cycles of exposure were applied for 5 seconds (10 seconds total with 5 seconds

x2 cycles) for SPR 220-3 PR, and two cycles of exposure were applied for 16 seconds (32 seconds total with 16 seconds x2 cycles) for SPR 220-7 PR. EVG 6200 Contact Aligner System was used for the UV exposure process shown in Figure 3.4.

Figure 3.4 EVG 6200 Contact Aligner System

3.2.4 Photoresist (PR) Development

After UV exposure was completed and unwanted parts of the PR were degraded with the help of this procedure, to strip away these parts from the wafer's surface, photoresist development was applied to the wafers. For this purpose, wafers were

soaked into the developer. To stop the reaction and prevent the over-developing used PR that may cause removing necessary PR parts and affect the metal deposition and bonding process, wafers were soaked into the Deionized Water (DI water) twice with two different beaker usage. In this thesis, the MF24A developer was used for PR development. For SPR 220-7 PR, 150 seconds development procedure was applied, while 55 seconds of development was applied for SPR 220-3 PR. For each applied development procedure, the wafers were soaked in two different DI water beakers for the same time as the development procedure. The photo of a used system for PR development is shown in Figure 3.5.

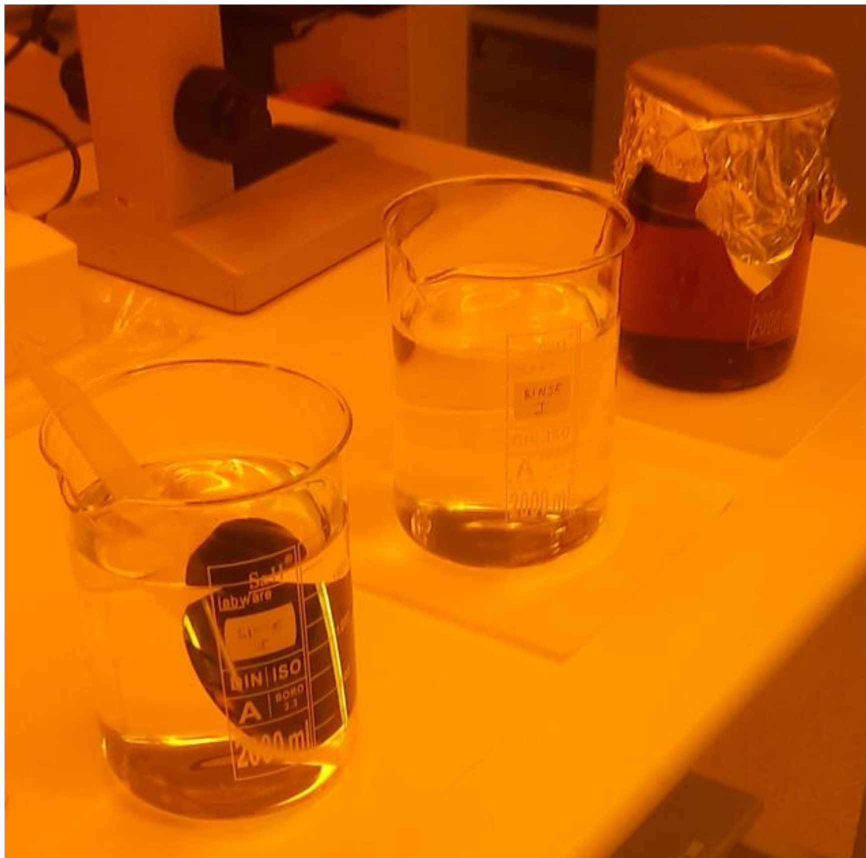

Figure 3.5 Development Procedure

3.2.5 Thin Film Metal Deposition

After the lithography stages, including dehydration, PR spinning, UV exposure, and development steps, wafers are ready to be coated with the candidate material stack. Since bonding material systems in this work require a seed layer that includes an adhesion and diffusion barrier layer, the coating procedure was started with these layers. While the adhesion layer provides sticking between the wafer and the bonding material system, the diffusion barrier layer is essential to prevent any diffusion occurrence between the wafer and bonding material system. For this purpose, Titanium (Ti) is used as an adhesion layer since that metal provides a good sticking phenomenon onto the wafer with respect to other metal systems. Nickel (Ni) and Titanium – Tungsten (TiW) metals were used as a diffusion barrier layer. TiW metal system used in this thesis consists of 10 wt % Titanium and 90 wt % Tungsten. To prevent oxidation and increase the wetting property of the bonding material system to the seed layer, thin Gold (Au) was coated onto the seed layer without breaking the vacuum at each metal deposition stage. Oxidation can be problematic for the bonding procedure because any oxide formation on the surface can be detrimental to bond integrity because of decreasing effect on sticking.

This thesis used Ti, TiW, Ni, Au, In, and Sn metals as-deposited materials. While Ti, TiW, and Ni metals were deposited with a magnetron sputtering, In and Sn metals were deposited with thermal evaporation. Since Au coating is possible with both sputtering and thermal evaporation methods, Au was coated onto the pre-coated metal stack with a determined thickness after each metal deposition step. For Ti-TiW-Au stack, AJA Sputtering System, for Ti-Ni-Au stack, BESTEC sputtering system, for In-Au stack, Nanovak NVTH 500 Thermal Evaporator system, and Sn-Au stack, Varian 3119 Thermal Evaporation System were used. Photos of the used metallization systems are shown in Figure 3.6.

Figure 3.6 a) Varian 3119 Thermal Evaporator System, b) BESTEC Sputtering System, c) AJA Sputtering System, and d) Nanovak NVTH 500 Thermal Evaporator System

Since combinatorial approaches were tried with varying thicknesses of In metal for the Au-In binary system, different holder types, where wafers are placed, were tested in this work. For this purpose, both a holder that can carry only one 4” wafer and a holder that can hold two 4” wafers simultaneously were used. A holder that can take two 4” wafers simultaneously was explicitly manufactured for the Nanovak NVTH 500 Thermal Evaporator system at METU MEMS Center to observe the combinatorial effect more efficiently. Photos of the used holders and placed situation of this holder inside the chamber were shown in Figure 3.7 and Figure 3.8, respectively.

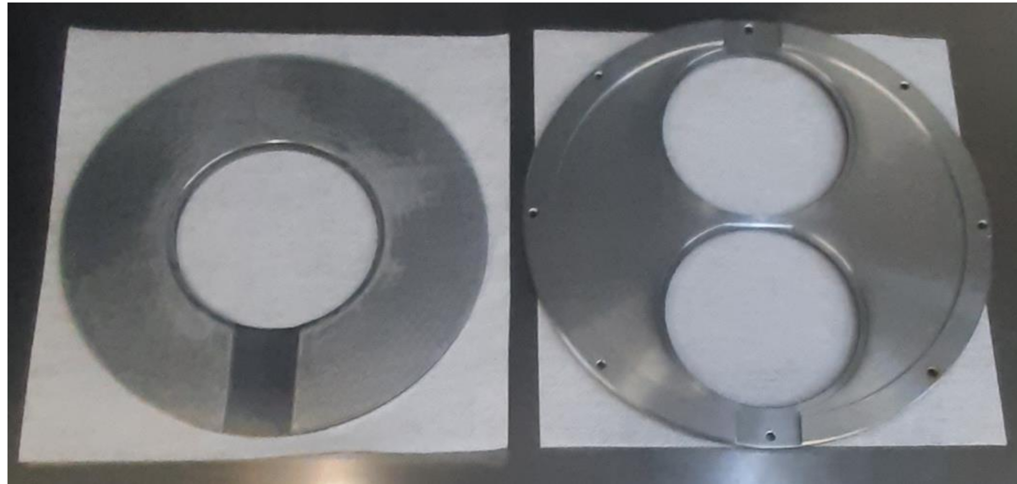

Figure 3.7 Holder Types of In Thermal Evaporator for 4" Wafer In Deposition

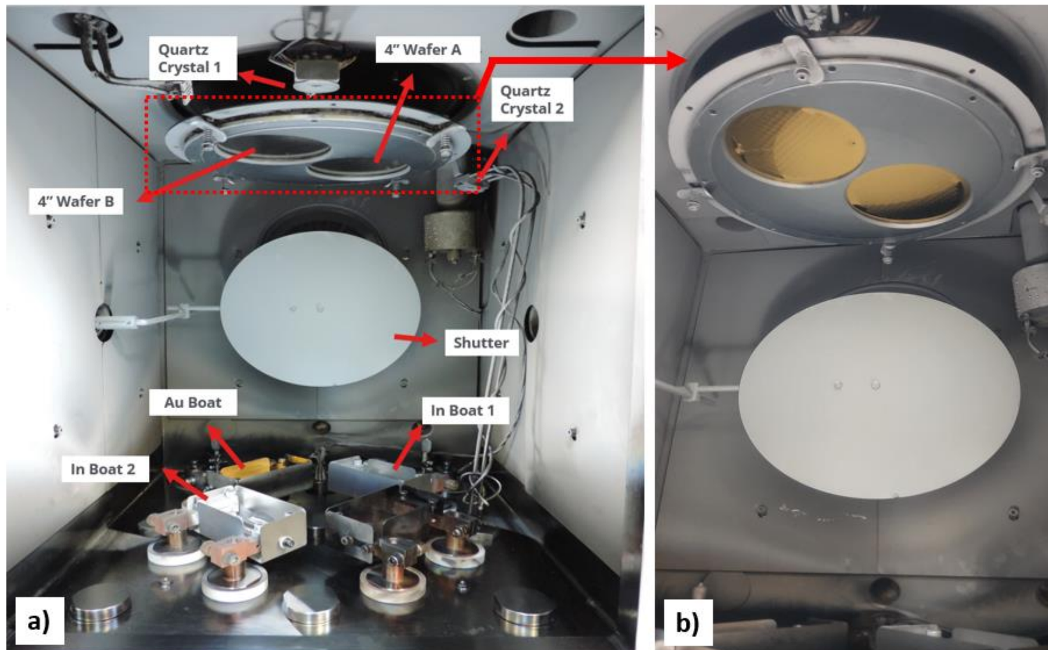

Figure 3.8 a) Nanovak NVTH 500 In Thermal Evaporator Inside the Chamber and b) Magnified View of Wafer Holder

3.2.6 Lift-Off

Later metal deposition, metals coated the entire surface of the wafer. A lift-off process was applied to strip off undesired metal parts from the wafer surface;

therefore, only metal parts that were desired with respect to the patterned structure remained on the wafer surface. Since both the surface of the pre-patterned PR and the remaining empty parts desired for bonding are covered with metal, when the PR part is removed, only the desired metal pattern remains, as it is removed with the metal on it. This patterning phenomenon is known as the lift-off process. From starting the photoresist coating to the final result of the lift-off procedure, a schematic illustration of the entire process flow is shown in Figure 3.9.

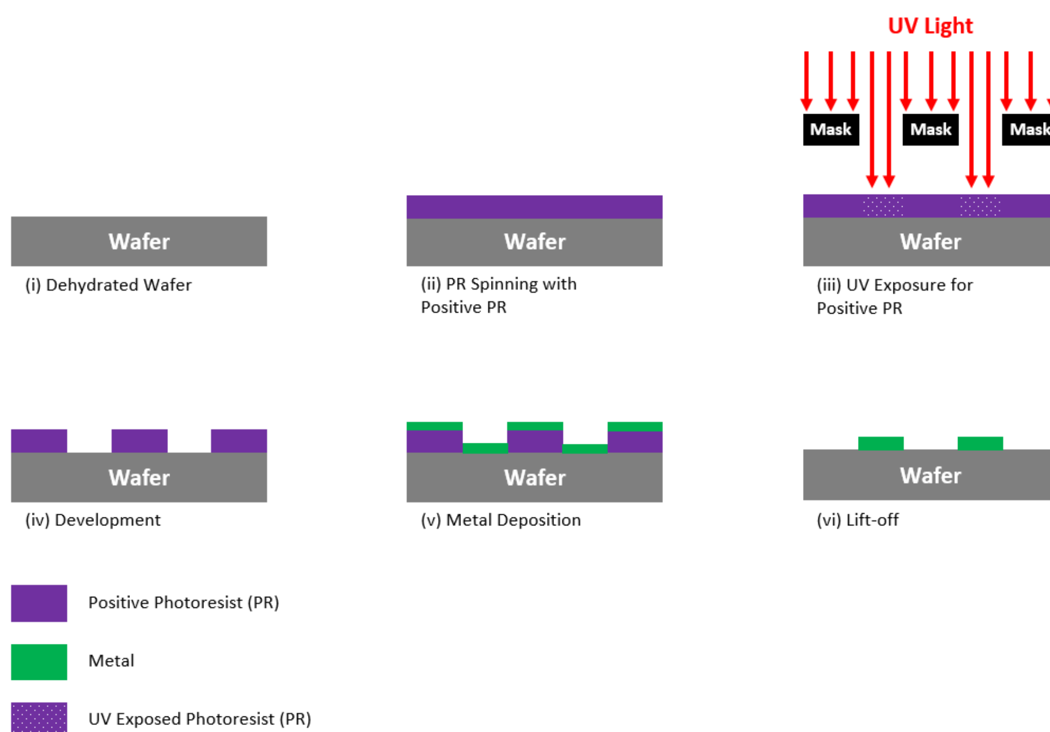

Figure 3.9 Schematic Representation of Process Steps for Patterning Metal Structure with Lift-off

To perform the lift-off process, wafers were placed into the glass petri, and acetone was added to an almost fulfilling volume of the petri. The wafers were usually kept in these petri dishes overnight to allow the complete dissolution of the PR by the acetone. Nevertheless, to complete removal, ultrasonic cleaning was applied. Then acetone and isopropyl alcohol cleaning were applied to remove some possible residual residue. After this process, the Avenger Ultra-Pure 8 SRD system that provides drying under an N_2 atmosphere was used to dry wafers. Photos of the

ultrasonic cleaning system and the Avenger Ultra-Pure 8 SRD system are shown in Figure 3.10.

Figure 3.10 a) Ultrasonic Cleaner for Lift-Off Process and b) Avenger Ultra-Pure 8 SRD System

3.2.7 Cap Cavity Opening

A cavity opening procedure was applied to one of the wafers before packaging to generate a certain package volume that provides checking hermeticity of the packaged system with cap deflection or He-Leakage test. The Deep Reactive Ion Etching (DRIE) dry plasma etching method was used with the STS Pegasus DRIE system. While etching is provided with SF_6 gas in this system, C_4H_8 gas flow is also applied inside the chamber as a passivation layer to protect any lateral etching. Therefore, a uniform, the controllable etching process can be applied for cavity formation. Since the DRIE dry etching process can only be used on Si wafers, the

metal types deposited on these wafers have been chosen accordingly because metals with low melting points like In or Sn can be damaged during this process. A photo of the STS Pegasus DRIE system is shown in Figure 3.11.

Figure 3.11 STS Pegasus DRIE System

Photolithography steps were applied to the wafer to protect the bonding metal from the dry etching procedure. Since bond metals must be protected by PR, negative PR is used instead of positive PR for sample manufacturing. For that purpose, AZ nlof 2070 negative PR was used. Besides soft bake, post-exposure bake after UV exposure and hard bake after development was also applied to provide standing of

the PR during the DRIE process. Soft and post-exposure bake steps were done at 110 °C for 90 seconds with a hot plate. The hard bake step, on the other hand, was done at 120 °C for 15 minutes in the Imperial oven from starting room temperature. After hard baking, furnace cooling was applied to the wafer up to room temperature.

After the DRIE process was completed, to remove PR, O_2 plasma treatment with Branson IPC Oxygen Plasma System. This treatment was applied at 300W for 20 minutes to remove. Later, the PR Strip process was used with the MLO-07 solution. The solution was heated to 80 °C, and the wafers were exposed to this solution for two cycles of 15 minutes each. In the second cycle, a different solution tank was used. After PR Strip, wafers were rinsed with De-Ionized (DI) water and dried with Avenger Ultra-Pure 8 SRD system. Photos of the Branson O_2 Plasma Cleaner and used the wet bench for the PR Strip are shown in Figure 3.12. A schematic representation of cap cavity formation with stages is shown in Figure 3.13.

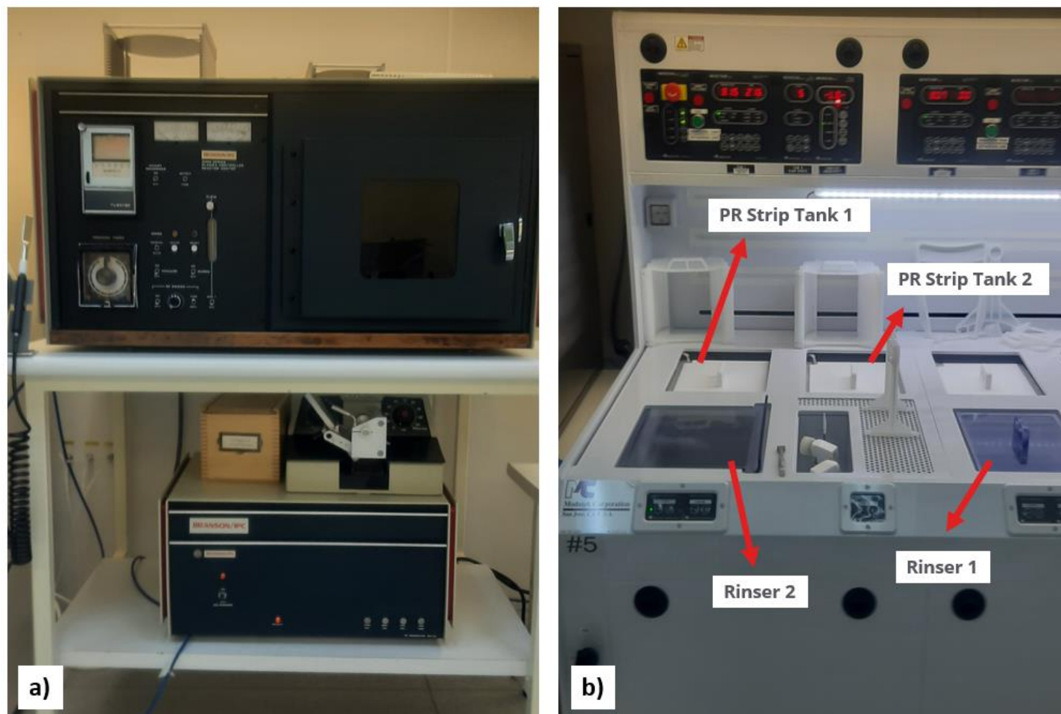

Figure 3.12 a) Branson O_2 Plasma Cleaner and b) Wet Bench of PR Strip Process

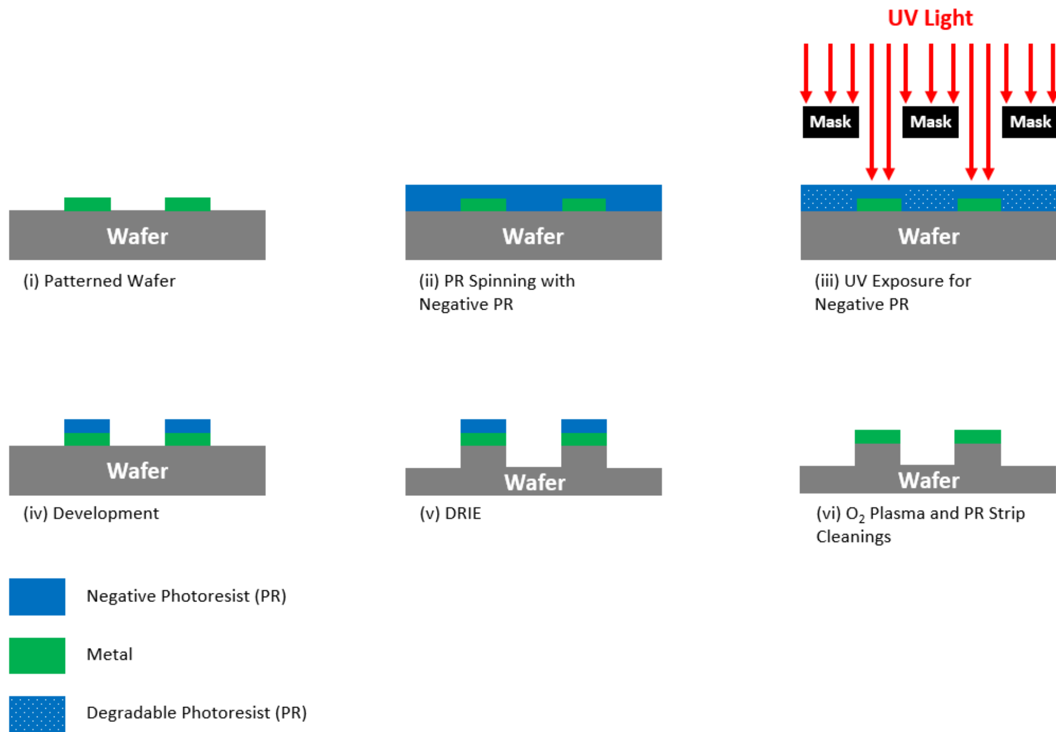

Figure 3.13 Schematic Illustration of Cap Cavity Opening Process

3.2.8 Bond Alignment

After the patterning process of both cap and substrate wafers is completed, the wafers are aligned with each other. For this purpose, EVG 6200 Contact Aligner System was also used for UV exposure. Since cap and substrate wafers have the same pattern, with aligning with the help of alignment marks, the wafers became the same position before the bonding procedure. Since Si and glass wafers were used in this study, the alignment process was performed without the need for back-side alignment due to the transparency of the glass wafer. Spacers were placed between wafers during alignment to prevent any contact before bonding. Furthermore, it can provide vacuum formation inside the package during bonding since bonding procedure is applied in a vacuum atmosphere.

3.2.9 Wafer Bonding

After the alignment of wafers, the bonding process was applied with an appliance of heat and force under a vacuum environment. For this purpose, EVG 520 IS Wafer Bonder system was used. Before the bonding process in the system, the chamber could be filled with forming gas containing 95% N_2 and 5% H_2 gases by volume. After creating the gas treatment, the chamber has to be vacuumed to obtain a vacuum inside the package. After these, the wafers' temperature was raised to a temperature with a specific heating rate. After pulling the spacers between wafers, the force was applied to obtain bond formation. A photo of the EVG 520 IS Wafer Bonder system is shown in Figure 3.14.

Figure 3.14 EVG 520 IS Wafer Bonder System

Since both Au-In and Au-In-Sn systems were studied in this thesis, different bonding recipes have been generated.

For combinatorial Au-In WLP trials, the same bonding process parameters were used to compare composition property relations between samples. For this purpose, the recipe was created and named Recipe CombAuIn 1. In this recipe, after forming gas application inside the chamber for 2 minutes, the temperature increased to 150 °C with a 45 °C/min rate. After melting In and avoiding any thermal stress failure, the temperature was raised to 170 °C with a 4 °C/min rate. During this state, In started to melt, so In was preparing for TLP bonding. After that system's temperature was increased to 200 °C with 45 °C/min, bonding procedure was started with 7200 N force for 45 minutes when spacers were pulled away from between wafers. This force provides 3 MPa pressure on wafers approximately during bonding with respect to the bonding area that is 2413 mm^2. After 45 minutes of the bonding cycle, the temperature decreased to 120 °C with 45 °C/min. The system was held at that temperature for 30 minutes to avoid any thermal stress effect and complete diffusion between Au and In. Later, the temperature was down to room temperature with the maximum cooling rate of the bonder system, and samples were taken from that system for characterization stages. The bonding process profile of that system is shown in Figure 3.15.

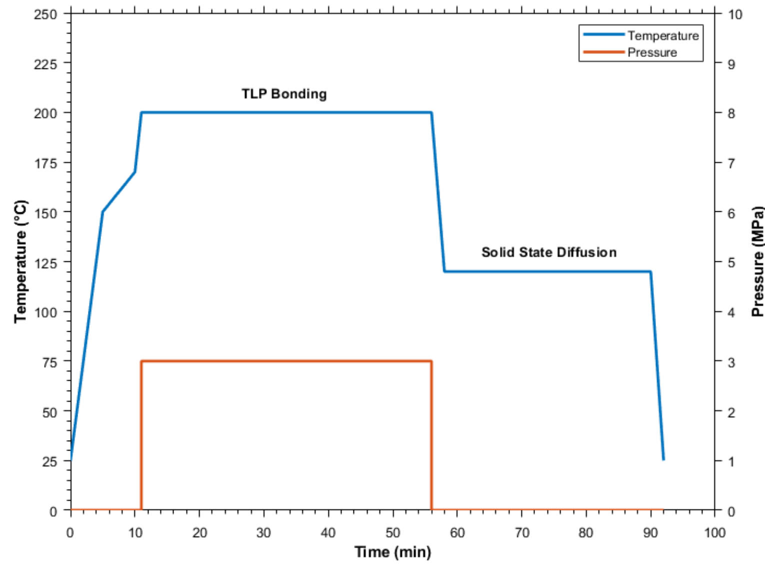

Figure 3.15 Recipe CombAuIn 1 Temperature and Pressure vs. Time Diagram

Since the ternary Au-In-Sn material system is not well known because this system has yet to be tried for WLP before in the literature, new bonding recipes were designed for that system. The first recipe, Recipe AuInSn 1, 700 N force (in other words, 0.3 MPa pressure), was applied while the system's temperature was raised to 100 °C for 10 minutes after the standard forming gas procedure. The main aim of this state was to provide solid-state bonding at this system to prepare the system for TLP bonding. After that, the temperature was increased to 350 °C, and 5000 N force (equal to 2 MPa pressure) was applied for 60 minutes for TLP bonding. After that system was cooled to room temperature. The temperature–time profile of this recipe concerning bonding pressure was schematized in Figure 3.16.

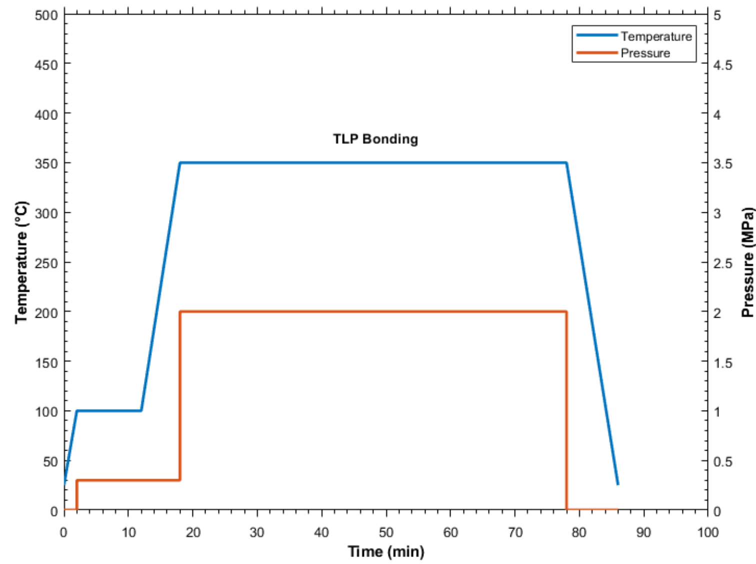

Figure 3.16 Recipe AuInSn 1 Temperature and Pressure vs. Time Diagram

Another recipe was generated for Au-In-Sn ternary system named Recipe AuInSn 2. This recipe has a similar property to Recipe AuInSn 1. The only pressure was increased to 6 MPa with 15000 N force, and the bonding time was raised to 90 minutes at 350 °C during bonding. A schematic illustration of this bonding recipe is shown in Figure 3.17.

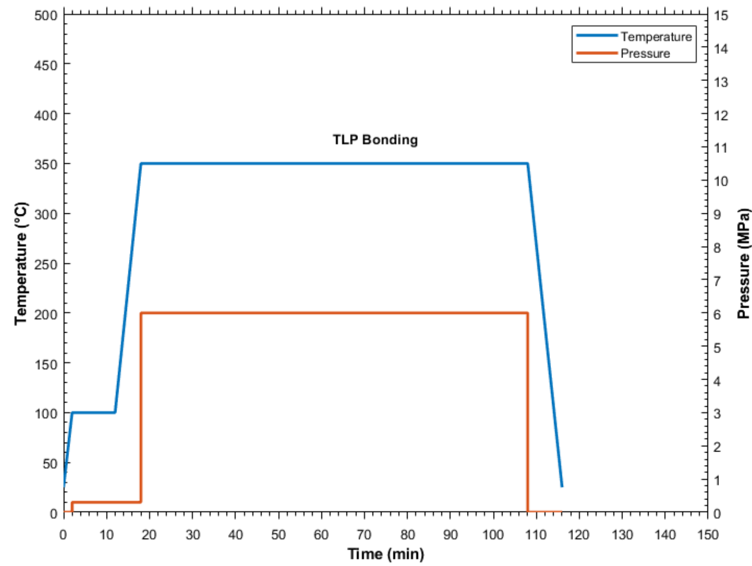

Figure 3.17 Recipe AuInSn 2 Temperature and Pressure vs. Time Diagram

3.2.10 Dicing

After the WLP stage had been completed with the bonding of glass and Si wafers, the dicing operation to obtain chips was done. Since bonded wafers are placed on an adhesive polymer sheet before dicing, dies obtained after dicing remain on this sheet. With the help of UV light exposure on a polymer sheet, dies can be separated from this sheet for characterization stages. For this purpose, DAD 3350 Dicing System was used. Photos of the used dicing system are shown in Figure 3.18.

Figure 3.18 DAD 3350 Dicing System

3.3 Characterization

After the WLP processes and dicing operation were completed, characterization steps were done to observe the properties of the bonded samples. Furthermore, some characterization processes were done before the bonding operation. For instance, Veeco DEKTAK 8 Surface Profiler system was used after the lift-off procedure to measure deposited metal thicknesses and cap deflection amount. With this method,

the thicknesses of both seed layers and used bonding material systems like In or Au-Sn were measured. Furthermore, since In thermal evaporator used in this thesis, Nanovak NVTH 500 Thermal Evaporator System, has a quartz crystal that provides measure coated In thickness in situ, obtained results from data of the quartz crystal were correlated with DEKTAK Surface Profiler system. These two systems were given the same thickness results. This surface profiler system is also used to detect cap deflection amount after the bonding operation. A photo of this system is shown in Figure 3.19.

Figure 3.19 Veeco DEKTAK 8 Surface Profiler

Additionally, samples were investigated with Optical Microscopy (OM) after some processes like development, lift-off, and dicing stages. While the existence of any remained PR was tried to be investigated with OM after development and lift-off stages, squeeze-out of bonding material and bond integrity was investigated with an observed amount of matching patterns of bonded wafers after dicing and WLP processes.

3.3.1 Scanning Acoustic Microscopy (SAM)

A Scanning Acoustic Microscopy (SAM) system was used in this thesis to analyze bond integrity and hermeticity of wafer-level packaged samples via using sound waves. In this system, WLP samples were sunk into the DI water since sound wave transmission is more efficient in DI water with respect to an air atmosphere. Later, the transducer was soaked into the DI wafer to produce a 200 MHz sound wave for scanning the WLP sample along the entire area. During scanning, as a result of the reflection and transmission of the sound waves sent by the transducer, the intensity vs. time data were collected according to the resulting peaks. Based on this information, the image of the WLP system was obtained. While the sound waves are reflected from the empty areas of the package system during imaging, peak and white contrast are obtained in the image, while the sound waves sent by the transducer pass directly through the bonding area without reflection, so no peak is obtained. Accordingly, dark contrast is obtained in the image. Therefore, a darker color in the imaging system indicates that the bound region has more efficient bond integrity. If water penetrates the packaged region since the water partially reflects the sound wave, a grayish contrast in the image is obtained, which indicates that the packaging is not hermetic. The bond integrity needs to be fully ensured.

This work examined WLP samples with the PVA TepLA 301 HD SAM system. Photos of the SAM system, characterization during scanning, and obtained SAM image are shown in Figure 3.20.

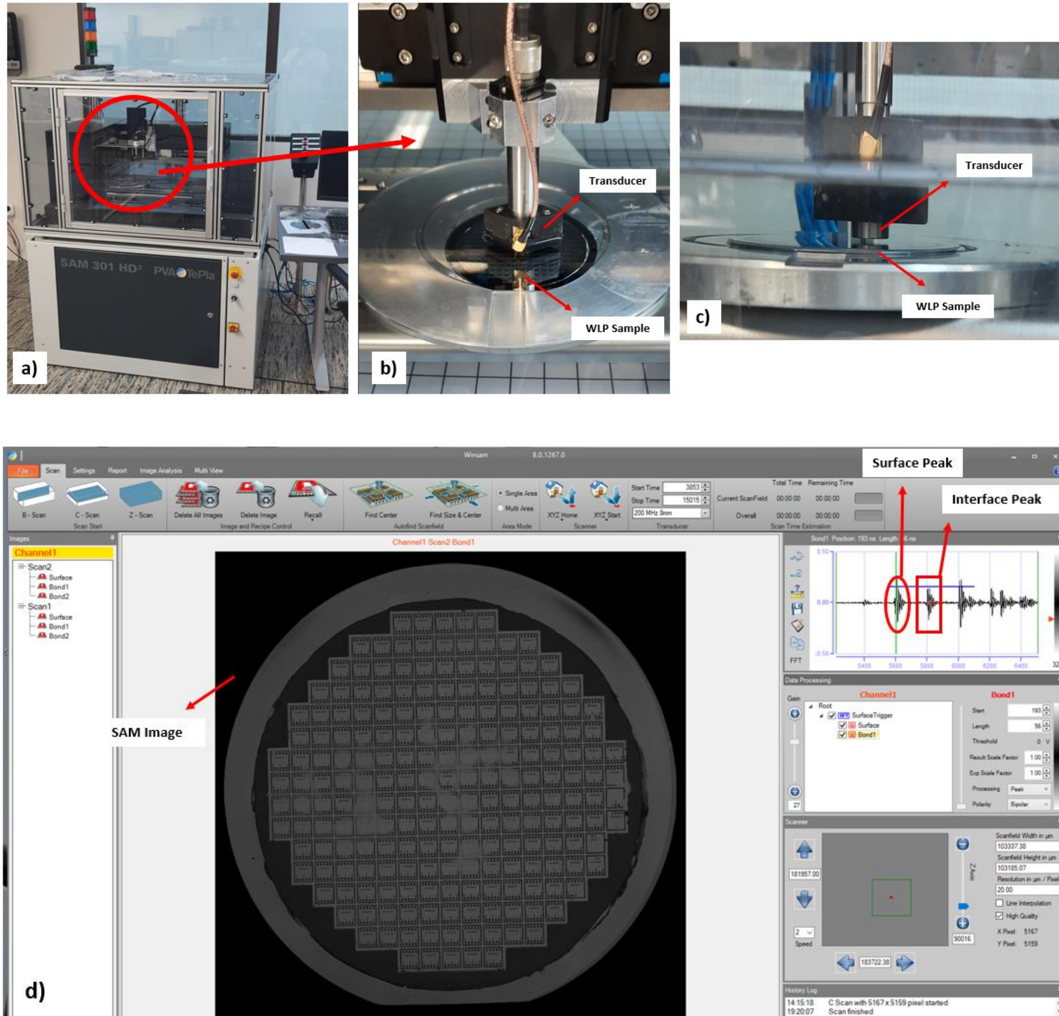

Figure 3.20 a) PVA TepLA 301 HD SAM System, b and c) Positions of the Transducer and WLP Sample during SAM Analysis, and d) SAM Software Interface with Peak Positions and SAM Image

3.3.2 Scanning Electron Microscopy (SEM) and Energy Dispersive Spectroscopy (EDS)

For microstructural analysis of the bond region of WLP samples, a Scanning Electron Microscope (SEM) was used. With this characterization system, the formatted Intermetallics (IMCs) crystal structure and bond integrity concerning the observation of any void or microcrack formation was also observed. For elemental analysis of the Au-In system and to investigate the composition amount of formatted

new IMC compounds, Energy Dispersive Spectroscopy (EDS) method was also used. With the EDS method, point, linear, and map EDS analyses were made to observe the bonding area in detail. Samples were examined along the cross-section of the bonding region to observe the bonding area efficiently at both SEM and EDS methods. In this thesis, Hitachi Regulus 8230 SEM system was used for both SEM and EDS analyses. A photo of the used device is shown in Figure 3.21.

Figure 3.21 Hitachi Regulus 8230 SEM System

3.3.3 Differential Scanning Calorimetry (DSC)

For the thermal characterization of the bond material system, Differential Scanning Calorimetry (DSC) system was used. With that characterization method, the temperature of the new phase formation, melting, and crystallization temperatures could be examined. Especially since Au-In-Sn ternary material system is a new system for the WLP procedure, DSC analyses could give temperature information about the formation of new phases or melting points beneficial for TLP trials. For this purpose, candidate materials were deposited along one side of the wafer since signals from the packaged structure were not give strong endothermic or exothermic peaks from DSC analysis to observations. Samples were heated at a 5 °C/min rate up to 550 °C from room temperature. After cooling was done at 5 °C/min per rate, a second heating procedure was also applied to the samples to ensure the formation of TLP bonding. Suppose no peak is observed after the second heating; newly formatted IMCs can withstand against Ti getter activation temperature, which is 400 °C since the second heating was done up to 550 °C with 5 °C/min. DSC analyses were done at the Middle East Technical University (METU) Central Laboratory. Experiments were done with the Perkin Elmer Diamond DSC system, shown in Figure 3.22.

Figure 3.22 Perkin Elmer Diamond DSC System

3.3.4 Die Level Shear Test

The die-level shear characterization method was applied to the samples to measure the robustness and mechanical strength of the produced dies after WLP and dicing processes. In that method, samples were placed in the device after the die. At the same time, the substrate part of the package was immobilized, and the shear force was applied with a force tool with adjusted height concerning the thickness of the wafers and bonding material. 650 µm height was adjusted for these experiments, and tests were used with standard shear test conditions. From this test, force vs. displacement data was obtained, and since the bonding area was known for packaged die, the shear strengths of each die were calculated based on that info. For each WLP sample, after coordination of dies were set for five divided regions of the WLP system, for each area, three samples were tested at least. These tests were done with Dage 4000 Bond Tester system. A photo of this system is shown in Figure 3.23.

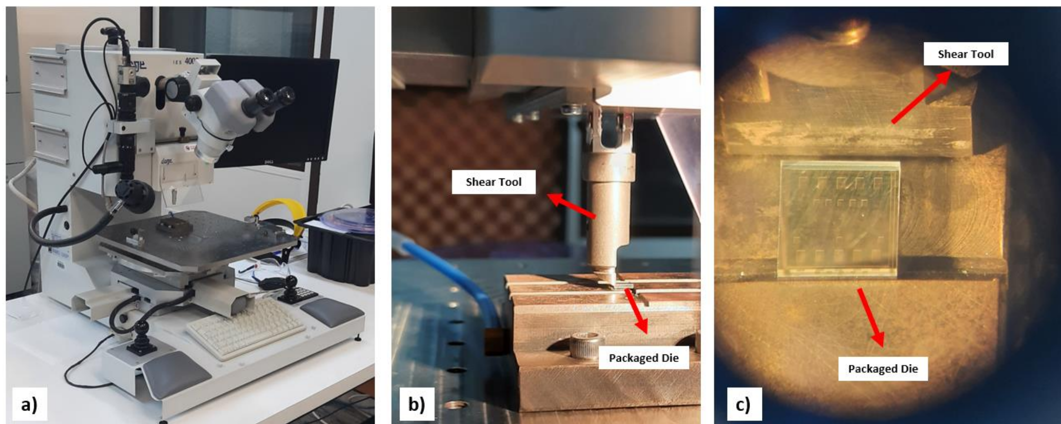

Figure 3.23 a) Dage 4000 Bond Tester System, b) Cross View of Shear Tool with Packaged Die During Die Level Shear Test, and c) Optic Microscope Image of Shear Tool and Sample

3.3.5 Cap Deflection Test

After the cap cavity was formed for the Si wafer, a specific volume was generated inside the package with a vacuum level since WLP was applied in a vacuum

atmosphere. With thinning the cap wafer with the DRIE method up to a specific thickness value, the pressure difference between the environment and inside the package would generate buckling at the cap wafer. The pressure level inside the package could be found by measuring specific buckling levels with a surface profiler and a particular equation for that approach. For this characterization method, the cap part of the dies was etched with DRIE up to 25 µm thickness to observe deflection. Schematic illustrations of the cap deflection system and the equation used for calculating the package pressure level are shown in Figure 3.24 and Figure 3.25, respectively.

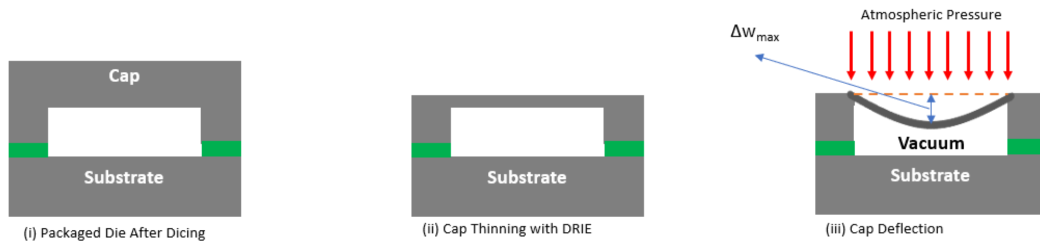

Figure 3.24 Schematic Illustration of Cap Deflection Process

$$\Delta P_{total} = \frac{32Eh^3(l^4+w^4)}{5(1-\vartheta^2)l^4w^4}\,\Delta\omega_{max}$$

Figure 3.25 Package Vacuum Level Equation

Where E is Young's Modulus of the Si wafer, h is the thickness of the cap wafer after thinning process, l and w are the length and width of the cap wafer, respectively, and ϑ is Poisson's Ratio of the Si wafer.

Furthermore, simulations were done with the COMSOL Multiphysics Simulation system to observe possible package vacuum levels with respect to varied thinned cap thicknesses; in other words, membrane thicknesses and displacement amounts due to these variables. Obtained graphs for this simulation approach for the cap deflection phenomenon are shown in Figure 3.26.

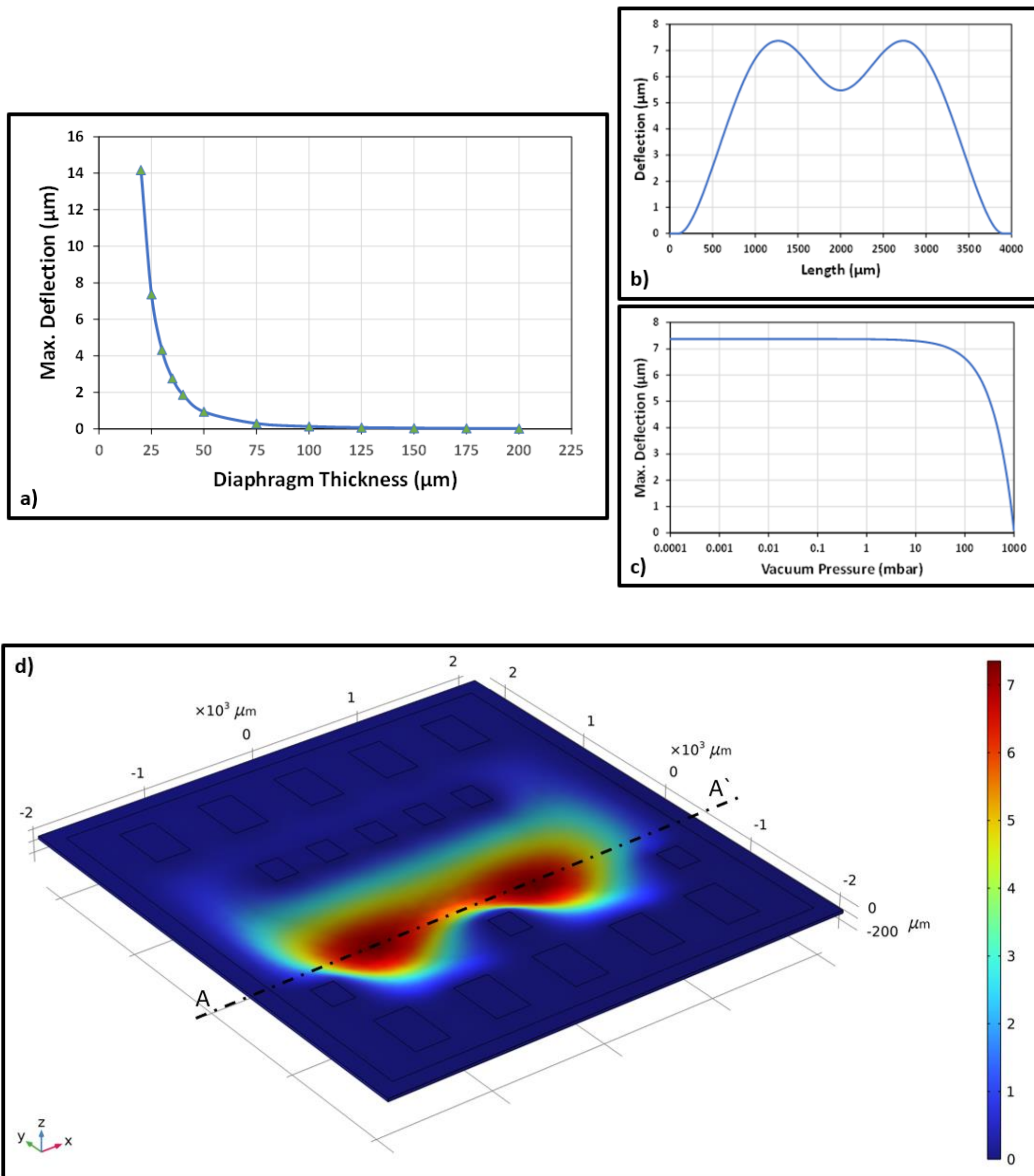

Figure 3.26 a) Maximum Deflection vs. Membrane Thickness from 20 µm to 200 µm for 10 mbar Package Pressure, b) Deflection Distribution vs. Length along Max. Deflection Cross Section for 25 µm Membrane Thickness, c) Max. Deflection vs. Pressure Inside the Package for 25 µm Membrane Thickness and d) Schematization of Deflection along Maximum Deflection Cross Sectional Region for 25 µm Membrane Thickness.

According to COMSOL Simulation data, the prepared die's cap side must be approximately 20-30 µm thick to observe visible cap deflection. Since inside the package was etched up to 130 µm for the cap cavity and the Si wafer has 525 µm

thickness approximately, the target DRIE etching procedure was set for 370 µm cap thinning operation to obtain 25 µm membrane thickness. For 370 µm etching procedure with DRIE, several etching process cycles were applied to the packaged die to eliminate anisotropic etching across the cap wafer surface and delamination of cap and substrate dies due to the probability of the overheating of samples.

3.3.6 He Leak Test

In this test, die samples were placed inside the chamber that contains He gas with specific pressure for a particular time. In this test, this step is also called He is bombarding. During that, The gas could penetrate inside the package with respect to the hermeticity property of the packaged system. After that, samples were transferred to another chamber that measures possible He leakage from inside to outside of the package with a specific leak detector. Regarding package volume, bombarding conditions such as pressure amount, exposure time, dwell time, and reject limit can be observed due to MIL-STD-883 specifications shown in Table 3.1 [12]. In this thesis, a used system for that characterization method is shown in Figure 3.27.

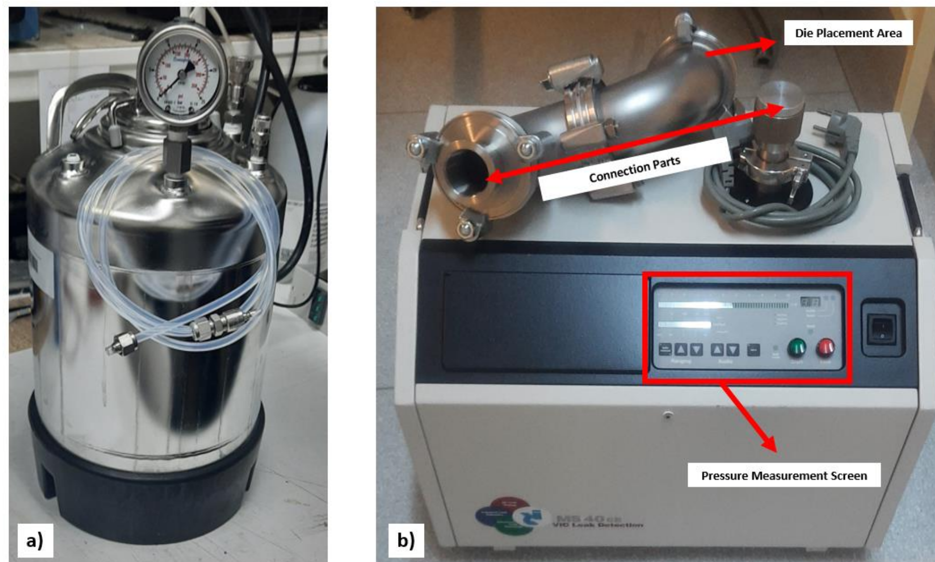

Figure 3.27 a) Pressure Vessel for He Bombardment and b) He Leak Detector

Table 3.1 He Leakage Test Rejection Limits Concerning MIL-STD 883 [12]

Volume of package (V) in cm^3	Bomb condition			R_1 Reject limit (atm cc/s He)
	Psia ±2	Minimum exposure time hours (t_1)	Maximum dwell hours (t_2)	
<0.05	75	2	1	5×10^{-8}
≥0.05 - <0.5	75	4	1	5×10^{-8}
≥0.5 - <1.0	45	2	1	1×10^{-7}
≥1.0 - <10.0	45	5	1	5×10^{-8}
≥10.0 - <20.0	45	10	1	5×10^{-8}

CHAPTER 4

RESULTS & DISCUSSION

To analyze the packaged system after characterization stages more efficiently quantitatively, wafers were divided into 5 regions with respect to patterned structure. Furthermore, each die was nomenclature with respect to their positions with numbering rows and columns. Schematic representations of regions of the wafers and the nomenclature of dies were shown in Figure 4.1 and Figure 4.2, respectively..

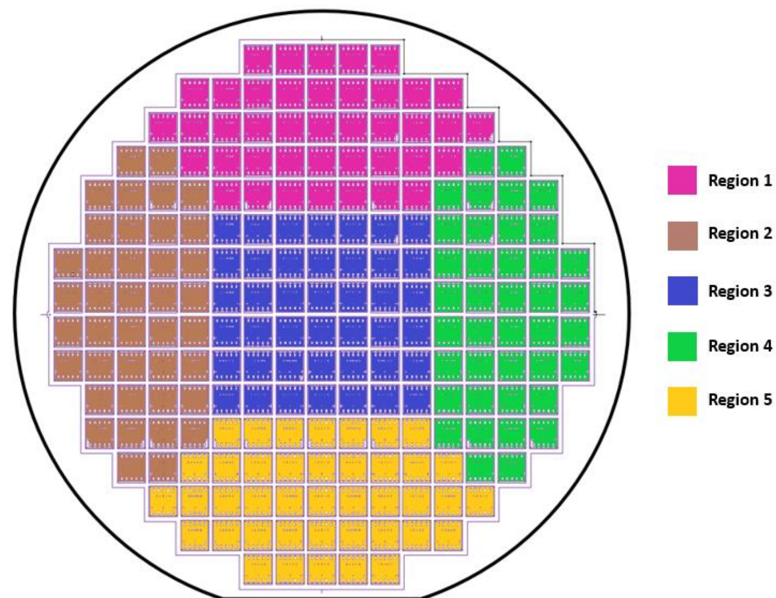

Figure 4.1 Schematic Representation of Regions of 4” Wafer

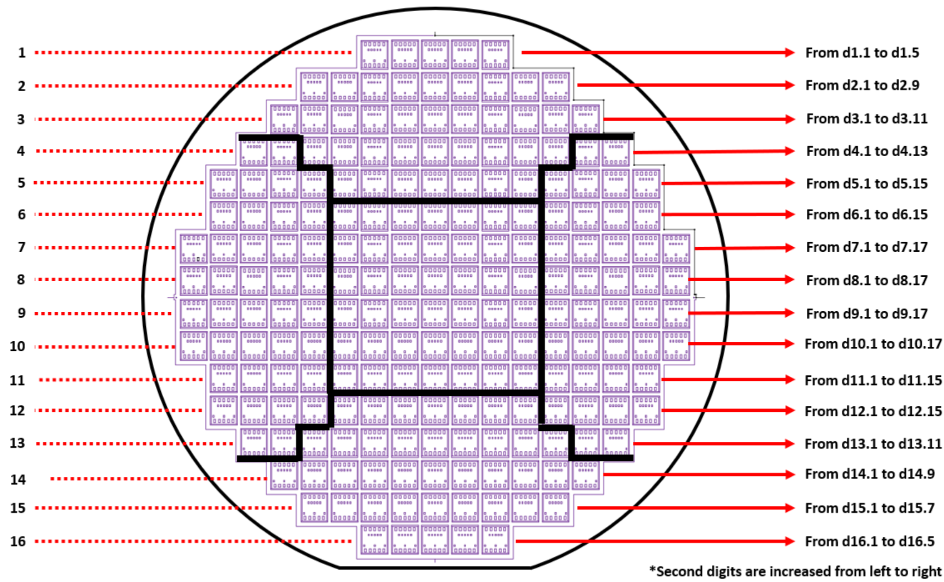

Figure 4.2 Representation of the Nomenclature of dies for 4” Wafer System

4.1 WLP Trials with Combinatorial Au-In Material System

4.1.1 Combinatorial Au-In Sample 1

To obtain compositional variance at Au-In binary system with alternating In thickness during thermal evaporation of In while Au thickness was kept constant, a holder that only carried one 4” wafer, which is shown in Figure 3.7, was used for the first combinatorial trial. For that purpose, 1500 nm In thickness was aimed due to pre-deposited 750 nm Au. While 1500 nm In thickness was measured at quartz crystal 2, which is the close crystal that In boat 1, 800 nm In thickness was measured at quartz crystal 1. Since the holder was not rotated and only one In boat was used for the thermal evaporation of In during the deposition of In, a thickness gradient was observed across the chamber with respect to measured values from quartz crystals. This situation was shown that obtaining thickness variance along the wafer is possible with this thermal evaporator system.

Furthermore, instead of the deposition of Au and In to different wafers that were studied generally in the literature and previous works on METU MEMS Center, the

Au-In stack was deposited directly onto the Si wafer while the glass wafer has only 60 nm Au for wetting and sticking during bonding. The reason for that design is to decrease metal deposition on the device side as much as possible in that way. Since photolithography and lift-off procedures can not be applied at real microbolometer packaging systems due to the existence of the device, deposition has to be held on with the shadow mask procedure. As metal thickness at that method is increased, the probability of over spraying phenomenon, in other words, deposition of metal to the near side of the bond ring area, is increased, which can cause undesired results at the device such as shortcuts, improper working situations, etc.

Schematized illustrations of In chamber and thickness values of the bonding material system with the seed layer are shown in Figure 4.3.

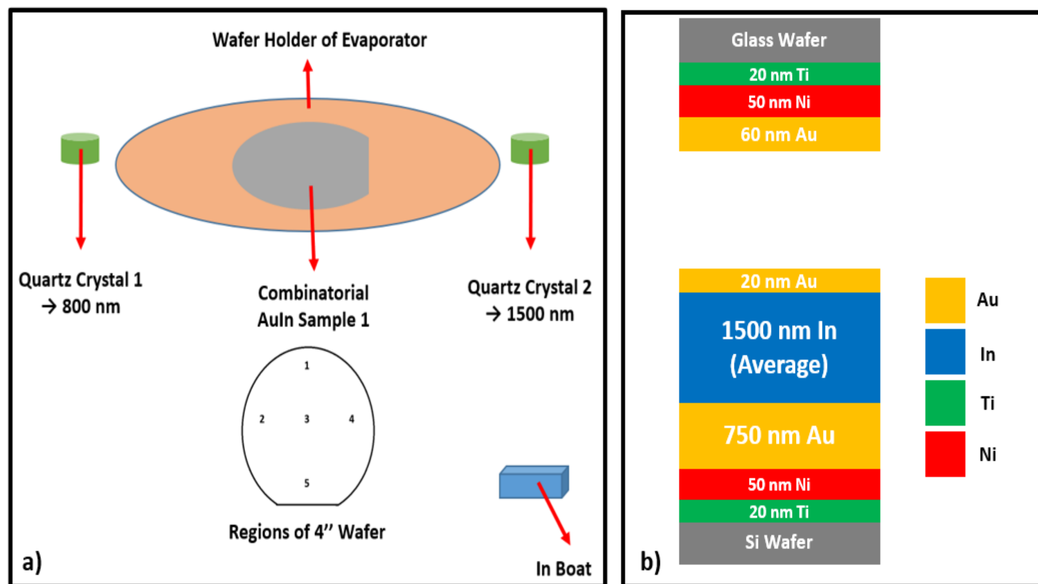

Figure 4.3 a) Schematized Illustration of Obtained Thickness Values Inside the In Chamber and b) Cross Sectional View of Deposited Thicknesses of Bonding Material System with Seed Layer

Since thicknesses of the seed layers for both Si and Glass wafers were measured with a surface profiler before In deposition, In thickness values were measured directly with the surface profiler. For each region of the 4" wafer, the thicknesses of 3 dies were measured. Obtained thickness data with respect to measured thicknesses of the

Au-In system and statistical values with respect to these data were shown in Table 4.1. Furthermore, compositional analysis with respect to In thickness data is shown in Table 4.2.

Table 4.1 Indium Thickness Values and Statistical Data for Combinatorial Au-In Sample 1

	Thickness (nm)				
	Region 1	**Region 2**	**Region 3**	**Region 4**	**Region 5**
1	1408	1492	1550	1477	1576
2	1369	1500	1559	1496	1533
3	1418	1459	1616	1528	1547
Mean of Regions	1398	1484	1575	1500	1552
Standard Deviation of Regions	21	18	29	21	18
General Mean	1502	**Maximum Mean**	1575	**Maximum Value**	1616
General Standard Deviation	65	**Minimum Mean**	1398	**Minimum Value**	1369

Table 4.2 Indium Composition Values and Statistical Data for Combinatorial Au-In Sample 1

	Composition (wt% In)				
	Region 1	**Region 2**	**Region 3**	**Region 4**	**Region 5**
1	39.1	40.5	41.4	40.3	41.8
2	38.5	40.6	41.6	40.6	41.2
3	39.3	40.0	42.4	41.1	41.4
Mean of Regions	39.0	40.4	41.8	40.6	41.5
Standard Deviation of Regions	0.4	0.3	0.4	0.3	0.3
General Mean	40.6	**Maximum Mean**	41.8	**Maximum Value**	42.4
General Standard Deviation	1.1	**Minimum Mean**	39.0	**Minimum Value**	38.5

With respect to Table 4.1 and Table 4.2, 350 nm In thickness variance was achieved, which corresponds to approximately 4 wt% In difference along the surface of the 4” wafer. Nevertheless, standard deviation values for measured thickness values correspond 1 wt% In thickness alternation average across all patterned surfaces. Also, the lowest thickness values were observed in Region 1, which makes sense because during In deposition, the furthest part of the wafer was determined as that region, the thickest region was found as Region 3 according to the measurements, while Region 5 was expected since this region is closer than other regions shown like Figure 4.3. The reason for this situation can be related to measurement error during surface profiler usage or misplacement of the sample diagonally with respect to In boat 1 during In deposition. This situation still showed compositional variance between regions since the intermetallic region, which is desired region of Au-In binary system for packaging, has 17 %wt In difference between AuIn and $AuIn_2$ IMCs due to the phase diagram that was shown in Figure 1.12. Changing the holder structure could achieve more compositional gradients in a single run. For this reason, other combinatorial experiments were done with a holder holding two 4” wafers.

SEM and EDS analyses were done to observe the bonding area's microstructure and corroborate the thickness/composition relation obtained from surface profiler data. Obtained results from these characterization procedures are shown in Figure 4.4.

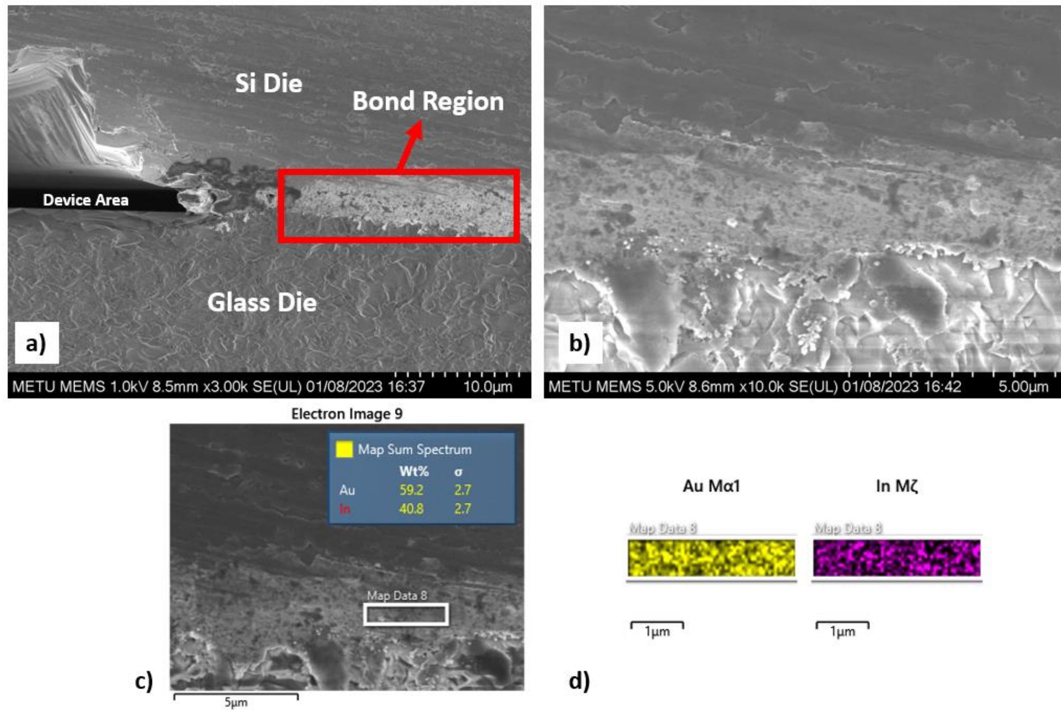

Figure 4.4 Combinatorial AuIn Sample 1 - d 10.9 a) Cross Sectional SEM Image with Package Parts, b) Cross-Sectional View of Bond Area, c) EDS Elemental Analysis and d) Elemental Distribution across Bond Area

As seen in Figure 4.4, the bond region was provided, sticking between glass and Si dies properly with efficient bond integrity. Near voidless structure was observed after observation with increased magnification at SEM. Furthermore, after map EDS analysis, obtained In composition was found to have almost the same value as the composition derived from surface profiler data. Therefore, data from the surface profiler were confirmed with EDS analysis. Furthermore, the elemental distribution of Au and In showed that proper IMC formed structure along the bonding region since these two elements covered almost the entire region at the selected EDS map.

After packaging was completed, SAM analyses were done to observe bond integrity. A visual inspection was also done to keep the structure after the SAM characterization step. Obtained results are shown in Figure 4.5.

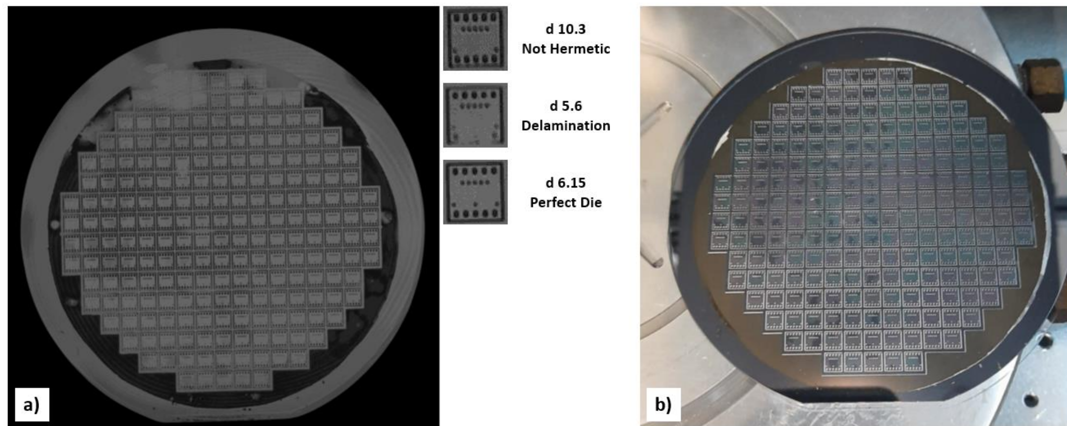

Figure 4.5 a) SAM Image of Combinatorial AuIn Sample 1 with Different Die Types and b) Optic Image of Combinatorial AuIn Sample 1 in Wafer just after SAM Analysis

As seen in Figure 4.5, water penetrated into some dies due to a lack of bond integrity and a delamination problem. To observe the package more efficiently, bonded area of these dies was investigated with an optic microscope. Obtained images are shown in Figure 4.6.

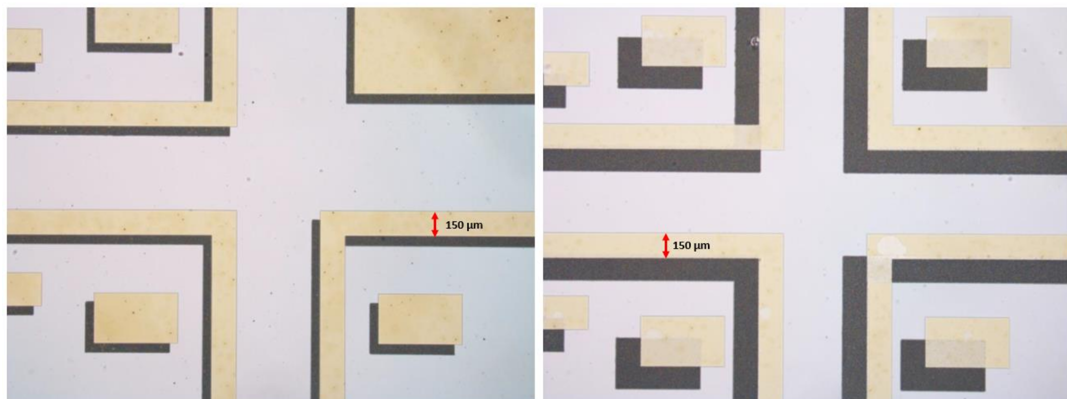

Figure 4.6 Optic Microscope Images of Combinatorial AuIn Sample 1 after WLP

As seen from 4.6, the bonding alignment of this sample was not done accurately in some regions. This situation caused water penetration into the dies and delamination problems; therefore, non-hermetic properties were observed with a lack of bond integrity. The reason for the misalignment of the bonding area can be related to experimental faults during the bond alignment procedure. During the transfer of the

sample from the EVG 6200 Bond Alignment system to the EVG 520 IS Wafer bonding system, wafers can be shifted from their positions due to small vibrations during transferring, even if the alignment was completely achieved after the bond alignment operation.

Even bond misalignment was observed in that sample, sample were diced after SAM analysis to other characterization steps. Cap and substrate parts of some dies were separated from each other during the dicing operation. Photo of the sample after the dicing operation and quantitative yield analysis with respect to visual inspection were shown in Figure 4.7.

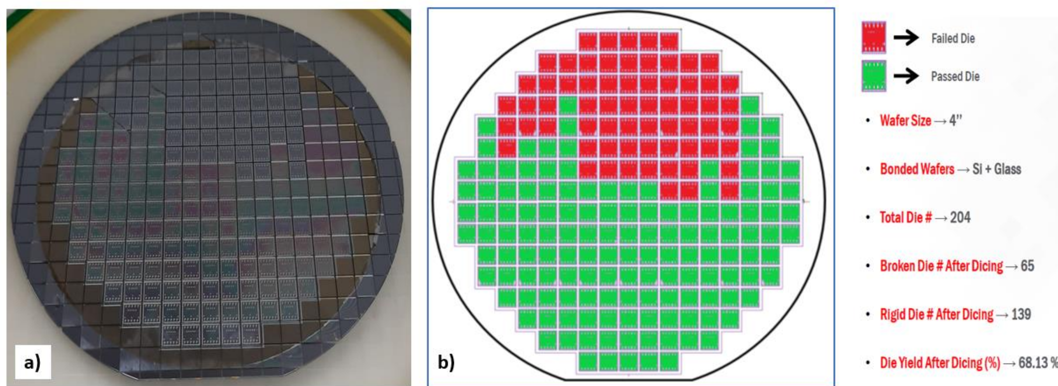

Figure 4.7 a) Photo of Combinatorial AuIn Sample 1 after Dicing and b) Dicing Yield Analysis of Combinatorial AuIn Sample 1 with Schematic Illustration

As seen in Figure 4.7, approximately 70 % yield was achieved after the dicing step. That can be an acceptable value; however, it should be increased to 80-90% value, at least for an efficient obtained sample amount.

Even bond misalignment existed in this sample; the shear test was done for rigid dies obtained from the dicing step. At least three tests were done for each region except Region 1 since only two die from region 1. Since the amount of misalignment was unknown for each die, to derive the strength value from the shear test operation, the force value obtained from this test with respect to displacement data was divided into the area of the bond region, which is 4.25 mm^2. With respect to that, shear strength values with statistical analyzes were given in Table 4.3.

Table 4.3 Shear Strength Values of Combinatorial AuIn Sample 1

	Shear Strength Values of Combinatorial AuIn Sample 1 (MPa) * At least 6 MPa required due to MIL-STD 883													
Region	1		2			3			4			5		
Die Number	d4.4	d5.5	d9.4	d11.4	d7.3	d10.10	d8.8	d11.10	d9.13	d7.14	d.11.12	d16.3	d14.6	d13.10
Shear Strength (MPa)	14	8	11	7	16	13	14	13	9	15	10	7	13	17
Mean of Regions	11		11			13			11			12		
Standard Deviation of Regions	3		3			1			3			4		
General Mean	12		**Maximum Mean**			13			**Maximum Value**			17		
General Standard Deviation	3		**Minimum Mean**			11			**Minimum Value**			7		

As seen from Table 4.3, shear strength values were above the 6 MPa value even bond misalignment was observed. Even with that misalignment, the standard deviation has a low value relatively. However, for instance, the highest and lowest values were observed in Region 5 with the highest standard deviation. This situation makes it challenging to correlate composition/property relations.

Furthermore, the maximum average shear strength value was observed at region 3 with minimum standard deviation. Since In thickness was also observed at the highest value in that region, the comment that increasing In thickness may increase the shear strength of the package can be made for the packaging system. However, since bond misalignment was observed in this sample and the amount of that misalignment varied region by region, more analyses about composition/property relation were done. For this reason, other combinatorial experiments were done with a holder holding two 4” wafers.

4.1.2 Combinatorial Au-In Sample 2 and Combinatorial Au-In Sample 3

A specific holder that can hold two 4” wafers was manufactured to obtain more compositional gradients in a single run, just as shown in Figure 4.8. For that purpose,

wafers were placed in the same In thermal evaporator chamber, and deposition was done without rotation and with only one single In boat. The placement of the wafers was done just like shown in Figure 3.8. Thicknesses of the seed and other layers were kept constant in the same order as a combinatorial AuIn Sample 1. With respect to quartz crystal 2, which is closer to In boat 1, the thickness of the In was set to 1600 nm. Therefore, the same deposition conditions applied to Combinatorial AuIn Sample 1 were used for these samples. Schematic illustrations of In deposition stage are shown in Figure 4.8.

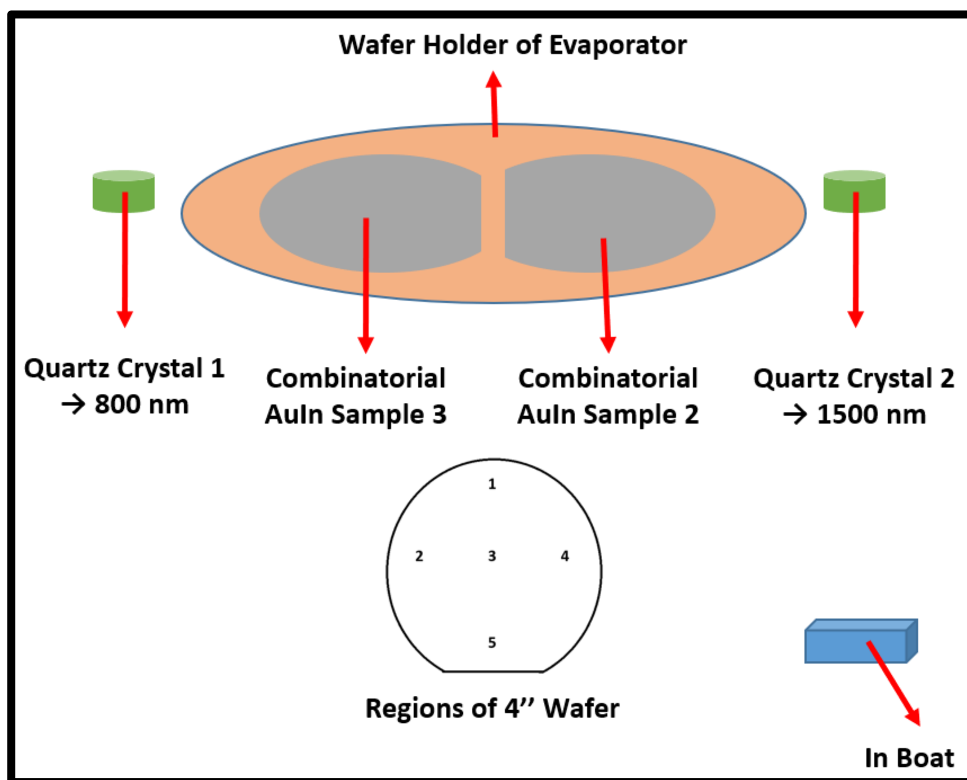

Figure 4.8 Schematic Representation of In Deposition Stage with Thickness Values

As Sample 2 was closer to the In boat with respect to Sample 3, a thicker profile was expected from Sample 2. Furthermore, as the total deposition area was increased by placing two 4" wafers, a higher compositional gradient was expected with respect to the amount of compositional gradient for one wafer trial. For this purpose, after In deposition, thickness values for both samples were measured with the surface

profiler. For each region, three measurements were done. Furthermore, measurements were done to the same dies for each sample to compare thickness values correctively. Obtained thickness values and composition values derived from thickness data for Combinatorial AuIn Sample 2 are shown in Table 4.4 and 4.5, respectively. The same results were shown in Table 4.6 and Table 4.7 for Combinatorial AuIn Sample 3.

Table 4.4 Indium Thickness Values and Statistical Data for Combinatorial Au-In Sample 2

	Thickness (nm)				
	Region 1	**Region 2**	**Region 3**	**Region 4**	**Region 5**
1	1427	1432	1473	1437	1418
2	1451	1428	1483	1456	1386
3	1433	1442	1469	1384	1390
Mean of Regions	1437	1434	1475	1426	1398
Standard Deviation of Regions	10	6	6	30	14
General Mean	1434	**Maximum Mean**	1475	**Maximum Value**	1483
General Standard Deviation	30	**Minimum Mean**	1398	**Minimum Value**	1384

Table 4.5 Indium Composition Values and Statistical Data for Combinatorial Au-In Sample 2

	Composition (wt% In)				
	Region 1	**Region 2**	**Region 3**	**Region 4**	**Region 5**
1	39.4	39.5	40.2	39.6	39.3
2	39.8	39.5	40.4	39.9	38.7
3	39.5	39.7	40.1	38.7	38.8
Mean of Regions	39.6	39.6	40.2	39.4	38.9
Standard Deviation of Regions	0.2	0.1	0.1	0.5	0.2
General Mean	39.5	**Maximum Mean**	40.2	**Maximum Value**	40.4
General Standard Deviation	0.5	**Minimum Mean**	38.9	**Minimum Value**	38.7

Table 4.6 Indium Thickness Values and Statistical Data for Combinatorial Au-In Sample 3

	Thickness (nm)				
	Region 1	**Region 2**	**Region 3**	**Region 4**	**Region 5**
1	1096	1225	1254	1120	1312
2	1153	1250	1237	1201	1299
3	1139	1248	1204	1157	1276
Mean of Regions	1129	1241	1232	1159	1296
Standard Deviation of Regions	24	11	21	33	15
General Mean	1211	**Maximum Mean**	1296	**Maximum Value**	1312
General Standard Deviation	64	**Minimum Mean**	1129	**Minimum Value**	1096

Table 4.7 Indium Composition Values and Statistical Data for Combinatorial Au-In Sample 3

	Composition (wt% In)				
	Region 1	**Region 2**	**Region 3**	**Region 4**	**Region 5**
1	33.3	35.9	36.4	33.8	37.5
2	34.5	36.3	36.1	35.4	37.2
3	34.2	36.3	35.5	34.6	36.8
Mean of Regions	34.0	36.2	36.0	34.6	37.2
Standard Deviation of Regions	0.5	0.2	0.4	0.7	0.3
General Mean	35.6	**Maximum Mean**	37.2	**Maximum Value**	37.5
General Standard Deviation	1.2	**Minimum Mean**	34	**Minimum Value**	33.3

As seen from thickness values obtained from the surface profiler, 220 nm In thickness difference between Sample 2 and Sample 3 was achieved, corresponding to 4 wt% In compositional difference due to that results. That provides a relatively high compositional gradient since the intermetallic region of the Au-In binary system has a 17 wt% In range between AuIn and $AuIn_2$. Furthermore, Sample 3 has more compositional fluctuations with respect to Sample 2. This situation was caused by the increased distance between In boat and the location of the sample. The thickest area was found as Region 3 at Sample 2, just like Sample 1, while the thinnest area was Region 5, which is the farthest part of this sample to the In boat. However, in Sample 3, the thickest and thinnest parts were found as expected, while the closest part, Region 5, in this case, gives the highest In thickness on average, and Region 1 gives the thinnest values.

After WLP was completed, SAM analyses were done for both samples. Obtained SAM results for Sample 2 and Sample 3 were shown in Figure 4.9 and Figure 4.10, respectively.

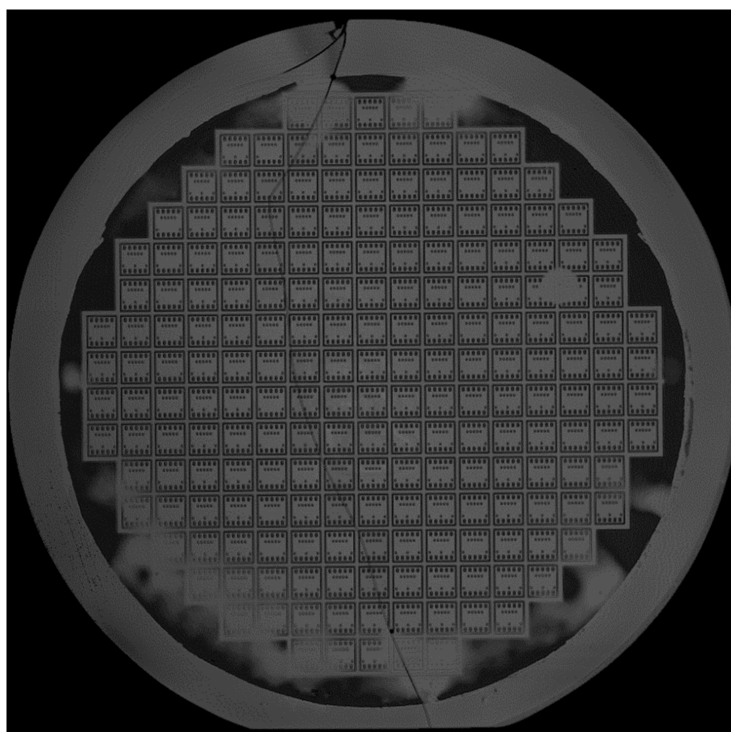

Figure 4.9 SAM Image of Combinatorial AuIn Sample 2

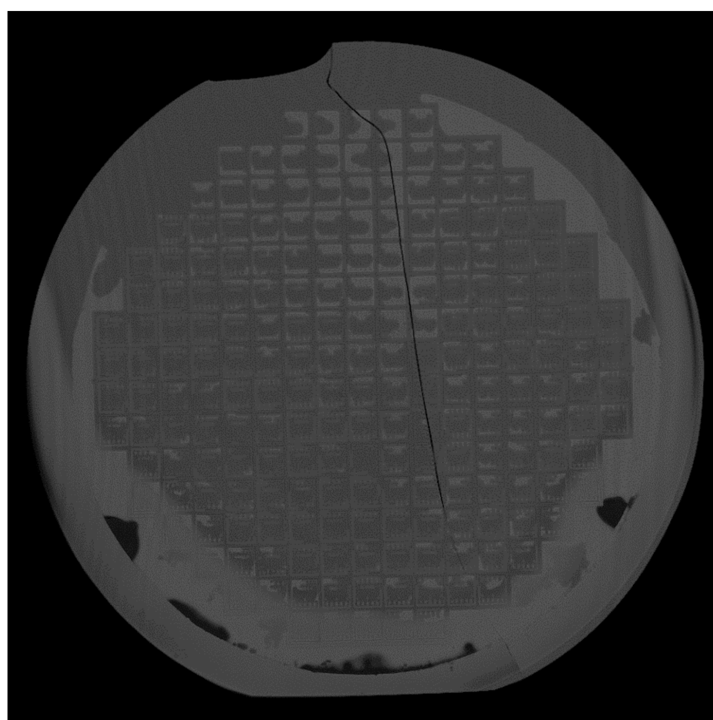

Figure 4.10 SAM Image of Combinatorial AuIn Sample 3

As seen in Figure 4.9, Sample 2 has relatively good bond integrity since the bond area of most of the dies has dark color except for some dies where the edge of the wafer. However, crack propagation was observed on the glass wafer after the WLP process. The reason for this may be related to the propagation of initial micro-cracks that may present at the wafer before processes or formed any process before packaging operation, during appliance of pressure and temperature at bonding process. Nevertheless, even though this crack exists, bond integrity was observed relatively enough for standing wafers together.

However, in Sample 3, the blurry profile was observed across the packaged area. Even some upper parts of the outside bond ring were given the same color as others, meaning the wafers were almost separated. Furthermore, water penetrated almost all dies since low bond integrity was observed in that sample. Similar crack propagation was observed just in Sample 2 due to the same reasons.

SEM and EDS analyses were also done to confirm the thickness/composition property obtained from the surface profiler. However, after dicing, the substrate and cap wafers of Sample 3 were almost completely separated. Therefore, no dies were obtained for SEM/EDS and Shear Test analyses. SAM image of Sample 3 was shown a lack of bond integrity already. Nevertheless, the sample was placed into the dicing process. The reason for this situation is probably related with In composition. From 37 wt% In to 54 wt% In is necessary to obtain the complete desired AuIn and $AuIn_2$ IMC structure at the bond area. Nevertheless, according to surface profiler data, Sample 3 has a lower composition value almost across the entire bonding area; therefore, that situation may cause insufficient bond integrity. Furthermore, since wafers are exposed to high vibrational effects and water duress during the dicing operation, the package's inadequate strength and bond integrity can cause the wafers' separation. A photo of Sample 3 after the dicing operation is shown in Figure 4.11. SEM and EDS analysis results for Sample 2 are shown in Figure 4.12.

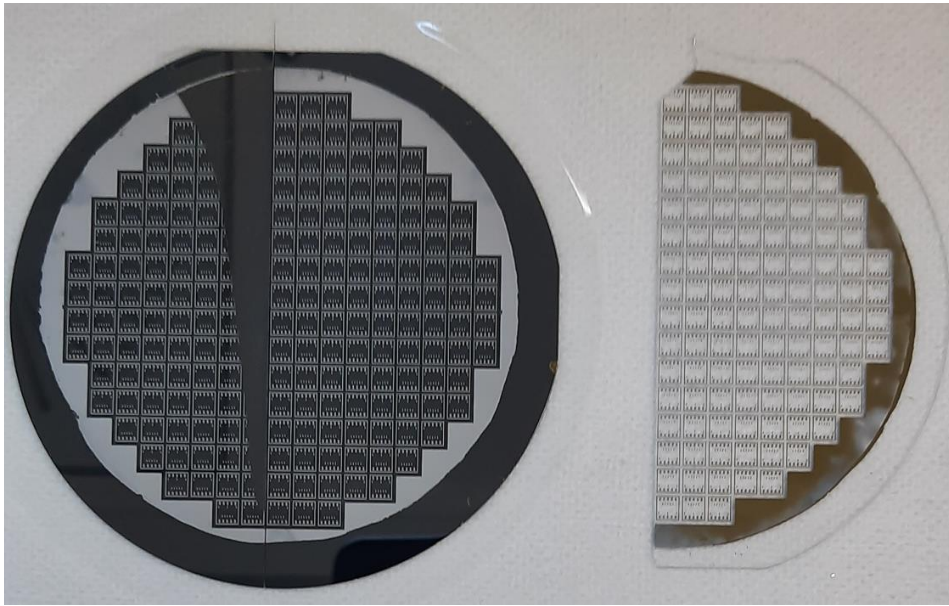

Figure 4.11 Optic Image of Combinatorial AuIn Sample 3 after Dicing Process

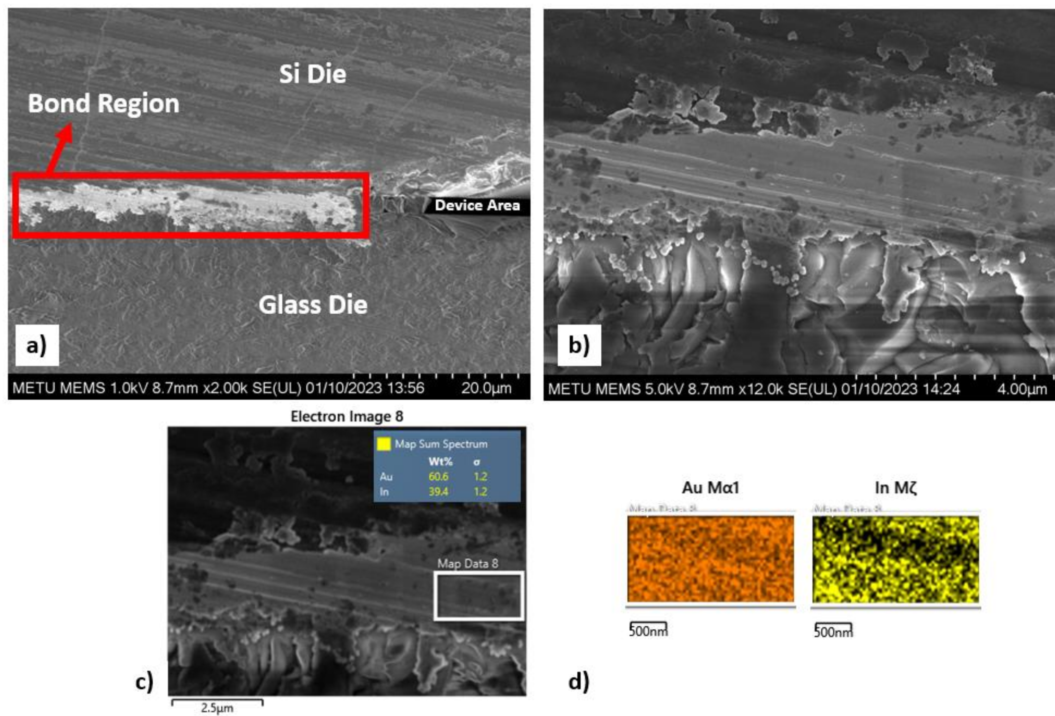

Figure 4.12 Combinatorial AuIn Sample 2 - d 10.9 a) Cross Sectional SEM Image with Package Parts, b) Cross-Sectional View of Bond Area, c) EDS Elemental Analysis and d) Elemental Distribution across Bond Area

As seen in Figure 4.12, bond integrity was satisfied along the bond region with a minimum amount of void structure. Some scratches on the surface of the cross-sectional part of the bond area were observed due to the dicing effect. However, with respect to EDS elemental analysis results, In composition was found as 39.4% wt, which is close to obtained data from the surface profiler that derived as 39.5% wt. The closeness of EDS elemental results and composition amount derived from surface profiler for both that sample and Combinatorial AuIn Sample 1 shows that thickness measurements were done in these experiments accurately. Furthermore, these data also show that In was completely mixed with Au at the bond region since no excessive or lesser amount of In was observed.

After the dicing process, most of the dies remained as the packaged structure at Combinatorial AuIn Sample 2. With respect to obtained results, statistical analysis for the yield of the sample after the dicing operation was done. Photo of Sample 2 after the dicing operation and the yield of successful dies after that operation with schematic illustration were shown in Figure 4.13.

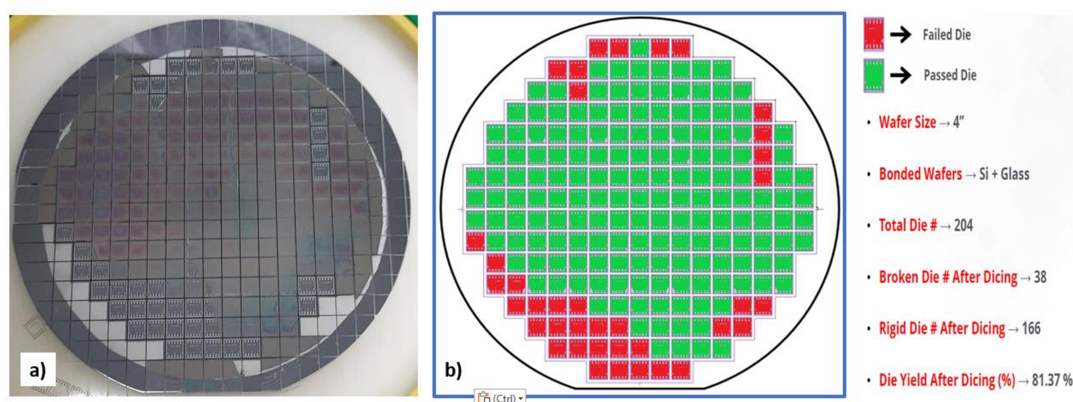

Figure 4.13 a) Photo of Combinatorial AuIn Sample 2 after Dicing and b) Dicing Yield Analysis of Combinatorial AuIn Sample 2 with Schematic Illustration

After the dicing operation of Combinatorial AuIn Sample 2, approximately 82% of the dies remained rigid, which is an acceptable ratio for the WLP process. For the remaining dies, a die-level shear test was applied. Obtained results are shown in Table 4.8.

Table 4.8 Shear Strength Values of Combinatorial AuIn Sample 2

	Shear Strength Values of Combinatorial AuIn Sample 2 (MPa) * At least 6 MPa required due to MIL-STD 883														
Region	1			2			3			4			5		
Die Number	d3.6	d4.9	d4.3	d7.4	d10.4	d8.3	d8.9	d10.11	d9.6	d9.13	d8.13	d.11.13	d14.7	d12.10	d12.11
Shear Strength (MPa)	16	14	18.	22	16	19	15	17	19	13	13	14	21	18	18
Mean of Regions	16			19			17			14			19		
Standard Deviation of Regions	2			2			2			0			1		
General Mean	17			**Maximum Mean**			19			**Maximum Value**			22		
General Standard Deviation	3			**Minimum Mean**			14			**Minimum Value**			13		

After the die level shear test, approximately 17 MPa average shear strength was achieved at Combinatorial AuIn Sample 2. Furthermore, alternation of the shear strength values was found to be relatively low due to close thickness values across regions of this sample. However, with respect to the comparison with Combinatorial AuIn Sample 3, increased In content was given better for both dicing yield and shear strength property. Nevertheless, to analyze In effect on package and bonding properties more efficiently, another combinatorial experience was tried with increasing In content for wafers.

4.1.3 Combinatorial Au-In Sample 4 and Combinatorial Au-In Sample 5

In thickness was increased due to previous samples to analyze the increased In composition effect on packaging structure. Moreover, a wafer holder that can hold two 4” wafers was used again to observe and vary in composition more efficiently. For that purpose, In deposition time was increased up to observing 2100 nm In thickness at quartz crystal 2, which is the closer crystal to In boat 1. The placement of the wafers was done just like shown in Figure 3.8. Compared to previous combinatorial studies, a 150 nm TiW diffusion barrier layer was used instead of 50

nm Ni since both diffusion layers have the same effectiveness. Schematized illustrations of In chamber and thickness values of the bonding material system with the seed layer are shown in Figure 4.14.

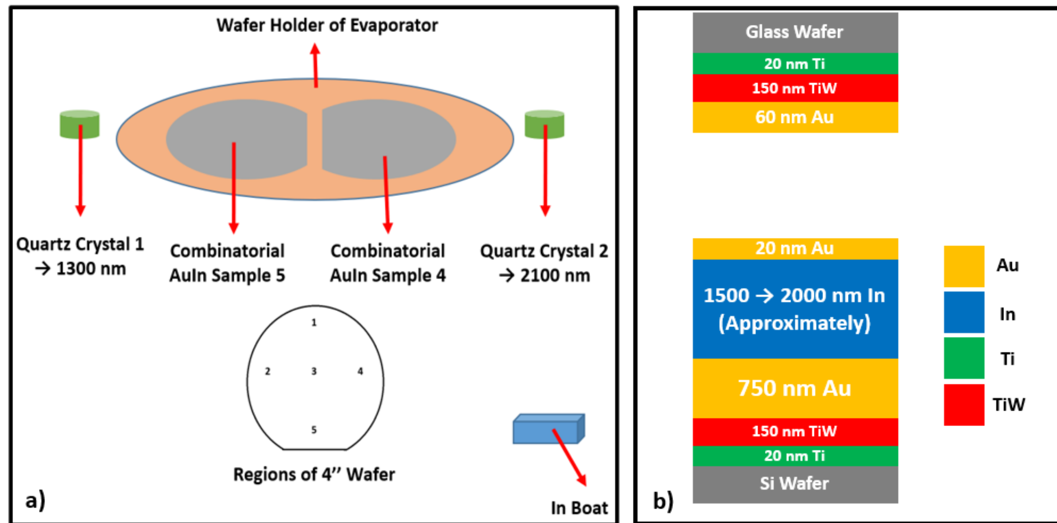

Figure 4.14 a) Schematized Illustration of Obtained Thickness Values Inside the In Chamber and b) Cross Sectional View of Deposited Thicknesses of Bonding Material System with Seed Layer

As seen in Figure 4.14, 2100 nm thickness was observed from quartz crystal 2, while 1300 nm In thickness was measured from quartz crystal 1 after In deposition. From data of these quartz crystals and also based on previous combinatorial samples, from 1500 nm to 2000 nm In thickness variance was expected. To correlate this, In thicknesses of these two samples were measured with the surface profiler. Obtained thickness values and composition values derived from thickness data for Combinatorial AuIn Sample 4 are shown in Table 4.9 and Table 4.10, respectively. The same results were shown in Table 4.11 and 4.12 for Combinatorial AuIn Sample 5.

Table 4.9 Indium Thickness Values and Statistical Data for Combinatorial Au-In Sample 4

	Thickness (nm)				
	Region 1	**Region 2**	**Region 3**	**Region 4**	**Region 5**
1	1917	1886	1882	1847	1832
2	1934	1865	1857	1861	1852
3	1929	1837	1888	1851	1813
Mean of Regions	1927	1863	1876	1853	1832
Standard Deviation of Regions	7	20	13	6	16
General Mean	1870	**Maximum Mean**	1927	**Maximum Value**	1934
General Standard Deviation	34	**Minimum Mean**	1832	**Minimum Value**	1813

Table 4.10 Indium Composition Values and Statistical Data for Combinatorial Au-In Sample 4

	Composition (wt% In)				
	Region 1	**Region 2**	**Region 3**	**Region 4**	**Region 5**
1	46.7	46.3	46.2	45.7	45.5
2	46.9	46.0	45.9	45.9	45.8
3	46.8	45.6	46.3	45.8	45.3
Mean of Regions	46.8	45.9	46.1	45.8	45.5
Standard Deviation of Regions	0.1	0.3	0.2	0.1	0.2
General Mean	46.0	**Maximum Mean**	46.8	**Maximum Value**	46.9
General Standard Deviation	0.5	**Minimum Mean**	45.5	**Minimum Value**	45.3

Table 4.11 Indium Thickness Values and Statistical Data for Combinatorial Au-In Sample 5

	Thickness (nm)				
	Region 1	**Region 2**	**Region 3**	**Region 4**	**Region 5**
1	1489	1573	1598	1593	1727
2	1456	1628	1667	1568	1774
3	1505	1690	1545	1662	1777
Mean of Regions	1483	1630	1603	1608	1759
Standard Deviation of Regions	20	48	50	40	23
General Mean	1617	**Maximum Mean**	1759	**Maximum Value**	1777
General Standard Deviation	96	**Minimum Mean**	1483	**Minimum Value**	1456

Table 4.12 Indium Composition Values and Statistical Data for Combinatorial Au-In Sample 5

	Composition (wt% In)				
	Region 1	**Region 2**	**Region 3**	**Region 4**	**Region 5**
1	40.5	41.8	42.2	42.1	44.1
2	39.9	42.6	43.2	41.7	44.7
3	40.7	43.5	41.4	43.1	44.8
Mean of Regions	40.4	42.7	42.2	42.3	44.5
Standard Deviation of Regions	0.3	0.7	0.8	0.6	0.3
General Mean	42.4	**Maximum Mean**	44.5	**Maximum Value**	44.8
General Standard Deviation	1.5	**Minimum Mean**	40.4	**Minimum Value**	39.9

As seen from obtained In thickness and composition data for Combinatorial AuIn Sample 4 and 5, almost 390 nm In thickness was measured, corresponding to 4.4% In composition variance. Furthermore, with deriving the thickest and thinnest regions data, almost nearly 17% wt In composition difference was observed. That value corresponds to 33% of the AuIn - $AuIn_2$ part since that region has 17% In the compositional range. Therefore, a relatively wide range of the aimed intermetallic region of Au-In has been tried for packaging applications with a single deposition run thanks to a combinatorial approach.

Just like Combinatorial AuIn Samples 2 and 3, a relatively high compositional variance was observed across the bonding area of Combinatorial AuIn Sample 5. In contrast, a much lower variance was observed in Combinatorial AuIn Sample 4. Similarly, this situation is related to the closeness of the sample to the In boat. As the wafer got farther away from In boat, more In thickness alteration was observed.

While the closest part, region 1, has the thickest In at Combinatorial AuIn Sample 4, region 5, the furthest part has the lowest In thickness, which is region 5. That was expected because an increment in the metal thickness was expected as part of the sample getting closer to the metal source. Furthermore, Combinatorial AuIn Sample 5 was shown the same regional In thickness results after measurements. Probably, on the contrary of Combinatorial AuIn Sample 2 and 3, these samples were placed to the wafer holder and In the thermal evaporator chamber more properly; thus, the expected regional In thickness gradient was observed with respect to the distance between samples and In source.

To analyze the bond integrity of the WLP samples, SAM analysis was done on both samples. Obtained SAM image and optic image for Combinatorial AuIn Sample 4 are shown in Figure 4.15. The SAM image of Combinatorial AuIn Sample 5 is shown in Figure 4.16.

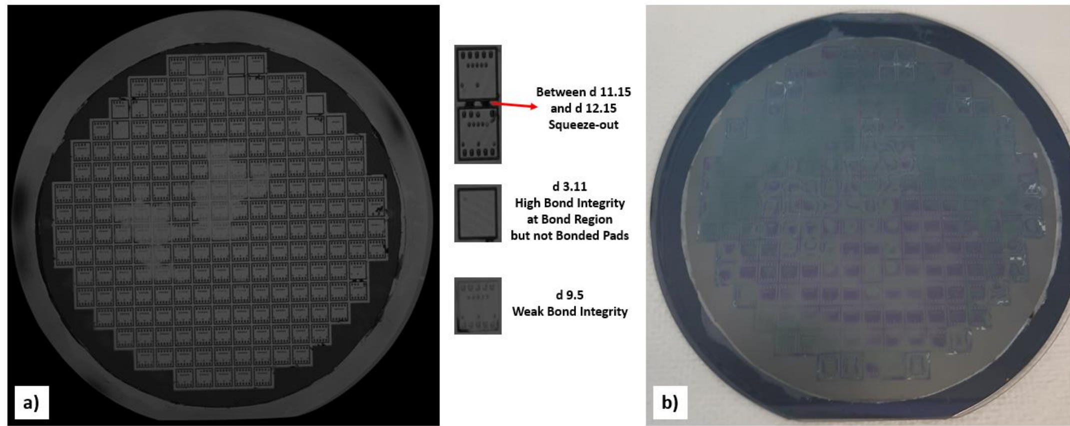

Figure 4.15 a) SAM Image of Combinatorial AuIn Sample 4 with Different Die Types and b) Optic Image of Combinatorial AuIn Sample 4 after WLP and SAM Analysis

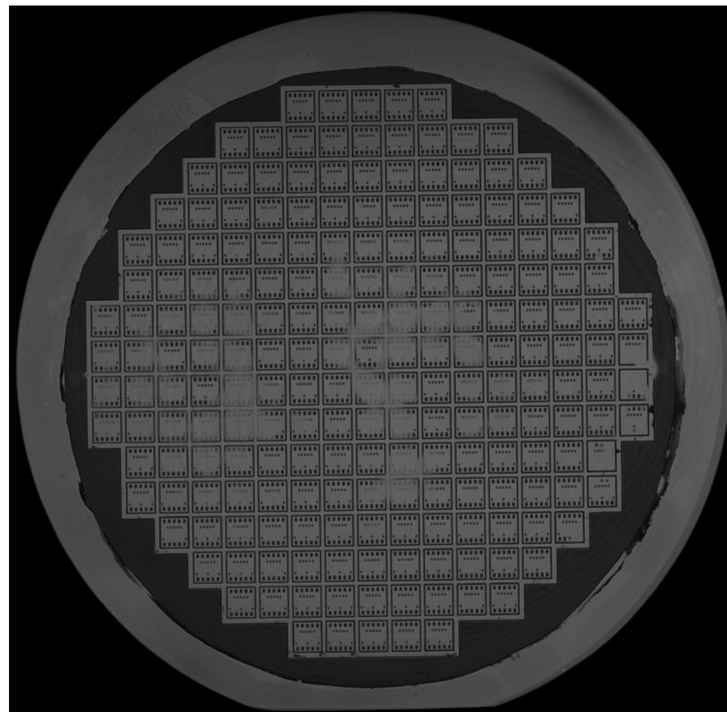

Figure 4.16 SAM Image of Combinatorial AuIn Sample 5

As seen from both SAM images of Combinatorial AuIn Samples 4 and 5, a whitish color was observed in the middle of the samples, which probably corresponds to low bond integrity. This contrast means reflection of the sound waves sent from the transducer was reflected instead of passing through so peak; in other words, white, a

like color, was observed in the image. This situation is probably related to non-uniform force appliances during the WLP process in some regions. As seen from the optic image in Figure 4.15, this region shows circular light reflection that also was shown non-regular sound wave reflection at SAM analysis, so whitish color was obtained.

Furthermore, some squeezed-out regions were observed at both wafers after SAM analysis, while Combinatorial AuIn Sample 4 had a higher amount, especially edge sides. Some liquefied In during bonding could overflow at the near side of the bond region during bonding due to pressure, and therefore these regions could be observed. Since most of the squeezed-out regions were observed at the edge sides of the package, this situation also shows the non-uniformity of the force appliance during bonding. While the edge sides of the wafer were exposed to relatively higher bonding pressure, the middle sides were exposed to relatively lower pressure; therefore, probably due to that, these structures were observed in these packages. Optical microscope images of the squeezed-out region between d 11.15 and d 12.15 of Combinatorial AuIn Sample 4 were shown in Figure 4.17 with different magnifications.

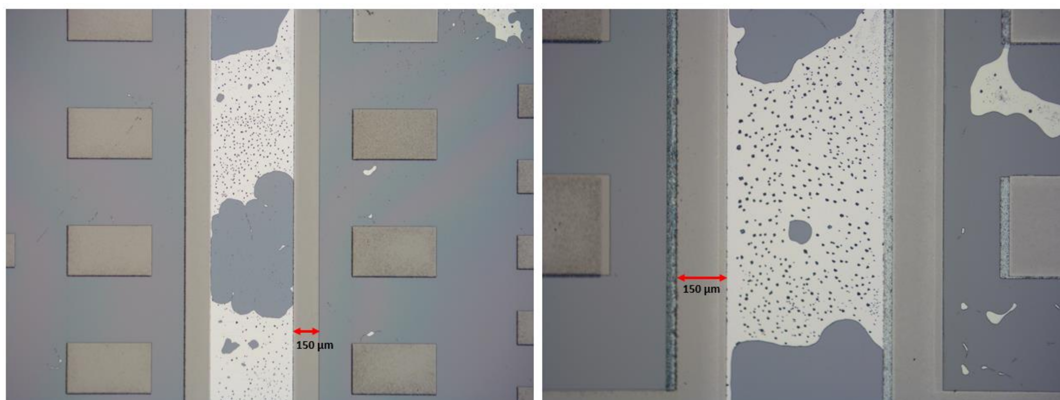

Figure 4.17 Optic Microscope Image of Squeezed-Out Region of Combinatorial AuIn Sample 4 between d 11.15 and d 12.15

As seen in Figure 4.17, the squeeze-out region has In based matrix structure with tetragonal-like precipitates. These precipitates are probably formed IMC structures

that have 5-10 μm size approximately. This situation shows that IMC formation during bonding has happened that provided proper bonding procedure.

Moreover, in both samples, while high bond integrity was observed at the bond region of some dies, pads inside the die package were shown no bond integrity, just like d3.11, shown in Figure 4.15. This situation is probably related to the deformation of the bond structure of these pads during the packaging process.

SEM and EDS analyses were done to check In composition and bond integrity to compare composition values derived from In thickness data from the surface profiler. Obtained results for Combinatorial AuIn Samples 4 and 5 were shown in Figure 4.18 and Figure 4.19, respectively.

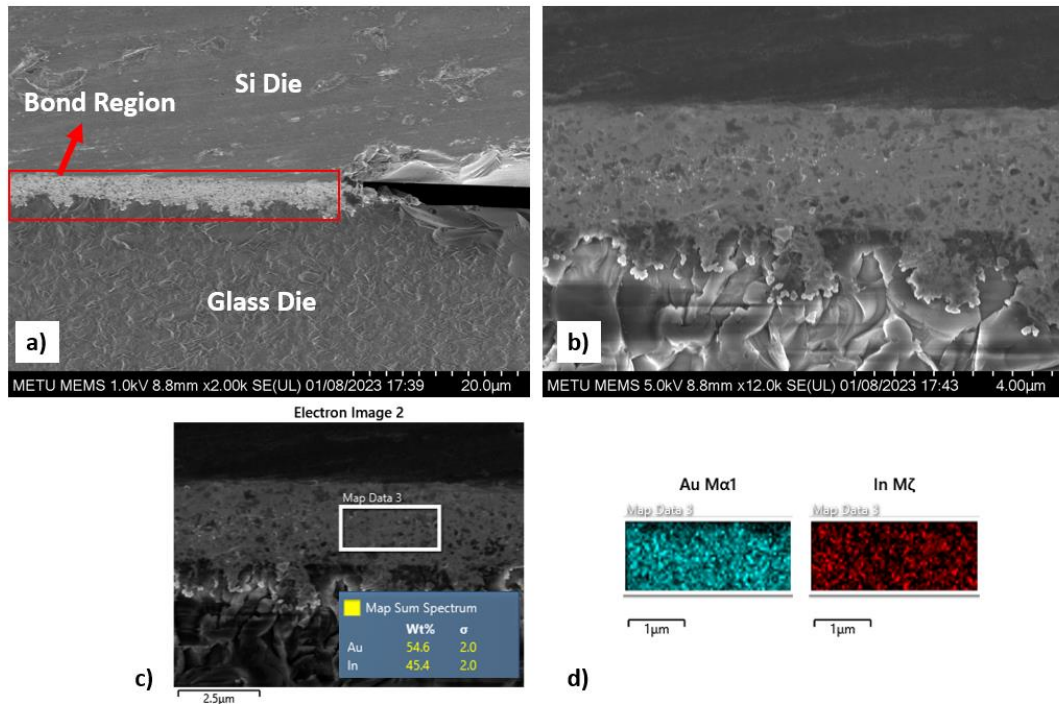

Figure 4.18 Combinatorial AuIn Sample 4 - d 10.9 a) Cross Sectional SEM Image with Package Parts, b) Cross-Sectional View of Bond Area, c) EDS Elemental Analysis and d) Elemental Distribution across Bond Area

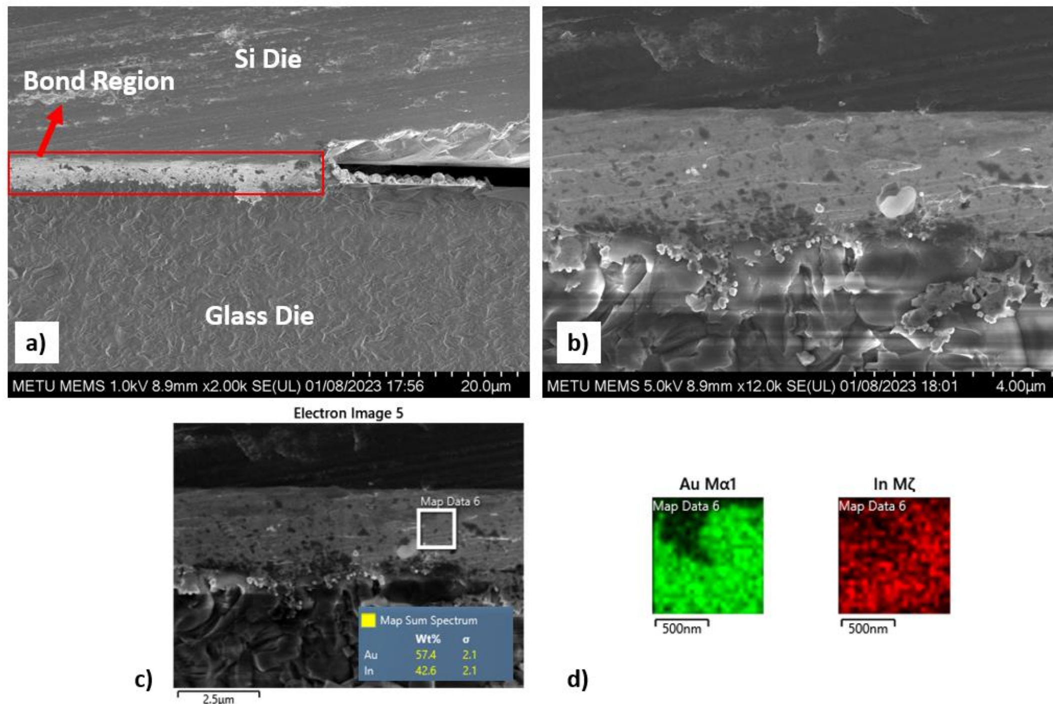

Figure 4.19 Combinatorial AuIn Sample 5 - d 10.9 a) Cross Sectional SEM Image with Package Parts, b) Cross-Sectional View of Bond Area, c) EDS Elemental Analysis and d) Elemental Distribution across Bond Area

As seen from Figure 4.18 and Figure 4.19, near voidless structure and, due to that, high bond integrity were observed. Furthermore, just like previous samples, obtained composition data derived from the surface profiler and EDS analysis shows the closeness, which means a uniform Au-In mixture was obtained across a bond area of the packaged samples. This also indicates that almost complete dissolution of In and Au in each other is achieved because the amount of In composition calculated via the measured In thickness was also obtained from the EDS analysis.

After SAM and visual inspection analyzes were done, WLP samples were diced. While only four dies were separated at Combinatorial AuIn Sample 4, corresponding to 98% yield, all packaged dies remained rigid at Combinatorial AuIn sample 5; therefore, 100% yield was obtained after the dicing operation. These samples were given higher efficient results with respect to other samples that show increased In content could provide more efficient bond integrity and packaging results. Photo of Sample 4 after the dicing operation and the yield of successful dies after that

operation with schematic illustration were shown in Figure 4.20. Photo of the Combinatorial AuIn Sample 5 after the dicing process was shown in Figure 4.21. Some packaged dies were taken to the shear test; therefore, some dies are missing even though they were rigid in Figure 4.21.

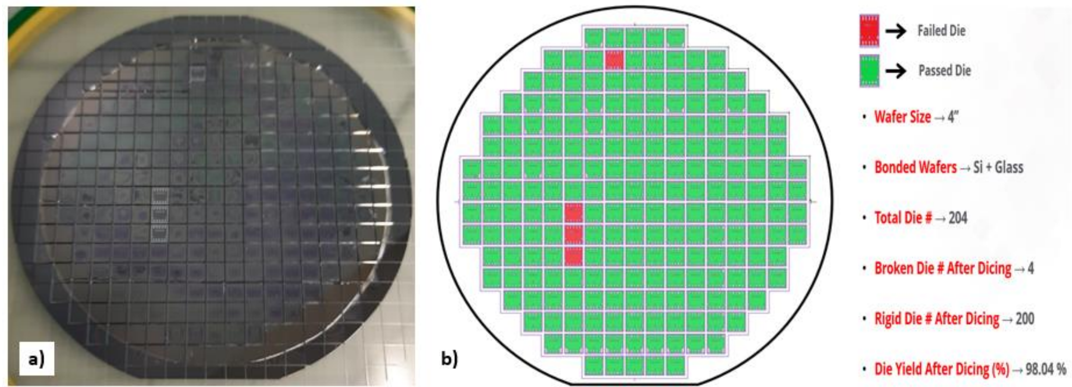

Figure 4.20 a) Photo of Combinatorial AuIn Sample 4 after Dicing and b) Dicing Yield Analysis of Combinatorial AuIn Sample 4 with Schematic Illustration

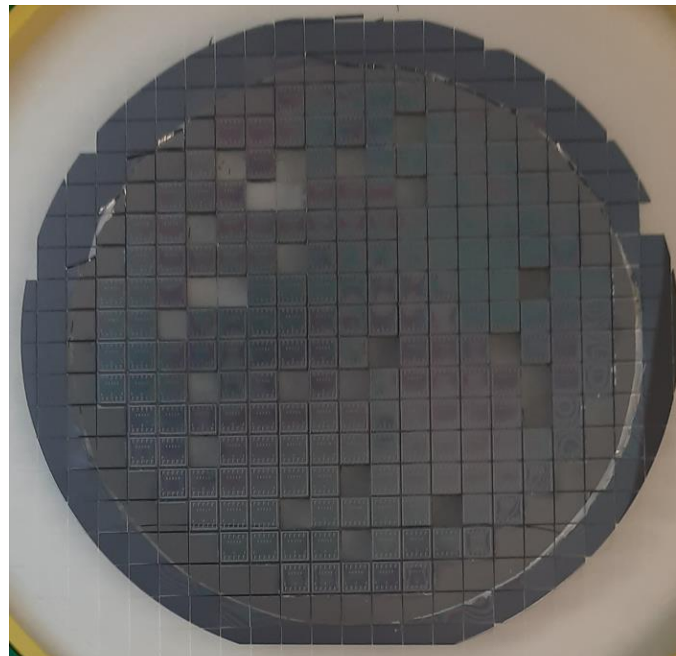

Figure 4.21 Optic Image of Combinatorial AuIn Sample 5 after Dicing Process (In this Figure, missing dies were taken for Shear Test)

After the dicing process was done for both samples, a die-level shear test was applied to these samples to observe the mechanical strength of the dies. Obtained results with

statistical data were shown in Table 4.13 and Table 4.14 for Combinatorial AuIn Samples 4 and 5, respectively.

Table 4.13 Shear Strength Values of Combinatorial AuIn Sample 4

	Shear Strength Values of Combinatorial AuIn Sample 4 (MPa) * At least 6 MPa required due to MIL-STD 883														
Region	1			2			3			4			5		
Die Number	d2.7	d4.4	d4.9	d8.3	d7.5	d10.4	d6.10	d9.10	d6.5	d9.14	d11.14	d.9.17	d13.7	d14.4	d14.9
Shear Strength (MPa)	28.	48	37	14	13	12	19	24	17	20	23	21	10	20	22
Mean of Regions	38			13			20			22			18		
Standard Deviation of Regions	8			1			3			1			5		
General Mean	22			**Maximum Mean**			38			**Maximum Value**			48		
General Standard Deviation	10			**Minimum Mean**			13			**Minimum Value**			10		

Table 4.14 Shear Strength Values of Combinatorial AuIn Sample 5

	Shear Strength Values of Combinatorial AuIn Sample 5 (MPa) * At least 6 MPa required due to MIL-STD 883														
Region	1			2			3			4			5		
Die Number	d3.6	d4.4	d4.9	d8.3	d5.3	d12.3	d9.10	d10.7	d6.6	d9.14	d7.15	d.11.14	d13.7	d14.4	d14.9
Shear Strength (MPa)	15	12	17	9	14	15	12	17	14	17	14	19	16	13	16
Mean of Regions	15			13			14			17			15		
Standard Deviation of Regions	2			3			2			2			1		
General Mean	15			**Maximum Mean**			17			**Maximum Value**			19		
General Standard Deviation	2			**Minimum Mean**			13			**Minimum Value**			9		

As seen from the shear strength values of Combinatorial AuIn Sample 4 and 5, higher shear strength values were obtained from Sample 5. Especially at region 1 of Combinatorial AuIn Sample 4, which is closer part to the In boat 1, was given the highest strength values. Both these results were shown that the shear strength of the packaged dies was increased with increased In composition.

However, even though Combinatorial AuIn Sample 4 has relatively lower In thickness alteration with respect to lower standard deviation value compared to Combinatorial AuIn Sample 5, higher shear strength alteration was observed. This situation can be related to non-uniform force appliances during the WLP process. As force value changes along the surface of the wafers regionally, different shear strength values could be obtained with respect to that. This problem makes it difficult to clear composition/property relationship analysis regionally across the wafer. In order to reduce this effect, a total of 15 dies were tested for both samples with 3 die selections from each region, and yet, since Combinational AuIn Sample 4 had a higher average shear strength value, a comparison of In thickness/shear strength based on composition could be obtained on the basis of samples.

4.1.4 Comparison of Combinatorial Au-In Samples

After all the combinatorial optimization steps, the data from these 5 samples were compared to obtain the optimum composition/property relationship of the Au-In binary system used for the WLP process. For this purpose, obtained data from these 5 samples were shown in Table 4.15 for comparison. Furthermore, investigated composition values with combinatorial approaches were shown on the phase diagram in Figure 4.22.

Table 4.15 Properties of Combinatorial AuIn Samples

	Combinatorial AuIn Sample 1*	Combinatorial AuIn Sample 2	Combinatorial AuIn Sample 3	Combinatorial AuIn Sample 4	Combinatorial AuIn Sample 5
Thickness of In (Surface Profiler) (nm)	1502	1434	1211	1870	1617
Composition of In (Surface Profiler) (%)	40.6	39.5	35.6	46.0	42.4
Standard Deviation of Composition of In (Surface Profiler) (%)	1.1	0.5	1.2	0.5	1.5
Composition of In (EDS) (%)	40.8	39.4	NA**	45.4	42.6
AuIn and $AuIn_2$ Ratio (%)	76.8% AuIn 23.2% $AuIn_2$	83.2% AuIn 16.8% $AuIn_2$	NA**	45.1% AuIn 54.9% $AuIn_2$	66.4% AuIn 33.6% $AuIn_2$
Dicing Yield (%)	68.13	81.37	0	98.04	100
Shear Strength	12	17	NA**	22	15

* Combinatorial AuIn Sample 1 has bond misalignment
** NA: Not Applicable

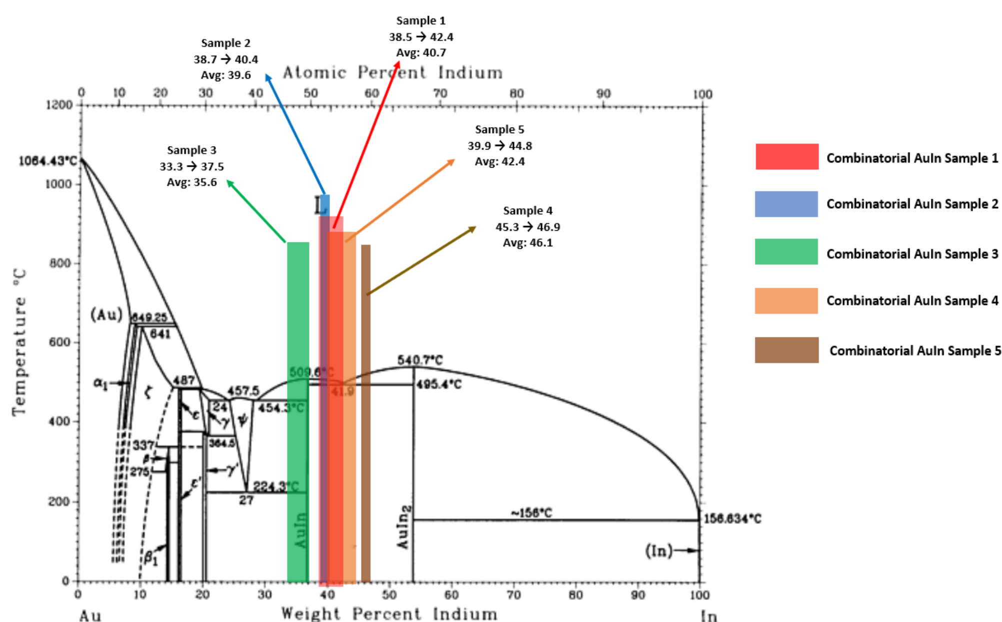

Figure 4.22 Position of All Combinatorial Samples in Au-In Phase Diagram and In Compositions Examined with Combinatorial Approach

As seen in Figure 4.22, a wide range of the Au-In phase diagram was investigated with a combinatorial approach. Besides inside the region of AuIn - $AuIn_2$ IMCs, the left side of the AuIn IMC region was also investigated to observe the effect of other phases on bonding. The packaged structure could not be obtained as a result of Combinatorial AuIn Sample 3 trials corresponding to the sample in that region. Therefore, it became clear that for successful packaging, the packaged structure should only have AuIn and $AuIn_2$ IMCs.

Furthermore, as seen in Figure 4.22, approximately 40% of the AuIn - $AuIn_2$ IMCs region in total was investigated for WLP by the combinatorial approach. Moreover, as seen from Table 4.15, composition data derived from the surface profiler and EDS analysis were shown closeness for all samples, which means Au-In elements were distributed homogeneously along bond structure for all samples. Furthermore, composition/property data was obtained from each sample, and with respect to that data, Combinatorial AuIn Sample 4 has the best properties due to other samples. This shows that increased In content, therefore, increased $AuIn_2$ ratio at bond structure gives better properties for packaging. For this purpose, at least, In composition of Combinatorial AuIn Sample 4 was aimed at a new WLP trial with a cap cavity for checking hermetic properties also. More than this amount of In content would also be suitable for the system because the theory that increased In content can better affect bond quality has been observed in previous studies.

4.1.5 Au-In WLP Sample with Cap Cavity

After the best composition/property relationship was found with combinatorial optimization for Au-In binary TLP bonding system at WLP, at least 2000 nm In thickness was aimed for 750 nm Au usage. For this purpose, instead of the non-rotating holder and usage of the one In boat during thermal evaporation, a regular In deposition procedure was used that included rotation of the sample holder with 10 rpm and usage of the two diagonal In boats. Therefore, totally uniform In thickness along all bond areas was aimed. The sample in this experiment was named Cavity

AuIn Sample 6. Since 1 sample was prepared for WLP, In holder that can hold only one 4” wafer was used for this experiment. Seed layers kept as same with Combinatorial AuIn Samples 4 and 5. Schematized illustration of setup during In thermal evaporation of Cavity AuIn Sample 6 and cross-sectional view of the system with seed and bonding material thicknesses as shown in Figure 4.23.

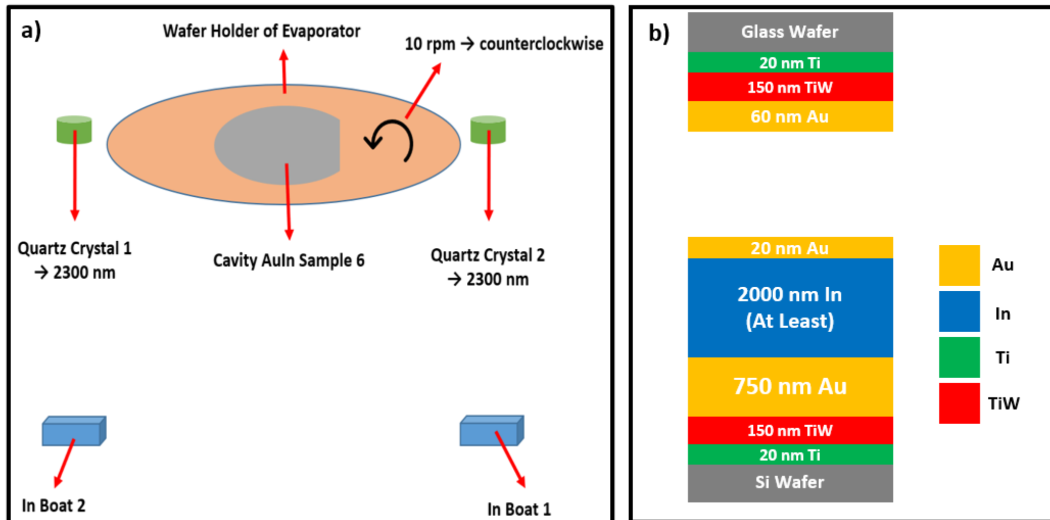

Figure 4.23 Schematized Illustration of Obtained Thickness Values Inside the In Chamber and b) Cross Sectional View of Deposited Thicknesses of Bonding Material System with Seed Layer

As seen in Figure 4.23, more than 2000 nm In thickness was observed from both quartz crystals because of the effect of observation of more In to bond quality was also want to be observed since positive effects of that phenomenon were observed from previous combinatorial experiments. After In deposition, In thicknesses were measured with a surface profiler. Since uniform In thickness distribution has been expected, 5 measurements were done with 1 measurement from each region of the wafer. Obtained In thickness values and In composition derived from thickness data were shown in Table 4.16 and Table 4.17, respectively.

Table 4.16 Indium Thickness Values and Statistical Data for Cavity AuIn Sample 6

	Thickness (nm)				
	Region 1	Region 2	Region 3	Region 4	Region 5
	2200	2203	2207	2208	2210
Mean	2206				
Standard Deviation	4				

Table 4.17 Indium Composition Values and Statistical Data for Cavity Au-In Sample 6

	Composition (wt% In)				
	Region 1	Region 2	Region 3	Region 4	Region 5
	50.1	50.1	50.2	50.2	50.2
Mean	50.2				
Standard Deviation	0.0				

As seen from Table 4.16 and Table 4.17, In has been uniformly deposited across all surfaces of the bond region since a low standard deviation value was observed after measurements. The composition of the In was exceed the values of the previous studies. However, since increased In content, in other words, increased $AuIn_2$ ratio on the bonding area, has a positive effect on bond quality, this situation was beneficial for package quality. Furthermore, to observe bond integrity SAM inspection was done. Obtained SAM image of that sample is shown in Figure 4.24.

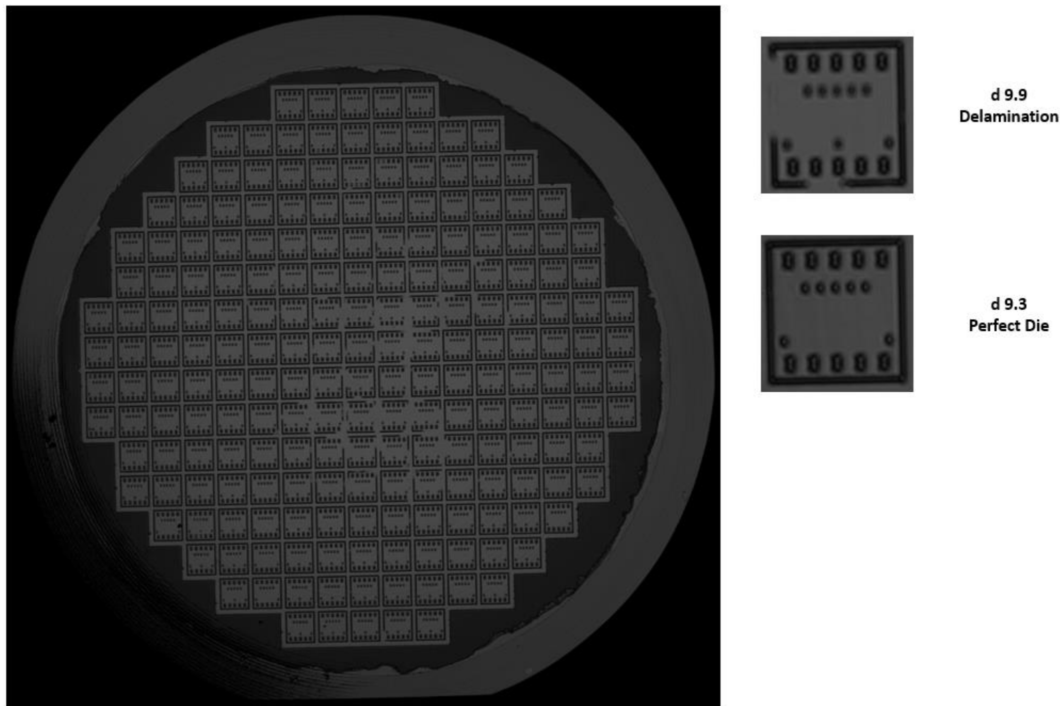

Figure 4.24 SAM Image of Cavity AuIn Sample 6 with Different Die Types

As seen in Figure 4.24, most of the dies stay rigid with high bond integrity. Nevertheless, some delaminated regions were observed on some of the dies, especially in the middle regions. The reason for that situation is probably experimental error during the photolithography stage of the production of this sample. If PR is not coated on the wafer properly during the deposition of the metal layers, the wafer gets heated due to the sputtering effect. Therefore, this causes the stripping away of the bond region during the lift-off process. Nevertheless, most of the dies remained rigid with respect to the SAM image. Therefore, after WLP, a dicing operation was done on that sample. After visual inspection, the obtained image is presented in Figure 4.25.

Figure 4.25 Image of Cavity AuIn Sample 6 After Dicing Process

As seen in Figure 4.25, due to the delamination problem mentioned before, some of the packaged dies were separated from each other. Even separation does not exist, due to vibration and water injection during the dicing process; the wafer was penetrated into the packaging area of that dies. Furthermore, some crack propagations were observed from the glass side of the package in some regions after the dicing process. This caused hermeticity loss of the package for these dies even though the bond quality was satisfied. Nevertheless, most of the dies remained as rigid after the dicing operation. Therefore, for these remaining dies, die-level shear tests were applied. Since In thickness was uniform along all bond regions of the sample, 4 dies were tested. Obtained results are shown in Table 4.18.

Table 4.18 Shear Strength Values of Cavity AuIn Sample 6 with Statistical Data

	Shear Strength Values of Cavity AuIn Sample 6 (MPa) * At least 6 MPa required due to MIL-STD 883			
Die Number	d 1.1	d 15.9	d 7.1	d 9.17
	23	33	31	26
Mean	28			
Standard Deviation	4			

As seen from Table 4.18, relatively low shear strength alteration was observed along dies due to uniform In thickness distribution. However, there is a small difference was still existed at these dies. This situation was probably related to non-uniform force distribution during the WLP process. Due to that, the sticking of dies was shown differently individually, which caused shear strength alteration. Nevertheless, obtained shear strength values are higher than in previous experiments, which confirmed the positive effect of increased In composition amount on package quality.

Furthermore, before the WLP operation, the cap cavity depth of the Si part of the package was measured with an optic surface profiler. Obtained results are shown in Figure 4.26.

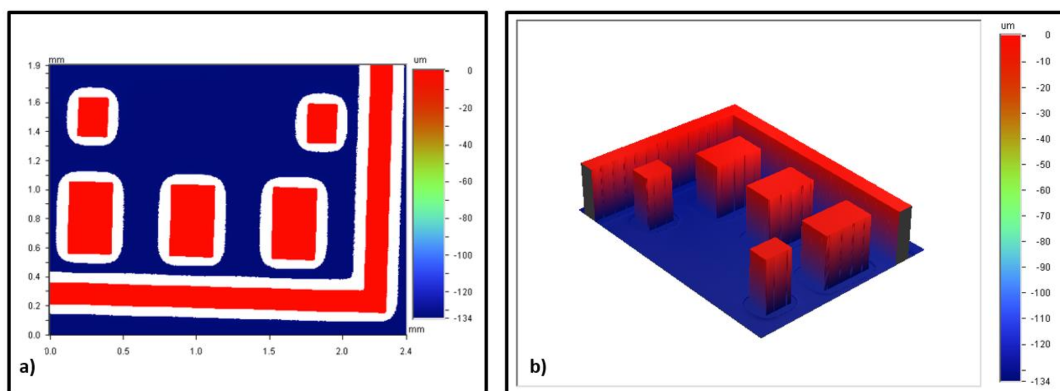

Figure 4.26 a) Cap Cavity Depth Measurement Result with Optic Surface Profiler for Cavity AuIn Sample 6 and b) Iso-sectional View of the Cap Cavity Depth with Optic Surface Profiler

As seen in Figure 4.26, approximately 130 µm cap cavity depth was observed from the optic surface profiler. That was the desired amount from DRIE process with respect to the applied procedure. Nevertheless, to check cap cavity depth, bond quality, and comparison obtained In composition from the surface profiler, SEM and EDS analyses were done. Obtained results are represented in Figure 4.27.

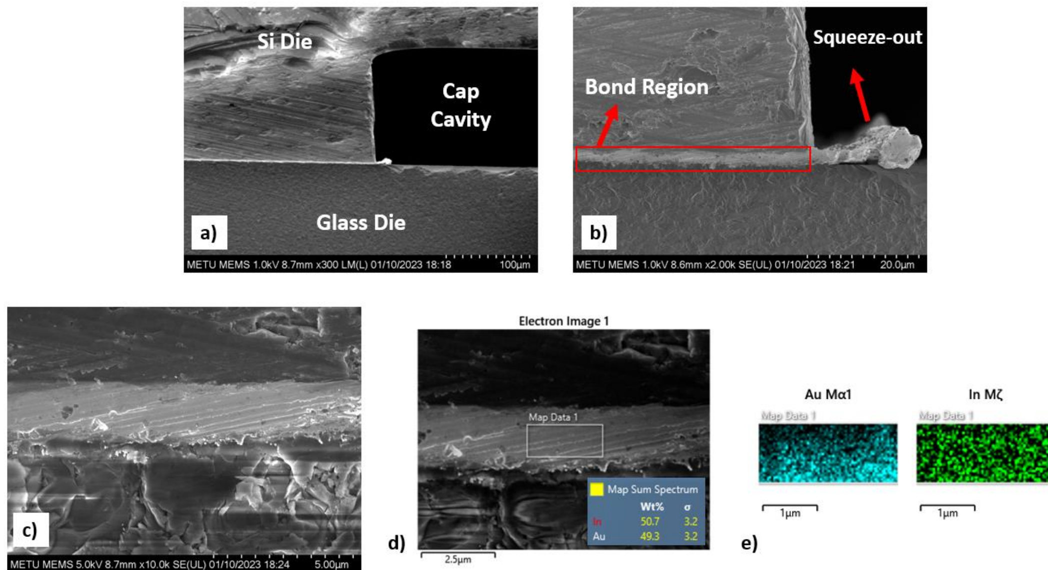

Figure 4.27 Cavity AuIn Sample 6 a) Cross Sectional SEM Image with Package Parts, b) Bond Region and Squeeze-out Parts of the Packaged System, c) Cross-Sectional View of Bond Area, d) EDS Elemental Analysis and e) Elemental Distribution across Bond Area

As seen in Figure 4.27, the cap cavity was observed as 130 µm approximately at SEM analysis. Obtained results were shown to be similar to the measured value from the optic surface profiler therefore, the amount of cap cavity was confirmed with these characterization methods. Furthermore, from EDS analysis, In composition was found as 50.7% wt, which was also shown similarity with the derived value from the surface profiler, that is 50.16% wt In. Therefore, just like in previous samples, the correlation between values of the surface profiler and EDS analysis was confirmed for that experiment. Nevertheless, even squeeze out existed for that sample shown at Figure 4.27; since compositional distribution was shown similarity at both surface profiler and EDS results, complete dissolution of bonding elements

between each other was obtained with adequate diffusion barrier properties since no elemental loss was observed.

Furthermore, since indium content was increased in that sample, the requirement of time and temperature during the bonding process also must have been increased for uniform dissolution of bonding metals into each other and complete TLP bonding. However, both shear test results and indium composition distribution after SEM/EDS analyzes were shown that Recipe CombAuIn 1 that used for all Au-In samples in this thesis was shown adequate temperature and time properties since complete dissolution was observed with respect to these characterization methods.

After elemental distribution with compositional value, shear strength, and bond integrity parameters have been confirmed via these characterization methods, to check the hermeticity quality of the packaged sample, the cap thinning procedure was applied with the DRIE process. With respect to the results of the COMSOL Simulation data, the aim was set to obtain at most 25 µm membrane thickness to observe the deflection effect. However, after the first DRIE trials, packaged dies were separated from each other. This situation was probably related to thermal stress generated during the dry etching process due to the difference in thermal expansion coefficient between Si and Glass materials. To eliminate this problem, dies were bonded onto the wafer by wax-type bonder material to increase thermal conductance between the holder and samples during the DRIE process. Dies were not separated from each other during the procedure however, due to anisotropic etching of the Si part of the packaged sample, some holes were formed while the remained surface has still certain thickness. Even DRIE process kept going, some Si parts of the package die were stripped away from the structure Nevertheless, one of the dies has been remained rigid, and therefore, cap deflection was observed. Photo of the die surface with cap deflection after the DRIE process is shown in Figure 4.28.

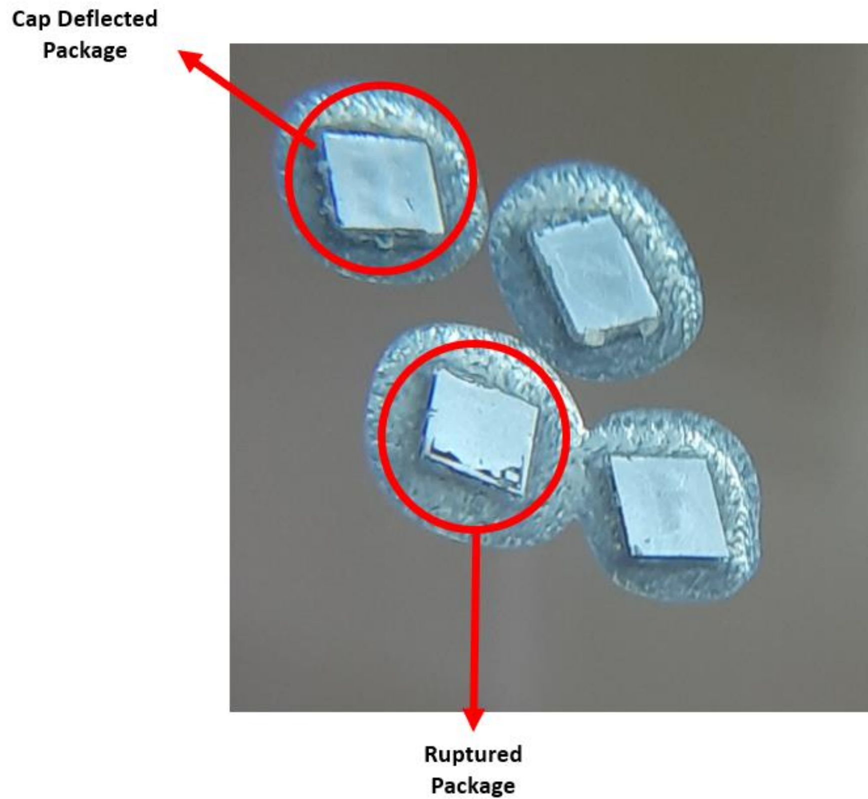

Figure 4.28 Photos of the Dies after DRIE Process with Cap Cavity Formation and Ruptured Si Part of the Die

To analyze the depth of the cap deflection amount, the surface of the die was inspected with an optic surface profiler. Obtained results were compared with simulation data of COMSOL Multiphysics. With respect to these, obtained images from the optic surface profiler, a comparison of these images with an iso-sectional view of the simulation result and 3 optic surface profiler measurement results is shown in Figure 4.29.

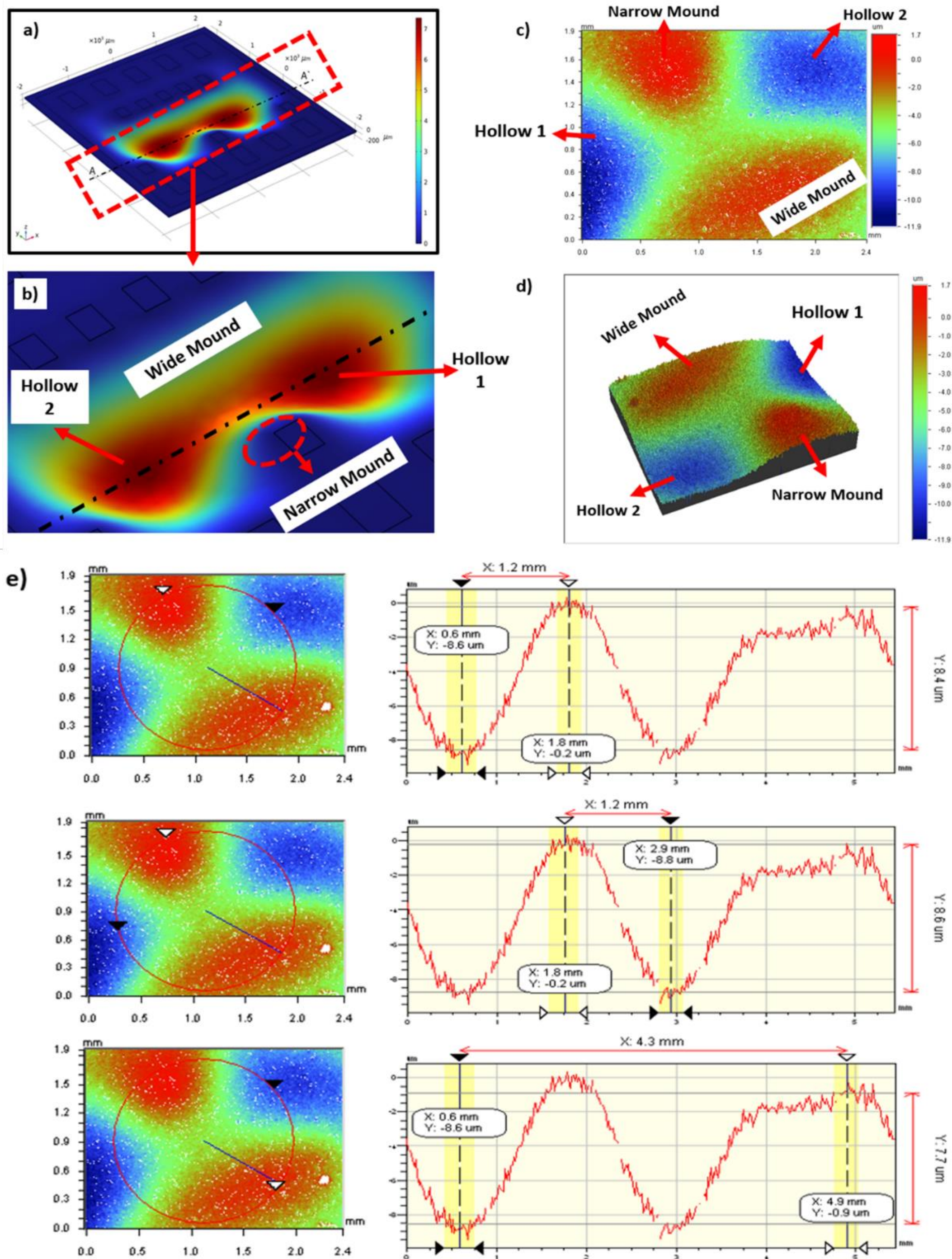

Figure 4.29 a) Iso-sectional View from COMSOL Multiphysics Software, b) Magnified View of the Cavity Deflection Area of the Image of COMSOL Multiphysics Simulation Image c) 2D Depth Image of Cap Deflection with Optic Surface Profiler, d) Iso-sectional Representation of Cap Cavity with Optic Surface Profiler and e) 3 Different Cap Cavity Depth Measurements with Optic Surface Profiler

As seen in Figure 4.29, the topological images obtained from the optical surface profiler show similar visuality to the image obtained from COMSOL Simulation. This correlation shows that obtained data from simulation has a similarity with experimental results. Furthermore, after 3 measurements, approximately 8.2 µm cap deflection depth was found from the surface profiler, which corresponds to approximately 24 µm membrane thickness with respect to simulation data. According to the cap deflection depth value obtained, approximately 0.2 mbar package pressure value was found through simulation, which shows that the obtained package has a hermetic structure.

Furthermore, the He Leak test was tried to check the vacuum pressure level inside the package. However, no pressure level was observed during the test. This situation was probably related to the lack of total volume of the package. To increase total volume during a test, several dies were inserted into the He Leak Test chamber. However, still, no value was observed after that test.

4.2 WLP Trials with Au-In-Sn Ternary System

Since the Au-In-Sn system has not been studied in the literature before for WLP, a designed amount of bonding material was deposited onto the wafers' surface to analyze the behavior and suitability for WLP of this candidate system. For this purpose, a combination of Au-Sn eutectic composition was designed with the addition of In to enhance TLP properties. Designed thickness values for that ternary system with seed layers were shown schematically with a cross-sectional view at Figure 4.30.

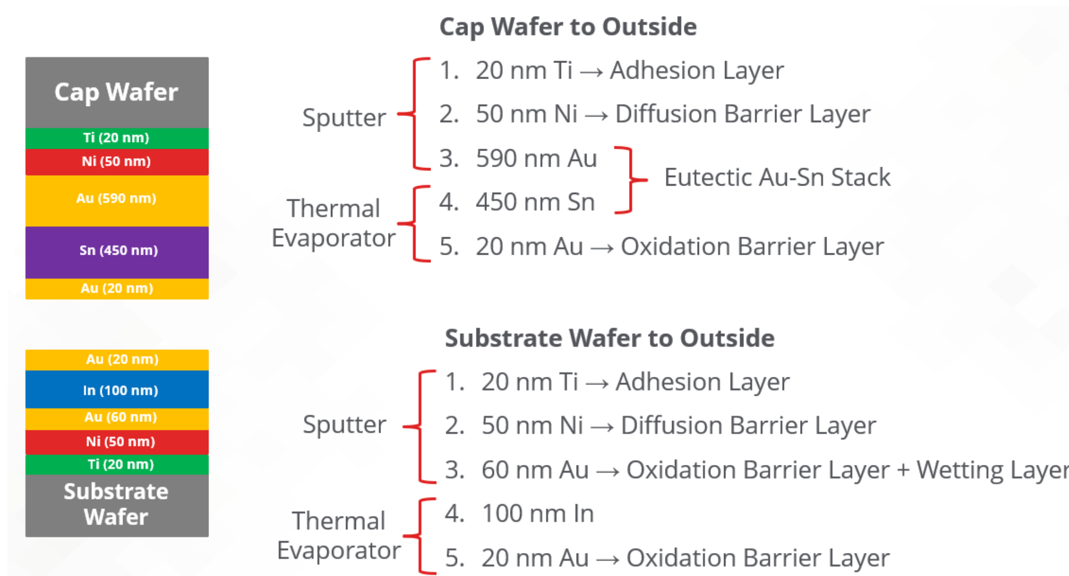

Figure 4.30 Schematic Representation of Bonding System for WLP with Au-In-Sn Ternary System with Definition of the Layers

As seen in Figure 4.30, for the 590 nm Au layer, 450 nm Sn thickness was aimed. With thickness to composition calculations, that amount of Sn thickness is excessive however, since porous Sn deposition was observed at previous studies in METU MEMS Research Center with Varian 3119 Thermal Evaporator, 450 nm Sn was aimed for obtain eutectic composition due to optimization parameters of previous studies [54], [32].

To understand the thermal profile of this ternary material stack, all candidate bonding materials with seed layers that are shown at Figure 4.30 were coated onto one 4” wafer’s surface for Differential Scanning Calorimeter (DSC) analysis. Obtained DSC graph is shown in Figure 4.31.

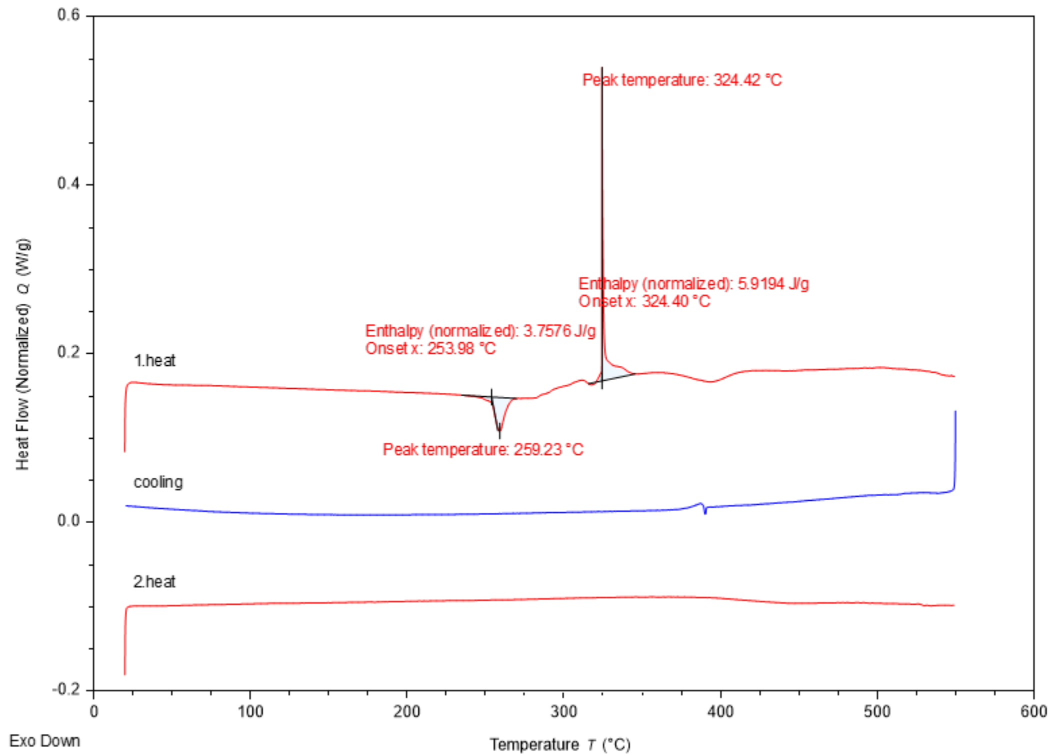

Figure 4.31 DSC Result of Au-In-Sn Ternary System

As seen in Figure 4.31, this candidate material stack gives an exothermic peak of around 260 °C. That peak probably corresponds to phase formation with respect to heat treatment. Furthermore, not any self-melting temperature of Sn or In was observed at the first heating procedure, which means elements were mixed into each other during heating. Moreover, a large endothermic peak was observed around 324 °C after the DSC test. This peak indicates melting temperature of this ternary alloy is a suitable temperature value for the WLP of many MEMS devices. Therefore, the bonding temperature has to be aimed at at least 324 °C temperature for this system. After cooling, any peak was not observed at the second heating operation, and this situation shows that the Au-In-Sn candidate material system was shown TLP behavior. Accordingly, with the bonding temperature above 324 °C and a certain time elapsed during bonding, this ternary material system can withstand at least 500 °C according to DSC results.

Furthermore, besides DSC analysis, the behavior of this ternary material system with respect to temperature was also simulated with Thermo-Calc Software. Due to that, isothermal ternary phase diagrams of this material system for 300 °C and 350 °C were generated via that software. Obtained phase diagrams are shown in Figure 4.32.

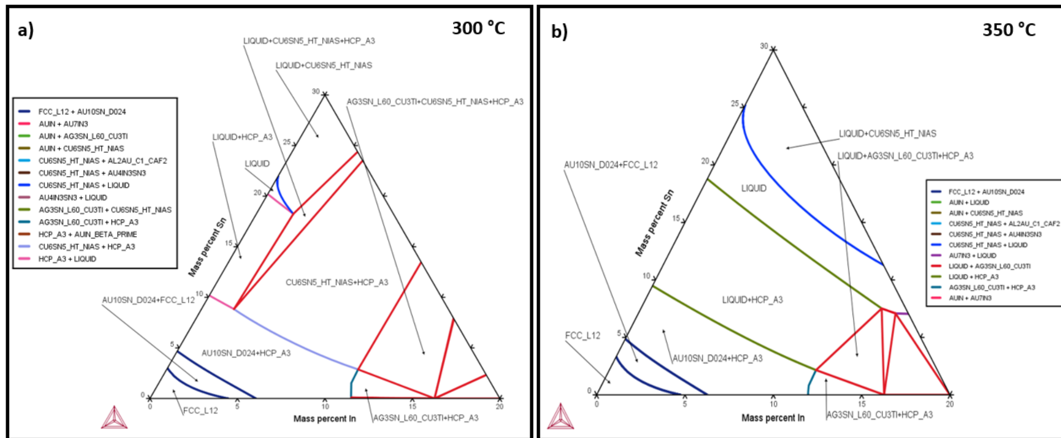

Figure 4.32 a) Isothermal Ternary Phase Diagram of Au-In-Sn Material System at 300 °C and b) Isothermal Ternary Phase Diagram of Au-In-Sn Material System at 350 °C

As seen in Figure 4.32, liquid phase formation could happen at both 300 °C and 350 °C with respect to phase diagrams. However, this material system gives more composition range for liquid formation at 350 °C, and since the melting point of this material system was found at 324 °C with respect to deposited thicknesses, 350 °C bonding temperature was selected for WLP.

Furthermore, SEM and EDS analyses were done to an inspection of the elemental composition and observation of the phase formation after some heat treatments. At first heat treatment, the sample was heated up to 350 °C and was held at that temperature for 1 hour in a vacuum atmosphere. At the second heat treatment, another identical sample was annealed at 350 °C for 5 hours in an N_2 atmosphere. Both samples were analyzed with SEM and EDS characterization methods. Obtained results for vacuum and N_2 atmosphere annealing conditions are shown in Figure 4.33 and Figure 4.34, respectively.

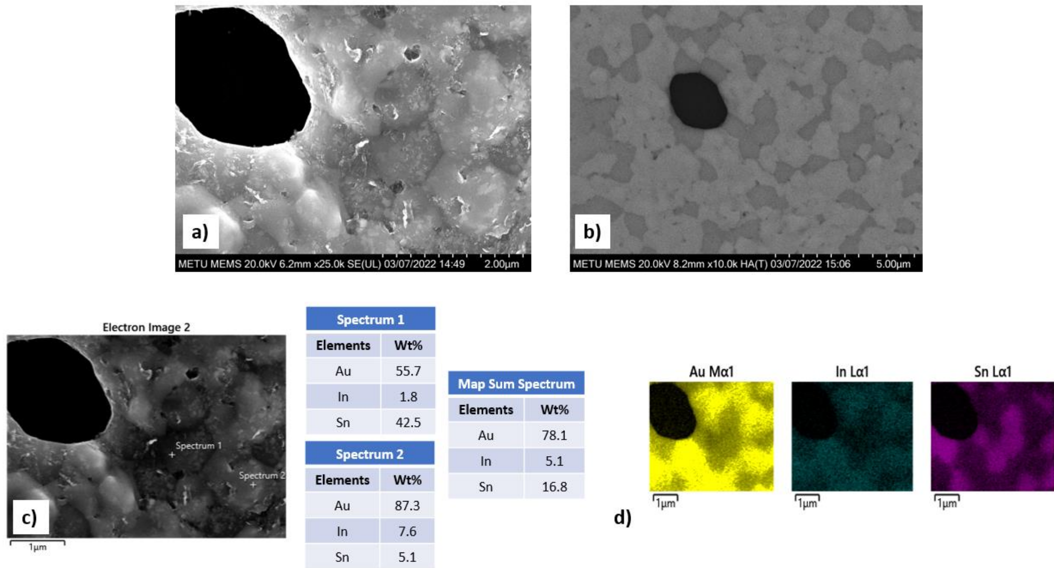

Spectrum 1	
Elements	Wt%
Au	55.7
In	1.8
Sn	42.5

Spectrum 2	
Elements	Wt%
Au	87.3
In	7.6
Sn	5.1

Map Sum Spectrum	
Elements	Wt%
Au	78.1
In	5.1
Sn	16.8

Figure 4.33 Sample that Annealed at 350 °C – 1 hour – Vacuum Atmosphere a) SEM Image with Secondary Electron Detector, b) SEM Image with High Angle Back Scattered Electron Detector c) Point and Map EDS Analyzes with Compositions and d) Elemental Distribution

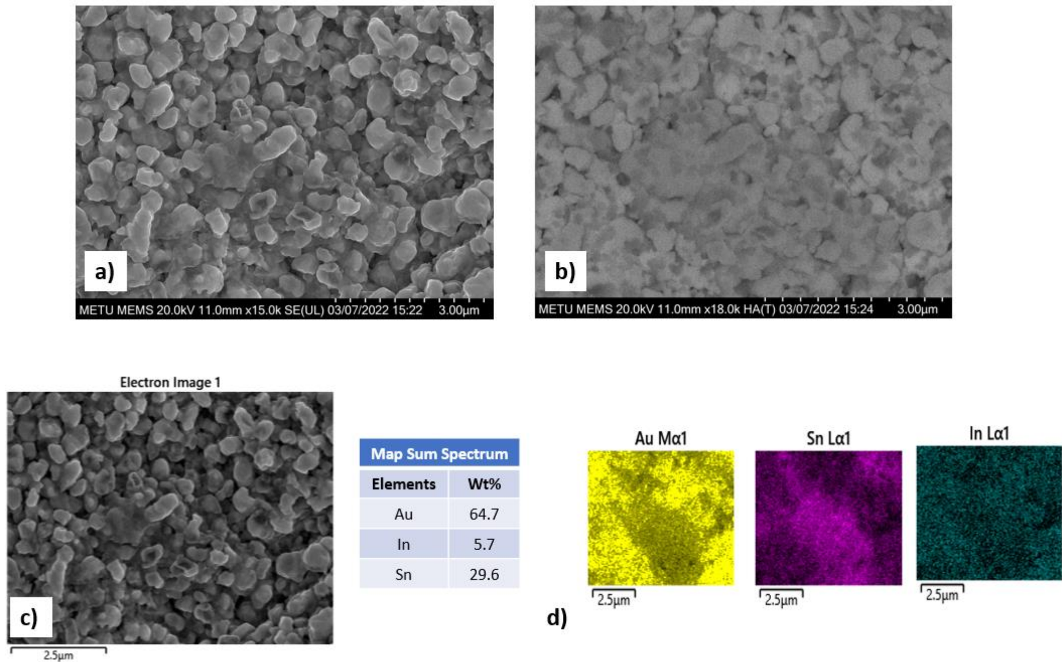

Map Sum Spectrum	
Elements	Wt%
Au	64.7
In	5.7
Sn	29.6

Figure 4.34 Sample that Annealed at 350 °C – 5 hours – N_2 Atmosphere a) SEM Image with Secondary Electron Detector, b) SEM Image with High Angle Back Scattered Electron Detector c) Point and Map EDS Analyzes with Compositions and d) Elemental Distribution

As seen from the SEM image of the vacuum-annealed sample, two different phases were observed. While the darker one has high Au-Sn content with an almost infinitesimal amount of In and a hexagonal-like structure, the lighter phase shows Au composition dominancy with almost equal In and Sn content with a higher amount along the deposited structure. At the darker phase, ternary phase formation existed probability due to elemental content. With respect to atomic percentages of the dark region, this phase probably indicates $In_3Sn_3Au_4$ IMC. In the total elemental composition diagram, Sn content was observed lower than aimed composition value. Furthermore, while Au and In distribution show similarity, Sn distributes almost opposite locations of these two elements. That situation could be shown that the tendency of Au-In phase formation is higher than the formation of phase between Au and Sn even if both existed in the total structure.

At 5 hours of the annealed sample, a completely different structure was observed. Due to the SEM image, small round-like structures were observed, and sintered formation was formed in some regions. Nevertheless, that kind of structure does not desire the formation of lots of topologies and formed void-like structures with respect to that. However, Au-Sn composition has relatively close values with the eutectic composition value of that system. That shows that selected thicknesses for Au and Sn can be suitable to create a eutectic stack with a small amount of In addition.

After these characterizations had been done, this ternary system was found suitable candidate material system for the WLP process. For this purpose, WLP packaging trials were done.

4.2.1 Au-In-Sn Sample 7

For the first WLP trial of this ternary material, packaging was done without lithography and patterning to observe the material bond quality and sticking properties more efficiently. For this purpose, two 4” Si wafers were bonded with

Recipe AuInSn 1, shown in Figure 3.16. After, for observation of the bond quality, SAM analysis was done. Obtained SAM image is shown in Figure 4.35.

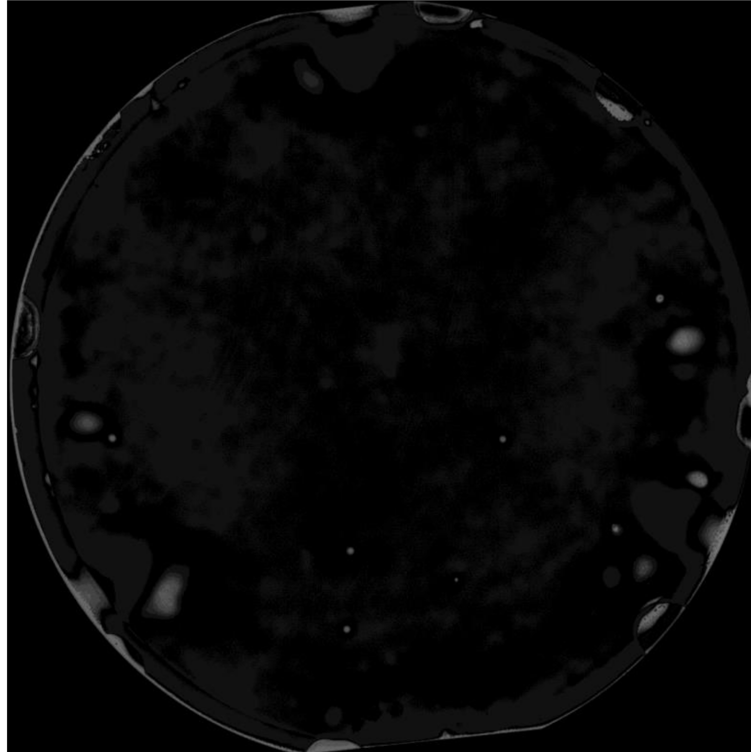

Figure 4.35 SAM Image of Au-In-Sn Sample 7

SEM and EDS analyses were done for two different locations to observe bond integrity and elemental compositions more accurately since this ternary system is one of the new material systems for WLP. From location 1 and location 2, obtained SEM and EDS results were shown in Figure 4.36 and Figure 4.37, respectively.

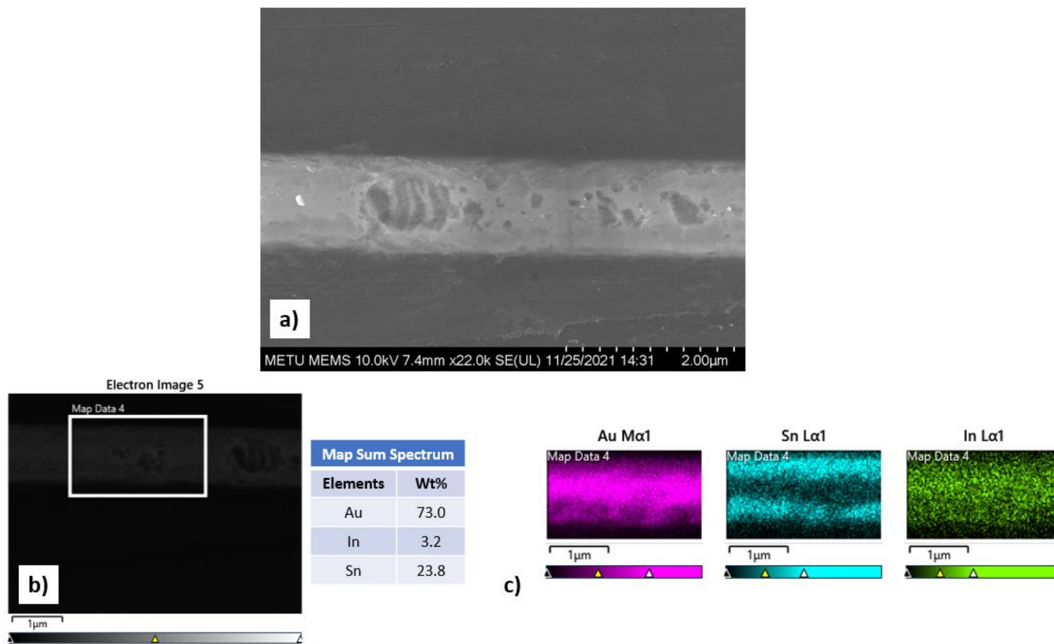

Map Sum Spectrum	
Elements	Wt%
Au	73.0
In	3.2
Sn	23.8

Figure 4.36 Au-In-Sn Sample 7 – Location 1 a) Cross Sectional SEM Image, b) Map EDS Analysis with Elemental Compositions and c) Elemental Distributions

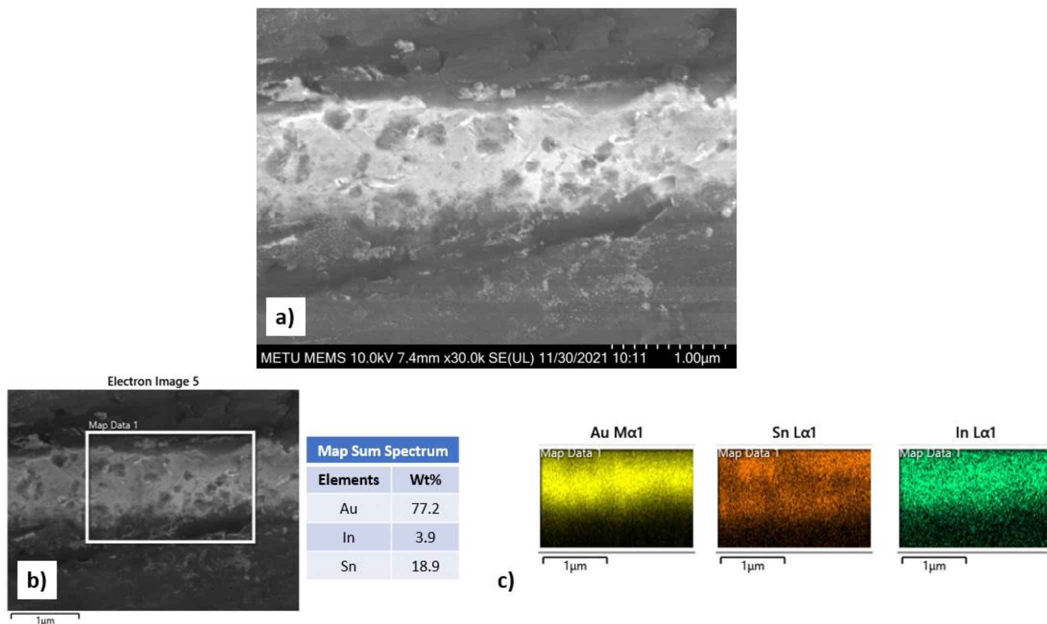

Map Sum Spectrum	
Elements	Wt%
Au	77.2
In	3.9
Sn	18.9

Figure 4.37 Au-In-Sn Sample 7 – Location 2 a) Cross Sectional SEM Image, b) Map EDS Analysis with Elemental Compositions and c) Elemental Distributions

As seen in Figure 4.36 and Figure 4.37, proper bond integrity has been obtained with respect to SEM images. Furthermore, at both locations, Sn was distributed upper and

lower parts of the bond region even though that element stayed middle part of the bonding system before packaging. The reason for this diffusion phenomenon was not understood clearly, but just like previous EDS analyses of that ternary system, Sn positions were shown opposite behavior to Au positions while Au and In showed similarity. Furthermore, the composition of the Au and Sn was shown variety at two different locations while In was approximately the same. The reason for that situation was probably related to the non-uniform or porous deposition of Sn at the Varian 3119 Thermal Evaporator. Nevertheless, the composition values of Au and Sn show closeness to the eutectic composition value of that binary system therefore, thickness optimization was done properly. Furthermore, just like in previous packaging studies, no bonding material has been diffused into the wafer side, which means seed layers were worked properly.

Samples were diced with 3 mm x 3 mm geometry. Since no pattern formation existed in this experiment and high bond integrity was observed with respect to SAM analysis, all dies remained rigid after the dicing operation. The mechanical strength of the samples was tested with die level shear test. Since each dies has approximately identical properties, 5 samples were tested. Obtained results are shown in Table 4.19.

Table 4.19 Shear Strength Values of Au-In-Sn Sample 7 with Statistical Data

	Shear Strength Values of Au-In-Sn Sample 7 (MPa) * At least 6 MPa required due to MIL-STD 883				
Sample Number	1	2	3	4	5
	57	42	60	52	38
Mean	50				
Standard Deviation	8				

As seen in Table 4.19, this ternary system has higher mechanical strength than the Au-In binary bonding system. These results show that this ternary system with these composition amounts can provide a robust package structure. However, even though identical bonding material thickness was expected along all package areas, shear strength values were shown to fluctuate with respect to the standard deviation value. The reason for this situation is probably related to the non-uniform deposition of Sn during coating even though proper conditions were satisfied such as rotation of the holder with maximum rpm and placement of the Sn boat at the middle of the system. In addition, this has been proven as compositional variance was observed with SEM and EDS analyses. Another reason for this situation could be related to non-uniform force distribution during the WLP process.

4.2.2 Au-In-Sn Sample 8

After the optimizations of this ternary material system in the patternless WLP processes, the first packaging experiment with a patterned structure was carried out with 4” glass and Si wafers. After the WLP step was done, SAM analysis was done. The obtained result is shown in Figure 4.38.

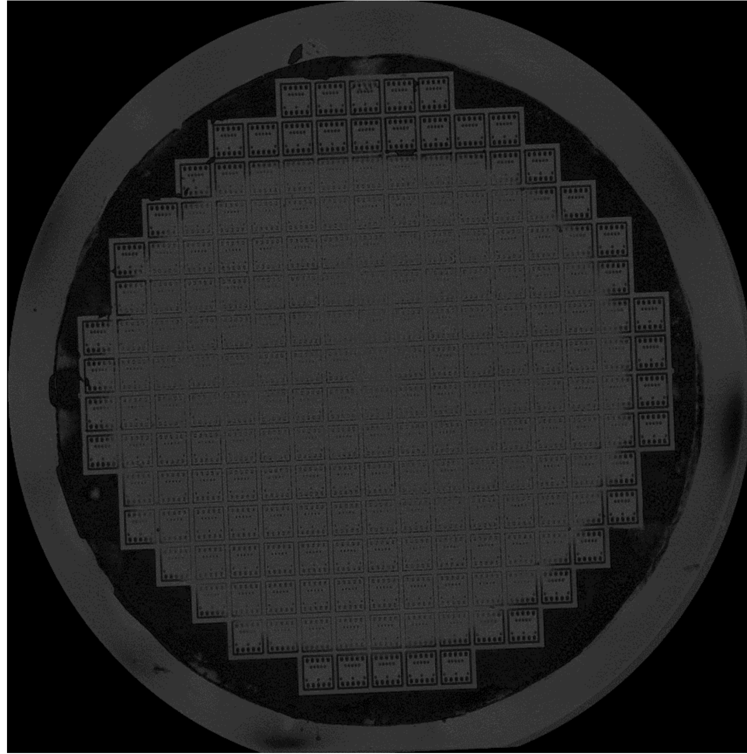

Figure 4.38 SAM Image of Au-In-Sn Sample 8

As seen in Figure 4.38, the edge sides remained rigid. However, in the middle circular part of the package, an almost completely whitish color was observed that indicating a lack of bond integrity in this region. The reason for this situation could be related to the lack of force appliances during packaging. Nevertheless, the outer ring part of the package still remained as a stacked structure that provides bond quality that can be achieved with this system since no water penetration was observed because of that.

After SAM analysis, the packaged sample was diced. A higher number of dies were separated from each other. Separation was especially observed at the low bond integrity region that was observed at SAM analysis. Photo of the packaged system after dicing is represented in Figure 4.39.

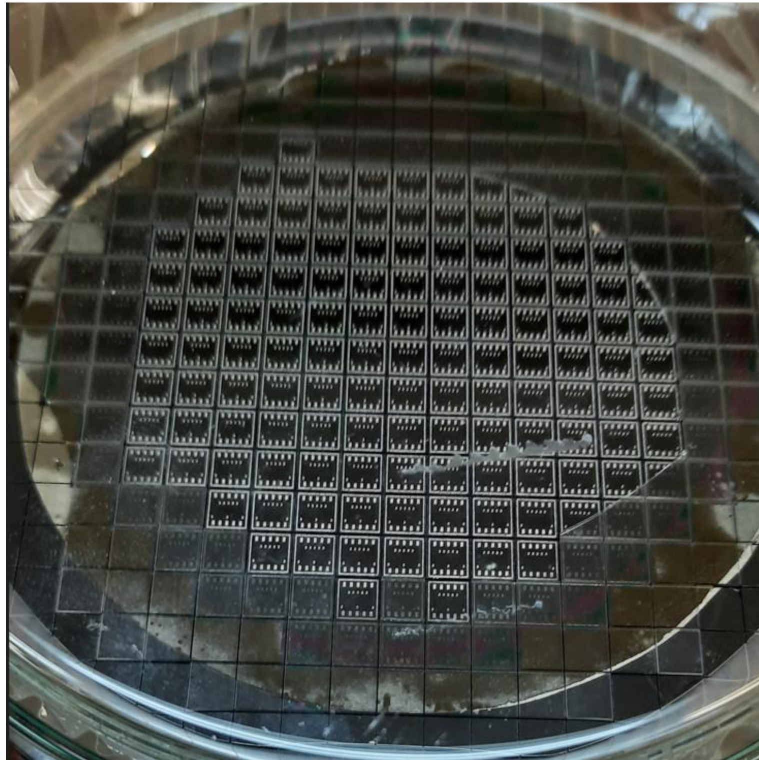

Figure 4.39 Photo of Au-In-Sn Sample 8 After Dicing Process

Die level shear test was applied to remained dies even though few numbers of dies remained after the dicing operation. 5 samples were taken for this test. Obtained data from this test are shown in Table 4.20.

Table 4.20 Shear Strength Values of Au-In-Sn Sample 8 with Statistical Data

	Shear Strength Values of Au-In-Sn Sample 8 (MPa) * At least 6 MPa required due to MIL-STD 883				
Sample Number	1	2	3	4	5
	122	90	126	110	80
Mean	106				
Standard Deviation	18				

As seen from Table 4.20, highly robust packages were obtained with respect to obtained shear test results. That samples have the highest shear strength with respect to previous samples. However, after dicing, a relatively low rigid die amount was obtained despite a high amount of shear strength. The reason for that situation can be related to high brittle IMC formation that can give high shear strength but low toughness. Since the bonding system has low toughness, the appliance of vibration and water duress during the dicing process can cause the separation of dies.

4.2.3 Au-In-Sn Sample 9

In this sample, WLP was tried with using the same bond and seed layer material thicknesses with Au-In-Sn Sample 8, but with changing the bonding parameters. Therefore, Recipe AuInSn 2 was used for that sample, that as shown in Figure 3.17. After WLP had been completed, SAM analysis was done. Obtained SAM image and photo of the sample after the SAM process are shown in Figure 4.40.

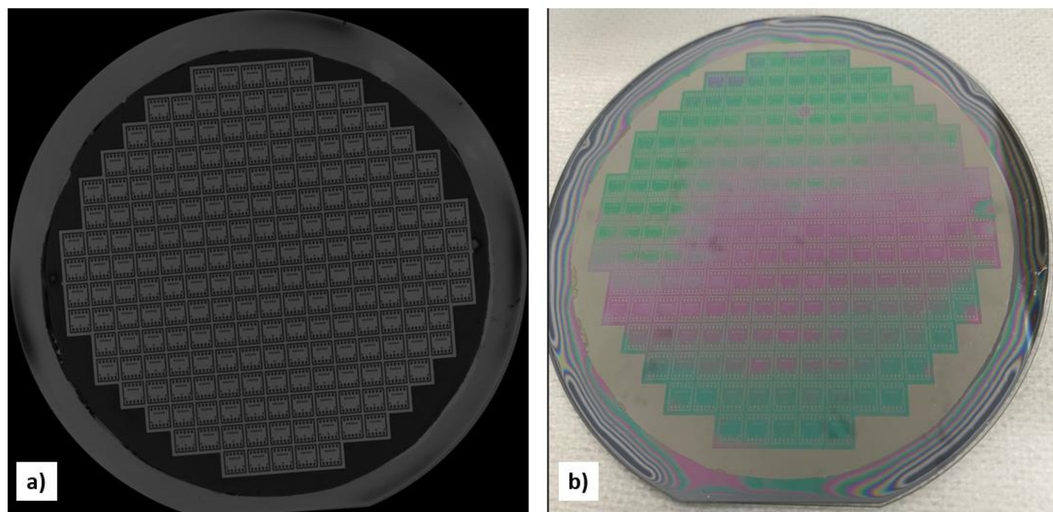

Figure 4.40 a) SAM Image of Au-In-Sn Sample 9 and b) Photo of Au-In-Sn Sample 9 after SAM Inspection

As seen in Figure 4.40, a perfectly bonded structure was observed with a full bond integrated. No water penetration, squeeze-out, or separation of dies was observed along all areas of the package. Besides the SAM image, a photo of this sample after packaging also shows high bond integrity and highly suitable bonding conditions.

After these inspections, the dicing process was done on this sample. Despite good results of SAM and visual inspections, almost all dies were separated from each other. Only 6 rigid dies on the right side of the package were left. A photo of the sample after the dicing operation is shown in Figure 4.41.

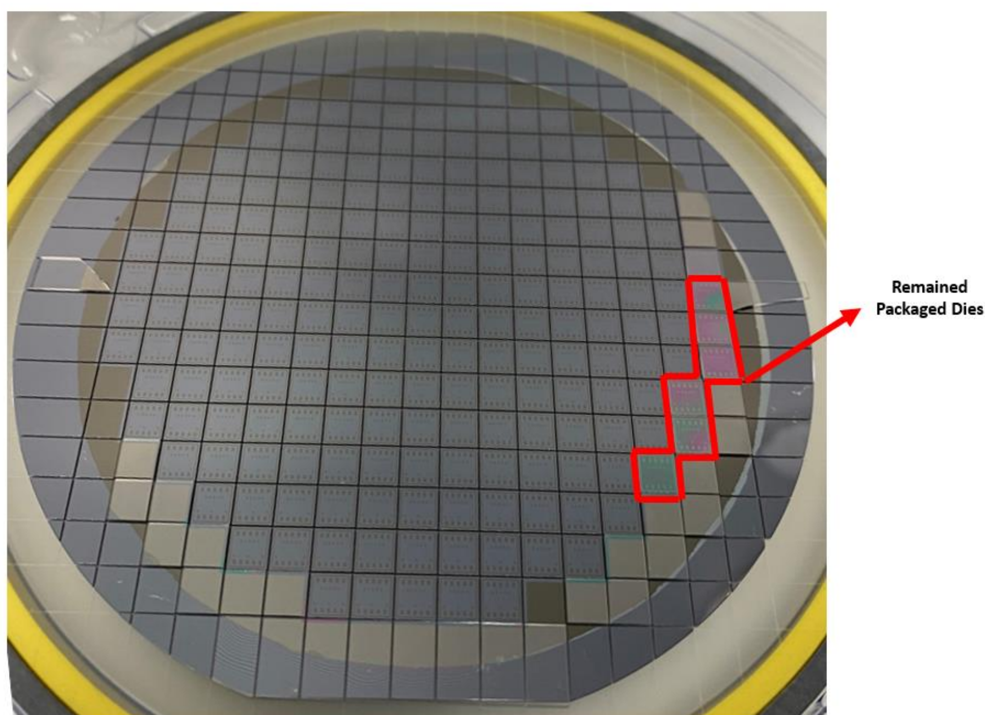

Figure 4.41 Photo of Sample Au-In-Sn Sample 9 After Dicing

Even if there are few dies left, a die-level shear test was applied for these packaged dies. 4 samples were taken for this purpose. Obtained data is shown in Table 4.21.

Table 4.21 Shear Strength Values of Au-In-Sn Sample 9 with Statistical Data

	Shear Strength Values of Au-In-Sn Sample 9 (MPa) * At least 6 MPa required due to MIL-STD 883			
Sample Number	1	2	3	4
	77	89	78	66
Mean	77			
Standard Deviation	8			

As seen from Table 4.21, high shear strength data were obtained from remained dies of Au-In-Sn Sample 9. However, even robust packaged dies were obtained just like Au-In-Sn Sample 8, and a much lower was obtained yield from dicing even though this sample has better SAM inspection results. The reason for this situation can be related to the reasons observed in Au-In-Sn Example 8. In both samples, due to the formation of brittle IMCs, the toughness of the bond structure is relatively low, causing the dies to separate during dicing process.

CHAPTER 5

CONCLUSION AND FUTURE RECOMMENDATIONS

In this study, experimental procedures have been done to obtain hermetic and robust wafer-level vacuum packaging with certain temperature-withstanding properties. For this purpose, first, packaging has been tried with Au-In binary metal system via TLP bonding with investigation composition/property relationship for improving the quality of the package via combinatorial optimization. Thanks to the combinatorial approach, this study investigated the In a range of about 8% by weight for package properties with only a single In deposition step. Therefore, although many WLP experiments are required for each composition, the number of experiments needed has been reduced, as the compositional variance is obtained along the bonding surface of the wafers with the combinatorial approach. According to the results obtained, the correlation between the composition and the packaging quality was found that the package properties improved with the increase in the In composition. With respect to that, 22 MPa average package strength was found with 46.0% wt In composition.

After the composition/property relationship has been done with combinatorial optimization to observe hermetic properties and repeatability of the obtained correlation between In composition and property, the sample has been prepared with the formation of a cap cavity. Therefore, in this experiment, to correlate the beneficial effect of In composition increment to package quality, In composition was raised to 50% wt In approximately. While after the shear test, average 28 MPa shear strength was found, hermetic properties have been obtained due to the observation of cap deflection. Therefore, with respect to optimizing the Au-In composition with a combinatorial approach, a successfully WLP packaged sample has been manufactured with adequate shear strength, bond integrity, and hermetic properties.

Furthermore, the Au-In-Sn ternary material system that has not been investigated in the literature was studied in this thesis for WLP. First, after the thickness design of each element, to observe the suitability of this candidate material system to WLP, a ternary phase diagram was generated with Thermo-Calc software. Later, with DSC analysis, the liquefaction temperature of that material system was found; therefore, the bonding recipe with 350 °C has been prepared for WLP. After optimizations were done with packaging without patterning, WLP experiments were done with the same patterned structure. After SAM analyses, high bond quality was obtained. Furthermore, 106 and 77 MPa shear strength values have been found after the die-level shear test. According to these, a more robust packaged structure has been obtained than the Au-In system. However, even though this material system provided DSC results suitable for TLP bonding, high bond integrity, and increased robustness according to SAM analysis, low yields were obtained in successfully packaged chips after dicing packaged samples.

Following this study, these recommended research topics can be considered in the future:

1) To optimize WLP studies, new material stacks that cannot be investigated in the literature can be studied with a combinatorial approach. Elemental compositions of this material stack can be optimized with a combinatorial approach that can provide less metal deposition experimental procedure. Moreover, optimum composition/property relationship can be investigated for new material systems to enhance the package quality.

2) Besides studies of WLP of MEMS devices, combinatorial optimization can be done for many research areas, such as discovering the materials' thermal, optic, electrical, or magnetic properties with varied composition values. For instance, solder material systems can be studied with the combinatorial approach to enhance the material properties.

3) The Au-In-Sn ternary material system can be re-evaluated for WLP of MEMS devices by optimizing the bonding parameters and thickness values, as the strength,

thermal properties for TLP bonding, and high bond integrity are met in the studies in this thesis. This ternary material system can provide successful WLP for MEMS devices with these improvements after the optimization stages.

REFERENCES

[1] Attoh-Okine, N., & Mensah, S. (2017). MEMS Application in Pavement Condition Monitoring-Challenges. *Proceedings of the 19th International Symposium on Automation and Robotics in Construction (ISARC)*, *September*. https://doi.org/10.22260/isarc2002/0061

[2] Obuh, I. E., Doychinov, V., Steenson, D. P., Akkaraekthalin, P., Robertson, I. D., & Somjit, N. (2018). Low-Cost Microfabrication for MEMS Switches and Varactors. *IEEE Transactions on Components, Packaging and Manufacturing Technology*, *8*(9), 1702–1710. https://doi.org/10.1109/TCPMT.2018.2834865

[3] A. A. M. Faudzi, Y. Sabzehmeidani, and K. Suzumori, "Application of micro-electro-mechanical systems (MEMS) as sensors: A review," *J. Robot. Mechatronics*, vol. 32, no. 2, pp. 281–288, 2020, doi: 10.20965/jrm.2020.p0281.

[4] H. Fujita, "A decade of MEMS and its future," *Proceedings IEEE The Tenth Annual International Workshop on Micro Electro Mechanical Systems. An Investigation of Micro Structures, Sensors, Actuators, Machines and Robots*, 1997, pp. 1-7, doi: 10.1109/MEMSYS.1997.581729.

[5] J. H. Lau, C. Lee, C. S. Premachandran, Y. Aibin, and E. Al, *Advanced MEMS Packaging*. New York: McGraw-Hill, 2009.

[6] S. Seok, *Advanced Packaging and Manufacturing Technology Based on Adhesion Engineering*, Springer Series in Advanced Manufacturing, https://doi.org/10.1007/978 3-319-77872-3_1

[7] M. Moraja, "Hermetic Packaging Design of MEMS," *Seminar Notes*, November 2009.

[8] Tanrıkulu, Y. (2007). *an Uncooled Infrared Microbolometer Detector Array Using Surface Micromachined Mems Technology a Thesis Submitted to the Graduate School of Natural and Applied Sciences of Middle East Technical University by in Partial Fulfilment of the Requirements for T. August*.

[9] Elßner, M. (2014). Vacuum quality evaluation for uncooled micro bolometer thermal imager sensors. *Microelectronics Reliability*, *54*(9–10), 1758–1763. https://doi.org/10.1016/j.microrel.2014.07.094

[10] He, X., Karunasiri, G., Mei, T., Zeng, W. J., Neuzil, P., & Sridhar, U. (2000). Performance of microbolometer focal plane arrays under varying pressure. *IEEE Electron Device Letters*, *21*(5), 233–235. https://doi.org/10.1109/55.841306

[11] Voronel, A. (2020). *Efficient Manufacture of IR Sensors – Combining Bonder and Vacuum Reflow Technology*.

[12] United States. Military Standard: Test Methods and Procedures for Microelectronics MIL-STD 883G. 2019.

[13] Jourdain, A., De Moor, P., Pamidighantam, S., & Tilmans, H. A. C. (2002). Investigation of the Hermeticity of BCB-sealed cavities for housing (RF-)MEMS devices. *Proceedings of the IEEE Micro Electro Mechanical Systems (MEMS)*, 677–680. https://doi.org/10.1109/memsys.2002.984361

[14] Santagata, F., Zaal, J. J. M., Huerta, V. G., Mele, L., Creemer, J. F., & Sarro, P. M. (2012). Mechanical design and characterization for MEMS thin-film packaging. *Journal of Microelectromechanical Systems*, *21*(1), 100–109. https://doi.org/10.1109/JMEMS.2011.2170817

[15] Welch W. C. "Vacuum and Hermetic Packaging of MEMS Using Solder" PhD Dissertation, The University of Michigan, 2008.

[16] A. Bosseboeuf *et al.*, "Effect of environment on activation and sorption of getter alloys and multilayers for hybrid wafer-level vacuum packaging," *Sensors Mater.*, vol. 31, no. 9, pp. 2825–2849, 2019, doi: 10.18494/SAM.2019.2312.

[17] J. S. Mitchell, "Low Temperature Wafer Level Vacuum Packaging Using Au-Si Eutectic Bonding and Localized Heating.," *Ph.D. Dissertation*, The University of Michigan, 2008.

[18] Aydın, G. D., & Akın, T. (2020). Resonance-Based Temperature Sensors using a Wafer Level Vacuum Packaged SOI MEMS Process. *Advanced Materials Letters*, 0–0. https://hdl.handle.net/11511/44208.

[19] Knowles, K. M., & Van Helvoort, A. T. J. (2006). Anodic bonding. *International Materials Reviews*, *51*(5), 273–311. https://doi.org/10.1179/174328006102501

[20] Wang, L., He, Y., Zhan, Z., Yu, L., Wang, H., & Chen, D. (2015). A novel sacrificial-layer process based on anodic bonding and its application in an accelerometer. *AIP Advances*, *5*(4), 3–10. https://doi.org/10.1063/1.4907930

[21] Cheng, Y. T., Lin, L., & Najafi, K. (2000). Localized silicon fusion and eutectic bonding for MEMS fabrication and packaging. *Journal of Microelectromechanical Systems*, *9*(1), 3–8. https://doi.org/10.1109/84.825770

[22] Dragoi, V., Mittendorfer, G., Thanner, C., & Lindner, P. (2008). Wafer-level plasma activated bonding: New technology for MEMS fabrication. *Microsystem Technologies*, *14*(4–5), 509–515. https://doi.org/10.1007/s00542-007-0437-7

[23] T. H. F.S., Lo, Chiang, C.C., Li, C., Lee, "Enhancement of Bonding Strength for Low Temperature Si3N4/Si3N4 Direct Wafer Bonding by Nitrogen-Plasma Activation and Hydrofluoric Pre-dip," *ECS Transcactions*, vol. 64, no. 5, pp. 11–117, 2014.

[24] Enoksson, P., Rusu, C., Sanz-Velasco, A., Bring, M., Nafari, A., & Bengtsson, S. (2005). Wafer bonding for MEMS. *Proceedings - Electrochemical Society*, *PV 2005-02*(April 2016), 157–172. https://doi.org/10.1149/ma2005-01/11/493

[25] Malik, N., Schjølberg-Henriksen, K., Poppe, E., Taklo, M. M. V., & Finstad, T. G. (2014). Al-Al thermocompression bonding for wafer-level MEMS sealing. *Sensors and Actuators, A: Physical*, *211*, 115–120. https://doi.org/10.1016/j.sna.2014.02.030

[26] Demirhan Aydın, G. (2022). *A WAFER LEVEL VACUUM PACKAGING TECHNOLOGY FOR MEMS BASED LONG-WAVE INFRARED SENSORS* [Ph.D. - Doctoral Program]. Middle East Technical University.

[27] Knechtel, R. (2005). Glass frit bonding: An universal technology for wafer level encapsulation and packaging. *Microsystem Technologies*, *12*(1-2 SPEC. ISS.), 63–68. https://doi.org/10.1007/s00542-005-0022-x

[28] Knechtel, R., Dempwolf, S., & Schikowski, M. (2020). Glass frit bonding. In *Handbook of Silicon Based MEMS Materials and Technologies*. INC. https://doi.org/10.1016/B978-0-12-817786-0.00025-6

[29] R. R. Tummala, "Fundamentals of Microsystems Packaging," Mc Graw-Hill, 2001.

[30] Wang, Q., Choa, S., Kim, W., Hwang, J., Ham, S., & Moon, C. (2006). *Application of Au-Sn Eutectic Bonding in Hermetic Radio-Frequency Microelectromechanical System Wafer Level Packaging*. *35*(3), 425–432.

[31] B. G. Dimez, “Al-Ge Eutectic Bonding for Wafer-Level Vacuum Packaging of MEMS Devices,” 2022.

[32] O. Temel, “Investigation of Solder Materials and Bond Formation for Wafer Level Vacuum Packaging of MEMS Devices,” 2020.

[33] Marauska, S., Claus, M., Lisec, T., & Wagner, B. (2013). Low temperature transient liquid phase bonding of Au/Sn and Cu/Sn electroplated material systems for MEMS wafer-level packaging. *Microsystem Technologies*, *19*(8), 1119–1130. https://doi.org/10.1007/s00542-012-1708-5

[34] Liu, Y., Joshi, S. N., & Dede, E. M. (2020). Novel transient liquid phase bonding for high-temperature automotive power electronics systems. Journal of Electronic Packaging, Transactions of the ASME, 142(1), 1–10. https://doi.org/10.1115/1.4044476

[35] Baker, H. (2004). ASM HANDBOOK, VOLUME 3, Alloy Phase Diagrams. In ASM Handbook.

[36] Mokhtari, O. (2019). A review: Formation of voids in solder joint during the transient liquid phase bonding process - Causes and solutions. *Microelectronics Reliability*, *98*(April), 95–105. https://doi.org/10.1016/j.microrel.2019.04.024

[37] G. Humpston and D. M. Jacobson, *Principles of Soldering*. ASM International, 2004.

[38] McGinn, P. J. (2019). Thin-film processing routes for combinatorial materials investigations - a review. *ACS Combinatorial Science*, *21*(7), 501–515. https://doi.org/10.1021/acscombsci.9b00032

[39] Bikowski, A., Holder, A., Peng, H., Siol, S., Norman, A., Lany, S., & Zakutayev, A. (2016). Synthesis and Characterization of (Sn,Zn)O Alloys. *Chemistry of Materials*, *28*(21), 7765–7772. https://doi.org/10.1021/acs.chemmater.6b02968

[40] Devulder, W., Opsomer, K., Meersschaut, J., Deduytsche, D., Jurczak, M., Goux, L., & Detavernier, C. (2015). Combinatorial study of ag-te thin films and their application as cation supply layer in CBRAM cells. *ACS Combinatorial Science*, *17*(5), 334–340. https://doi.org/10.1021/acscombsci.5b00025

[41] Golim, O., Vuorinen, V., Ross, G., Wernicke, T., Pawlak, M., Tiwary, N., & Paulasto-Kröckel, M. (2023). Achieving low-temperature wafer level bonding with Cu-Sn-In ternary at 150 °C. *Scripta Materialia*, *222*(September 2022), 2022–2024. https://doi.org/10.1016/j.scriptamat.2022.114998

[42] Grummel, B. J. (2012). *Design and Characterization of High-Temperature Packaging for Wide-Bandgap Semiconductor Devices*. *2012*, 2004–2019.

[43] Grummel, B., Mustain, H. A., John Shen, Z., & Hefner, A. R. (2011). Comparison of Au-In transient liquid phase bonding designs for SiC power semiconductor device packaging. *Proceedings - 2011 IMAPS International Conference on High Temperature Electronics Network, HiTEN 2011*, 77–83. https://doi.org/10.4071/hiten-paper6-bgrummel

[44] Welch, W. C., & Najafi, K. (2007). Nickel-tin transient liquid phase (TLP) wafer bonding for MEMS vacuum packaging. *TRANSDUCERS and EUROSENSORS '07 - 4th International Conference on Solid-State Sensors, Actuators and Microsystems*, 1327–1328. https://doi.org/10.1109/SENSOR.2007.4300385

[45] Choi, W. K., Premachandran, C. S., Chiew, O. S., Ling, X., Ebin, L., Khairyanto, A., Ratmin, B., Chen Wei Sheng, K., Thaw, P. P., & Lau, J. H. (2009). Development of novel intermetallic joints using thin film indium based solder by low temperature bonding technology for 3D IC stacking. *Proceedings - Electronic Components and Technology Conference*, 333–338. https://doi.org/10.1109/ECTC.2009.5074036

[46] Cai, J., Wang, Q., Li, X., Kim, W., Wang, S., Hwang, J., & Moon, C. (2005). Microstructure of AuSn wafer bonding for RF-MEMS packaging. *2005 6th International Conference on Electronics Packaging Technology*, *2005*. https://doi.org/10.1109/ICEPT.2005.1564660

[47] Torunbalci, M. M., Demir, E. C., Donmez, I., Alper, S. E., & Akin, T. (2014). Gold-tin eutectic bonding for hermetic packaging of MEMS devices with vertical feedthroughs. *Proceedings of IEEE Sensors*, *2014-December* (December), 2187–2190. https://doi.org/10.1109/ICSENS.2014.6985473

[48] Vuorinen, V., Dong, H., Ross, G., Hotchkiss, J., Kaaos, J., & Paulasto-Kröckel, M. (2021). Wafer Level Solid Liquid Interdiffusion Bonding: Formation

and Evolution of Microstructures. *Journal of Electronic Materials*, *50*(3), 818–824. https://doi.org/10.1007/s11664-020-08530-y

[49] Ludwig, A., Cao, J., Brugger, J., & Takeuchi, I. (2005). MEMS tools for combinatorial materials processing and high-throughput characterization. *Measurement Science and Technology*, *16*(1), 111–118. https://doi.org/10.1088/0957-0233/16/1/015

[50] Pişkin, F., Akyildiz, H., & Öztürk, T. (2015). Ti modified Pd-Ag membranes for hydrogen separation. *International Journal of Hydrogen Energy*, *40*(24), 7553–7558. https://doi.org/10.1016/j.ijhydene.2014.11.049

[51] Siol, S., Dhakal, T. P., Gudavalli, G. S., Rajbhandari, P. P., Dehart, C., Baranowski, L. L., & Zakutayev, A. (2016). Combinatorial Reactive Sputtering of In2S3 as an Alternative Contact Layer for Thin Film Solar Cells. *ACS Applied Materials and Interfaces*, *8*(22), 14004–14011. https://doi.org/10.1021/acsami.6b02213

[52] Li, J., Du, P., Li, S., Liu, J., Zhu, M., Tan, Z., Hu, M., Luo, J., Guo, D., Ma, L., Nie, Z., Ma, Y., Gao, L., Niu, G., & Tang, J. (2019). High-Throughput Combinatorial Optimizations of Perovskite Light-Emitting Diodes Based on All-Vacuum Deposition. *Advanced Functional Materials*, *29*(51), 1–8. https://doi.org/10.1002/adfm.201903607

[53] Mardare, A. I., Yadav, A. P., Wieck, A. D., Stratmann, M., & Hassel, A. W. (2008). Combinatorial electrochemistry on Al-Fe alloys. *Science and Technology of Advanced Materials*, *9*(3). https://doi.org/10.1088/1468-6996/9/3/035009

[54] Demir E. “Bonding Material Development At Wafer Level Vacuum Packaging For MEMS Devices by Transient Liquid Phase (TLP) Method”, Master Thesis, Middle East Technical University, 2016